Effect of Polymeric Properties on the Operation of Gel-Type Audio Transducers

by

Minsung Cho

A thesis submitted in partial fulfilment of the

requirements of Edinburgh Napier University,

for the award of

Doctor of Philosophy

School of Engineering and the Built Environment
Edinburgh Napier University

September 2013

Declaration of originality

The material presented in the thesis "Effect of Polymeric Properties on the Operation of Gel-Type Audio Transducers" is entirely the result of my own independent research under supervision of Dr. Mike Barker and Dr. Elena Prokofieva.

Name: Minsung Cho   14/02/2013

Signed:

Abstract

A novel design of a moving-coil transducer coupled with a low-hardness elastomer called "the gel surround" is presented in this thesis. This device is termed a "gel-type audio transducer". The gel-type audio transducer has been developed to overcome the problems that conventional loudspeakers have suffered - that is, the problem with size of the audio device against the quality of sound at low frequency range. Therefore the research work presented herein aims to develop the "gel-type audio transducer" as a next-generation audio transducer for miniaturized woofers.

The gel-type audio transducer consists of the magnetic and coil-drive plate assembly, and these parts are coupled by the gel surround. The transducer is driven by the electromagnetic conversion mechanism (a moving-coil transducer) and its output driving force can be greatly enhanced by applying the novel mechanism of the gel surround especially at low frequency range, resulting in the enhanced acoustic efficiency. The transducer can be attached to a stiff and light panel with both the optimized impedance matching and minimised wave collisions.

The performance of the gel-type audio transducer is greatly influenced by the mass of the magnetic assembly M_m and compliance C of the "gel surround". But as the size of the magnet and its weight have to be kept minimal for a miniaturisation of the device, the focus of the research is on the effect of the C of the gel surround. As a result, the effect of the gel surround, made of the RTV (room-temperature vulcanising) silicone elastomer, TPE (thermoplastic elastomer), and the silicone foam, on generation of the

output driving force, the energy transfer from the transducer to a panel to which the transducer is attached, and sound radiation from the vibrating panel, was investigated. This effect was studied by COMSOL multiphysics (FE analysis) and thereby, the simulated results were verified by experiments such as the laser scanning measurement, DMA (dynamic mechanical analyzer), and the acoustic test.

Successful development of prototypes of the gel-type audio transducers, with an enhanced acoustic efficiency at reduced size and weight, was achieved. Implementation of the transducers into consumer applications was also demonstrated with their commercial values.

Acknowledgements

Contents

List of Tables

List of Figures

Table of Symbols

SYMBOL	DESCRIPTION	SYMBOL	DESCRIPTION
M_m	Mass of a magnetic assembly	ε	Strain
M_c	Mass of the voice coil assembly	N_c	Number of network chains unit volume
Z_p	Mechanical impedance of the panel	K_f	Force constant
X_m	Displacement of the magnet	T	Absolute temperature
X_p	Displacement of the panel	T_g	Glass transition temperature
r	Damping	$E^{"}$	Loss modulus
k	Stiffness	$\hat{\varepsilon}$	Total strain
F_e	Electrical force	ε_e	Elastic strain
E	Young's modulus	ε_c	Creep strain
G	Shear modulus	$J(t)$	Creep compliance
t_s	True tensile stress	σ	Constant stress
t	Time	m	Mass
δ	Phase angle	ω_0	Natural angular frequency
$\bar{\sigma}$	Sinusoidal force	R_m	Mechanical resistance

$\bar{\varepsilon}$	Resulting displacement	r_c	Constant
σ_0	Stress amplitude	F_0	Magnitude of the driving force
ε_0	Strain amplitude	A'	Constants
ω	Angular frequency	φ	Angle – ratio of imaginary to rear part
E'	Elastic modulus	V^*	Complex velocity
i	Imaginary unit	V_0	Magnitude of the velocity
E^*	Complex modulus	Z_s	Complex mechanical impedance
$tan\,\delta$	Loss factor or tan delta	Z_c	Mechanical impedance of damping
Q_m	Mechanical quality factor	Z_k	Mechanical impedance of spring
x	Distance	Z_m	Mechanical impedance of mass
ζ	Damping ratio	W	Mechanical energy
C_C	Critical damping coefficient	W_s	Energy stored
h	Thickness of a plate	W_d	Dissipated energy
M_{xx}	Bending moment in x axis	B	Bending stiffness
M_{xy} or M_{yx}	Bending moment in x-y axis	μ	Mass per area of plate

M_{yy}	Bending moment in y axis	v_B	Bending wave velocity
q	Load of intensity in the z direction	K_b	Wave number of the bending wave
V	Shear force	c	Speed of sound
D	Flexural rigidity	T	Temperature
ρ	Density of the material	c_l	Longitudinal wave speed
n	This denotes the normal to the edge	c_t	Transverse wave speed
λ	Wave length	k_n	Wave number
f	Frequency	$\hat{p}$	Pressure of a plane wave
$\hat{u}$	Acoustic particle velocity	$\hat{P}$ and $\hat{Q}$	Magnitude of high and low pressure respectively
I	Sound intensity	W_p	Sound power
$|\hat{p}|$	Root-mean-square pressure	S	Unit area
$\hat{q}$	Volume velocity	Z_a	Acoustic impedance
r_a	Radius	R_a	Real part of Z_a
W_{sp}	Sound power of the monopole	X_a	Imaginary part of Z_a
R_0	Observation point	P_0	Atmospheric pressure

N_m	Total number of monopole	r_n	Distance from the monopole
$\widehat{q_n}$	Volume velocity of monopole	$\widehat{q_p}$	Volume velocity of the plate
$\widehat{u_p}$	Acoustic particle velocity of the plate	W_{pp}	Sound power with volume velocity of the plate
$\widehat{S_p}$	Sound radiating area of the plate	BL	Force factor
Z_b	Blocked coil impedance	V_{emf}	Back electro magnetic force
B	Magnetic flux density	v	Velocity
L	Coil length	M_{cdp}	Mass of the coil-drive plate assembly
I_e	Total electric current	x_{cdp}	Displacement of the coil-drive plate assembly
N	Number of coil turns	v_m	Velocity of the magnetic assembly
A	Cross-sectional area	v_p	Velocity of the panel
B_r	Remanent magnetic flux density	v_{cdp}	Velocity of the coil-drive plate assembly
V_I	Input voltage	F_{total}	Total output driving force
φ_m	Phase of the forced oscillation of the magnetic assembly	φ_{cdp}	Phase of the forced oscillation of the coil-drive plate assembly

f_0	Resonant frequency	v	Poisson's ratio
R_b	Electrical resistance	L_b	Blocked coil inductance
R	Real part of the acoustic radiation impedance	A_s	Cross-sectional area of a sample
$W(j\omega, r_p)$	Displacement of a panel	K_s	Stiffness of a system
ρ_p	Density of the panel	ρ_0	Density of the air
r_{ra}	Radius of sound radiating area		

Table of Acronym

ACRONYM	DESCRIPTION	ACRONYM	DESCRIPTION
DML	Distributed mode loudspeaker	DMA	Dynamic mechanical analysis
EPDM	Ethylene propylene diene monomer	SDOF	Single degree of freedom
SBR	Styrene-butadiene rubber	RTV	Room-temperature vulcanising
SPL	Sound pressure level	TPE	Thermoplastic elastomer
ABS	Acrylonitrile butadiene styrene	FE	Finite element
LDV	Laser Doppler Vibrometer	DSA	Peak to peak dynamic strain amplitude
EMF	Electro magnetic force	THD	Total harmonic distortion
PML	Perfectly matched layer	CES	Consumer electronics show
PMMA	Poly(methyl methacrylate)	PVC	Poly(vinyl chloride)
ERM	Eccentric rotating masses		

CHAPTER 1 – INTRODUCTION

1.1 Introduction to the thesis

Since Alexander Graham Bell had patented a first electric transducer which was capable of reproducing intelligible speech as part of his telephone invention in 1876, a large amount of research and development work has been carried out to improve the sound reproduction system trying to playback the sound through the loudspeakers as close as possible to the original. As the result, a remarkable development has been achieved throughout the last century, and now listeners are able to appreciate orchestra music in high-fidelity at a convenient place, i.e. at home. However despite multiple efforts and inventions came and gone, the main principle of how the sound is produced by the diaphragm of the electric device stays almost the same since the time it was originally invented.
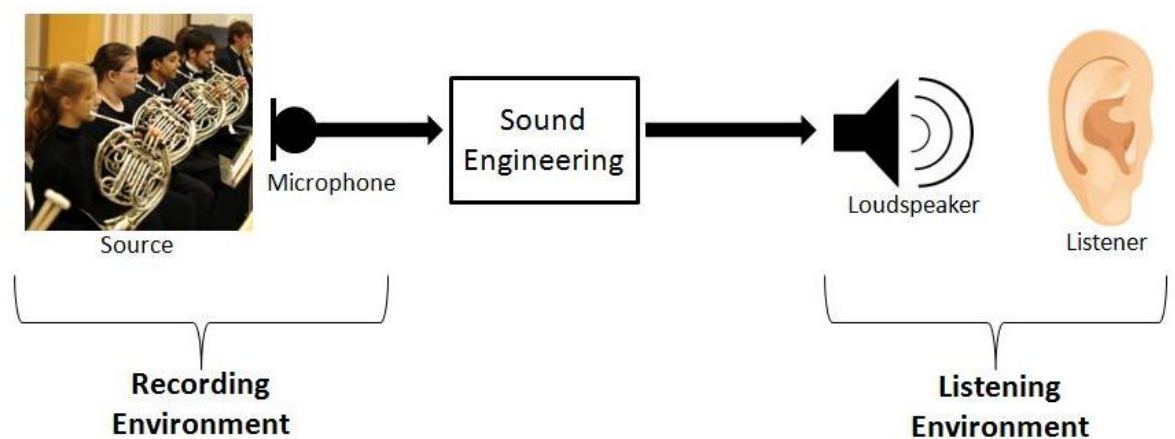
Fig 1.1 Sound reproduction system

Figure 1.1 shows a process of the sound reproduction. The analogue sound signal picked up by a microphone at the source location is converted by a process of digitization into the recording, allowing it to be stored and transmitted by a wider variety of media. Then the stored digital audio signal is reconverted to an analogue form and it is applied to a loudspeaker to reproduce the original sound recorded to the listener. In the sound reproduction system, the loudspeaker plays an important role as quality of the reproduced sound is greatly dependent on a loudspeaker device which reproduces it. But current loudspeaker devices face some limitations and challenges. In this thesis, those limitations will be considered, thereafter a newly developed loudspeaker called "a *gel-type audio transducer*" will be discussed as one of potential solutions.

1.1.1 Historical background of loudspeaker development

Many consumer electronic devices such as a mobile phone, laptop, and TV, which are equipped with various types of loudspeakers, have become an essential part of everyday life.

Alexander Graham Bell developed a first electric loudspeaker for his telephone application in 1876. In the following year, an improved version of the loudspeaker was developed by Ernst. W. Siemens and he explained the function of moving coil transducer and the circular coil of wires in the magnetic field. The first practical application of the modern design of moving-coil drivers was introduced by Peter L. Jensen and Edwin Pridham in Napa, California in 1915 [1] [2]. Since that time, a large amount of research has been carried out with commercial success and many patents had been issued with regard to mechanics and construction of loudspeakers.
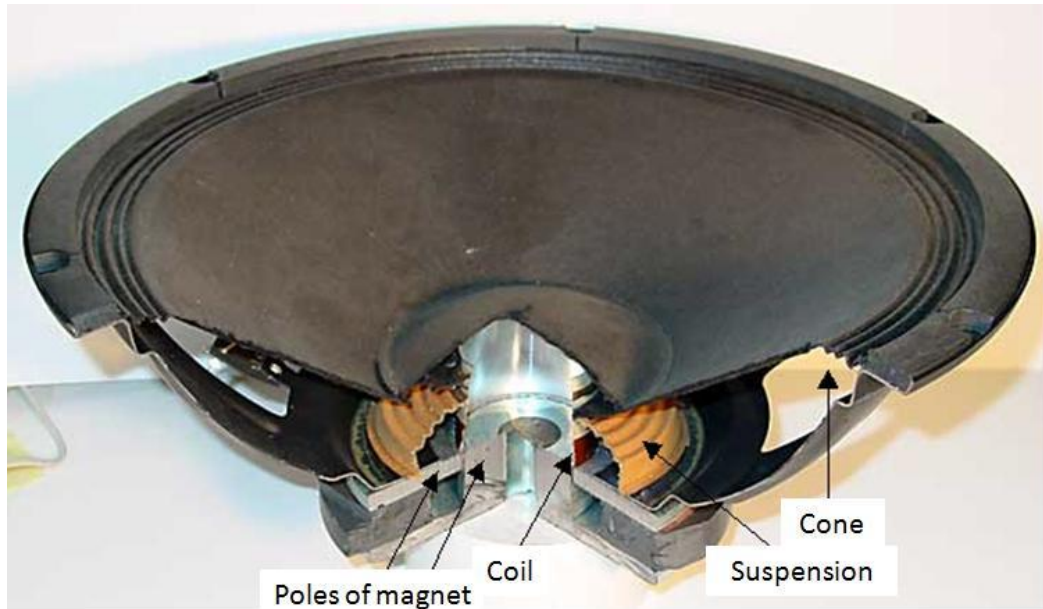
Fig 1.2 Cross-section of a dynamic cone speaker

In general, the most common type of a loudspeaker called a dynamic loudspeaker (or a cone speaker) consists of a magnetic assembly, voice coil, and a diaphragm (or cone), connected to a rigid frame via a flexible suspension as shown in Figure 1.2. The electrical interaction between the magnetic assembly and voice coil causes the diaphragm to move back and forth in response to the electrical signal input, thereby reproducing the sound by means of the change of pressure in the air. Due to a simple mechanical construction and low production cost, a cone-type speaker has been used in many applications [3].

1.1.2 Current problems for loudspeaker design

The sound wave length changes at each frequency band, and a single loudspeaker unit struggles to create the high level uniform sound pressure across the audible frequency range (20 Hz ~ 20 KHz). Throughout this thesis, unless specifically stated otherwise, the frequency ranges are designated as follows:

Low frequency range: 20 Hz to 300 Hz

Medium frequency range: 300 Hz to 3,000 Hz

High frequency range: 3,000 Hz to 20,000 Hz

To create the uniform sound the loudspeakers are combined into the systems employing two or three different drivers – a tweeter for high frequency, woofer for low frequency, and sometimes mid-range speaker for medium frequency in order to reproduce the sound in full spectrum. These speakers are wired up with each other and connected to a passive or active "crossover" network to ensure that the audio signal is accurately split and reproduced by all the different sub-speakers. Figure 1.3 shows a crossover network diagram. When multiple drivers, and crossovers are required, the overall construction becomes too complicated and bulky, and requires extensive additional work from the developer to be constructed and operated.
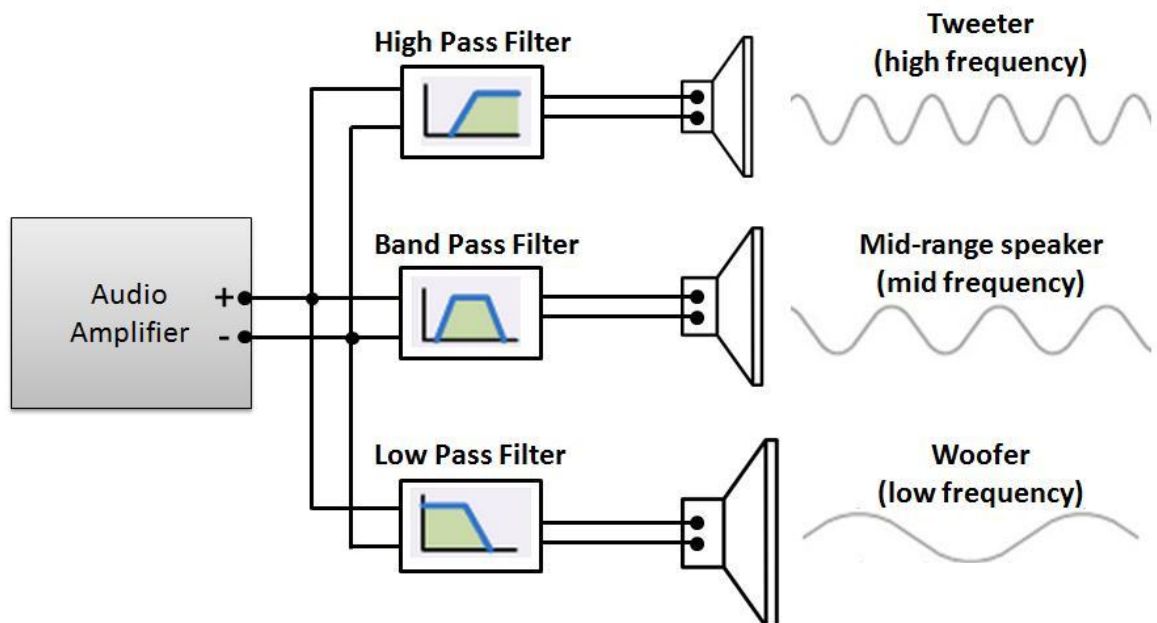
Fig. 1.3 Crossover network diagram

A woofer reproduces low frequency sound, typically below 300 Hz. Since the sound wave at low frequency is longer than at medium and high frequency, the woofer requires a large diameter of a diaphragm and big air cavity for higher excursion of a diaphragm to move more air and thereby, a large enclosure is used. For example, a typical woofer with the frequency range between 20 Hz and 300 Hz uses a diaphragm between 8″ (203mm) and 21″(533mm) in diameter and requires the air cavity relative to its diaphragm size. Furthermore, to accurately reproduce low frequency sound without unwanted resonances (typically from enclosures), those woofer speakers must be solidly constructed and properly braced. Thus woofers are typically heavy and big compared to other types of speakers designed for med-high frequency band.

In spite of enormous research work done over the century, the original construction of a woofer has not been changed since it was invented. However this issue had not appeared great in the past where applications incorporating a loudspeaker system were bulky [4].

Fig. 1.4 Next generation consumer electronics and electric car

However the remarkable advancement of technology over past a few years has brought such issue back to the surface. Figure 1.4 shows some of examples of current products, which identify the trend of the market and industry standard. For instance, as portable devices require smaller, lighter, and more power-efficient components, many devices are being developed to achieve a compact form factor [5] [6]. Traditionally, dynamic cone speakers have been used for mobile phones because of their lower price and great performance. However, they have suffered from a limiting factor of their thickness as mobile devices become more compact. Especially conventional woofers suffer greatly from this issue. Therefore most of consumer electronics that are equipped with loudspeakers do not have ability to produce the high-fidelity sound, that lacks the low frequency sound. This is a major reason why most of users utilise audio accessories such as an earphone and sound docking station in order to listen to the better sound with the enhanced bass. It also applies to the car industry. Since the weight of a car has a direct impact on fuel efficiency, especially for an electric car, weight saving emerges as a major challenge. Considering the fact that a minimum of two woofers (each weighing 1 kg) are used in a low-end compact car, e.g. the Kia *Soul*, the development of a smaller and lighter woofer is an important objective for automotive manufacturers.

1.1.3. New transducer development proposals

Thus far, a number of studies on other type of speakers as alternatives to dynamic cone speakers have been presented [7] [8] [9] [10] [11] [12]. Three examples of those alternatives will be discussed in section 1.2. However they still experience the limitations in the sound reproduction at low frequencies so there are no woofers available in a small and thin size for the applications.

The work conducted by multiple researchers in previous years clearly demonstrates that for development of new technology loudspeaker, the problem with size of the unit against the quality of sound should be addressed.

To try to eliminate these problems, a gel-type audio transducer was developed by SFX Technologies Ltd in 2004. This audio transducer was designed to attach to a range of solid panels that are light and stiff, in order to radiate the sound from its entire surface. This will be discussed in section 1.3.

1.1.4 Aims of the thesis

Each mechanical part of the gel-type audio transducer is coupled by an enclosure called, a gel surround that is made of an elastomer. The gel surround plays very important role in generation of the output driving force and the energy transfer from the transducer to a panel that the transducer is attached, and radiation of the transferred energy in the form of acoustic waves. Although the initially developed gel-type audio transducer has got limitations as mentioned in sections 1.1.2 and 1.3, its unique operating principle by means of the gel surround, showed a possibility that the gel-type audio transducer can deliver a solution required in the market – that is, miniaturisation of a woofer device.

Thus, aims of this thesis are as follows:

• Identification of factors governing the performance of the gel-type audio transducer;

• Investigation of the effect of the gel surround, that is made of different types and hardness of elastomers, on (a) generation of the output driving force, (b) energy transfer from the transducer to a panel that the transducer is attached, and (c) the sound pressure level (SPL) radiated from the panel excited by the transducer;

• Development of prototypes of next-generation gel-type audio transducers with an enhanced acoustic efficiency at especially low frequencies;

• Implementation of the gel-type audio transducer into commercial applications as a miniaturised woofer device.

1.1.5 The structure of the thesis

The current problems of conventional loudspeakers and objectives of this thesis are identified in Chapter 1. Furthermore, the three of the alternative loudspeakers and initial concept of the gel-type audio transducer are described in section 1.2 and 1.3. The literature review in Chapter 2 discusses, identifies and establishes the theoretical backgrounds of the raised problems. That is, the sound energy reproduction in the gel-type audio transducer can be explained with three different coupling mechanisms, between the transducer and gel surround made of an elastomer, the gel surround and panel that the transducer is attached, and the panel and air. Thus the relevant literature review according to those mechanisms is discussed.

Chapter 3 summaries the measurement techniques adopted for the research and fabrication process of a next-generation gel-type audio transducer is also discussed in detail. In Chapter 4, three theoretical problems – effect of the soft elastomer on, 1) generation of the output driving force, 2) mechanical energy transfer from the transducer to a panel that the transducer is attached, and 3) radiation of the transferred

energy in the form of acoustic waves, are studied. The FE analysis is used to simulate the problems, and thereafter, experimental analysis are carried out for verification. In Chapter 5, some of consumer applications incorporating the gel-type audio transducers developed throughout the thesis are demonstrated with the commercial values. Finally the summary of the thesis, main findings, and the future work are discussed in Chapter 6. Figure 1.5 shows the chart of the thesis' structure.
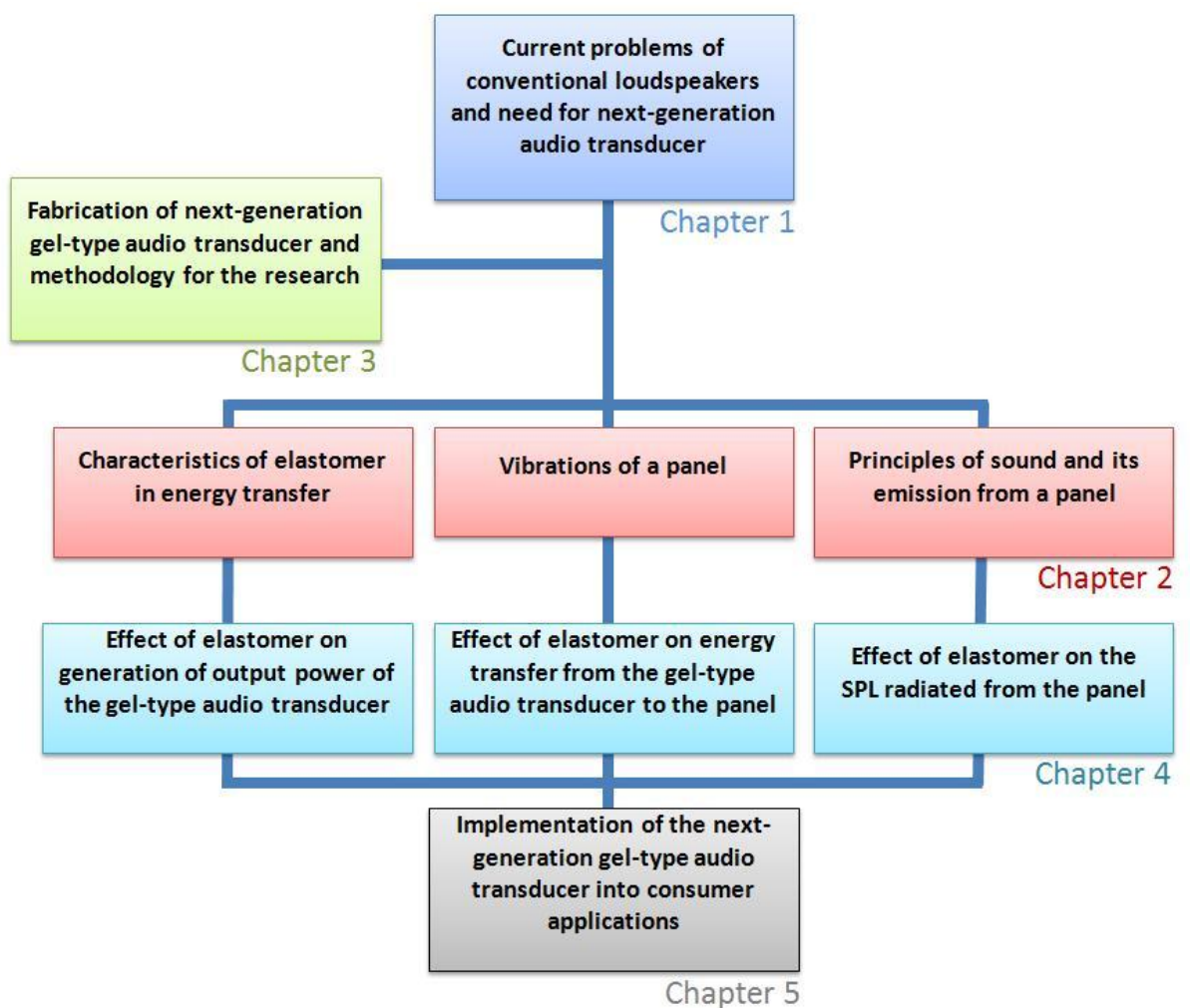
Fig. 1.5 Chart of the thesis' structure

1.2 Examples of alternative loudspeakers and their limitations

In recent years, many alternatives to conventional cone speakers were developed to satisfy the need on the fast-developing consumer electronics. Among them, a DML transducer, electrostatic transducer, and a piezoelectric transducer have received attention as the most remarkable options. Thus characteristics of those three loudspeakers with their advantages and disadvantages were considered in following sections.

1.2.1 Distributed-mode loudspeaker (DML transducer)

A DML is a well-known alternative to standard conventional cone speaker design [13]. It is a transducer attached to a light and rigid flat panel (or plate), as shown in Figure 1.6, that radiates acoustic energy by sustaining bending waves of the panel.
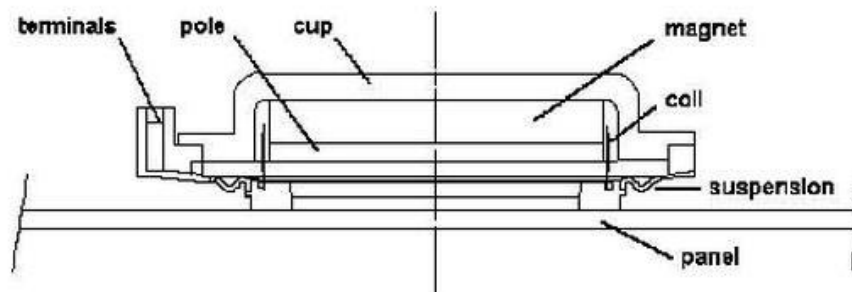
Fig. 1.6 Cross-section of a DML transducer
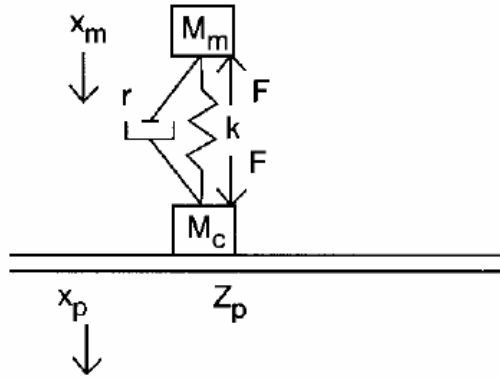
Fig. 1.7 Mechanical element model of a DMLtransducer [13]

Figure 1.7 represents a mechanical element model of the DML transducer. M_m, M_c and Z_p represent the mass of magnet, voice coil assembly, and mechanical impedance of the panel respectively. X_m and X_p, are displacement of the magnet and panel respectively and the suspension of the system is represented with r and k, which are damping and stiffness respectively. Electrical force F_e is applied to the panel and thereby the standing waves are created on the panel. As a result, the bending modes are formed and spaced uniformly across the panel. In general, the DML transducer is placed where there are fewer nodal lines (points of near zero vibration) so the location of the transducers is carefully chosen depending on the nodal map of the panel. The assumption is that the panel has a low mechanical loss and it can suppose that all the energy supplied to the panel will be dissipated by acoustic radiation [14].

In a conventional cone speaker, the directivity of the sound field depends on the path-length between each small element of the diaphragm and the receiving point. At frequencies where radiated wavelengths are small relative to the diaphragm dimensions, interference takes place between the radiation from different regions of the diaphragm,

and this increases in severity off-axis. So the characteristic radiation pattern exhibits strong beaming as shown in Figure 1.8 (a).
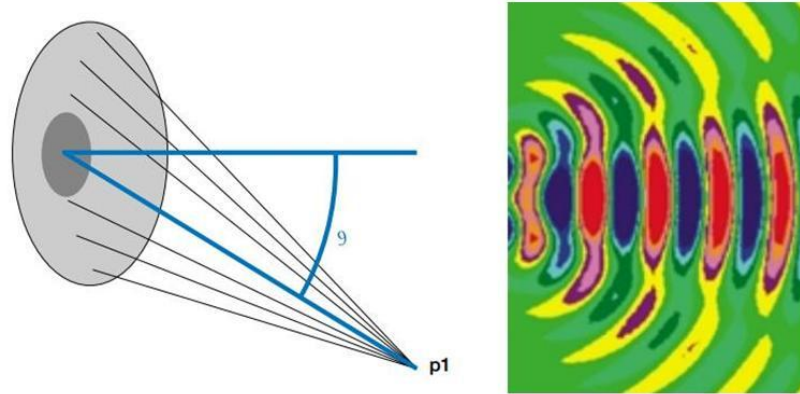
(a) Cone diaphragm of 160 cm^2 (radius = 7.1 cm) surface area
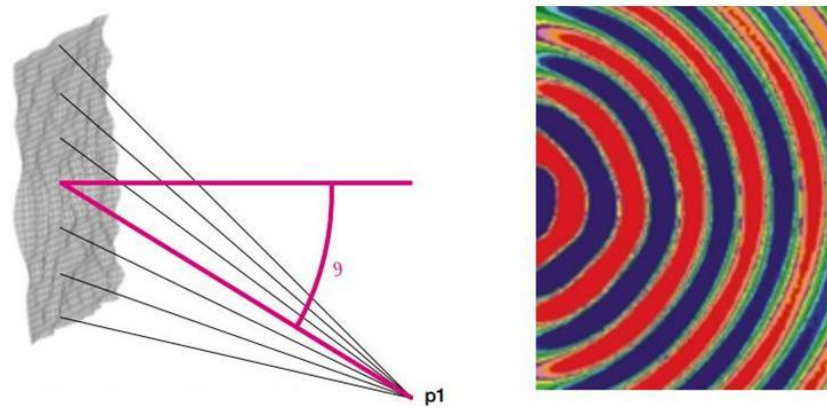
(b) DML panel of 163 cm^2 (12 cm × 13.6 cm) surface area

Fig. 1.8 Sound wave fields (FE simulation) [15]

In a randomly vibrating panel excited by the DML transducer, there exists a random distribution of diaphragm velocity with respect to magnitude and phase. The disparity in path-length between different areas of the diaphragm and the receiving point is also present in a manner similar to the conventional cone speaker at the same frequencies, but because there is no correlation between the source points' output, there can be no global interference. Hence the radiated sound is dispersed evenly in all

directions as presented in Figure 1.8 (b). As a result, the broad directivity of the sound field radiated from the panel at various frequencies can be achieved as shown in Figure 1.9.
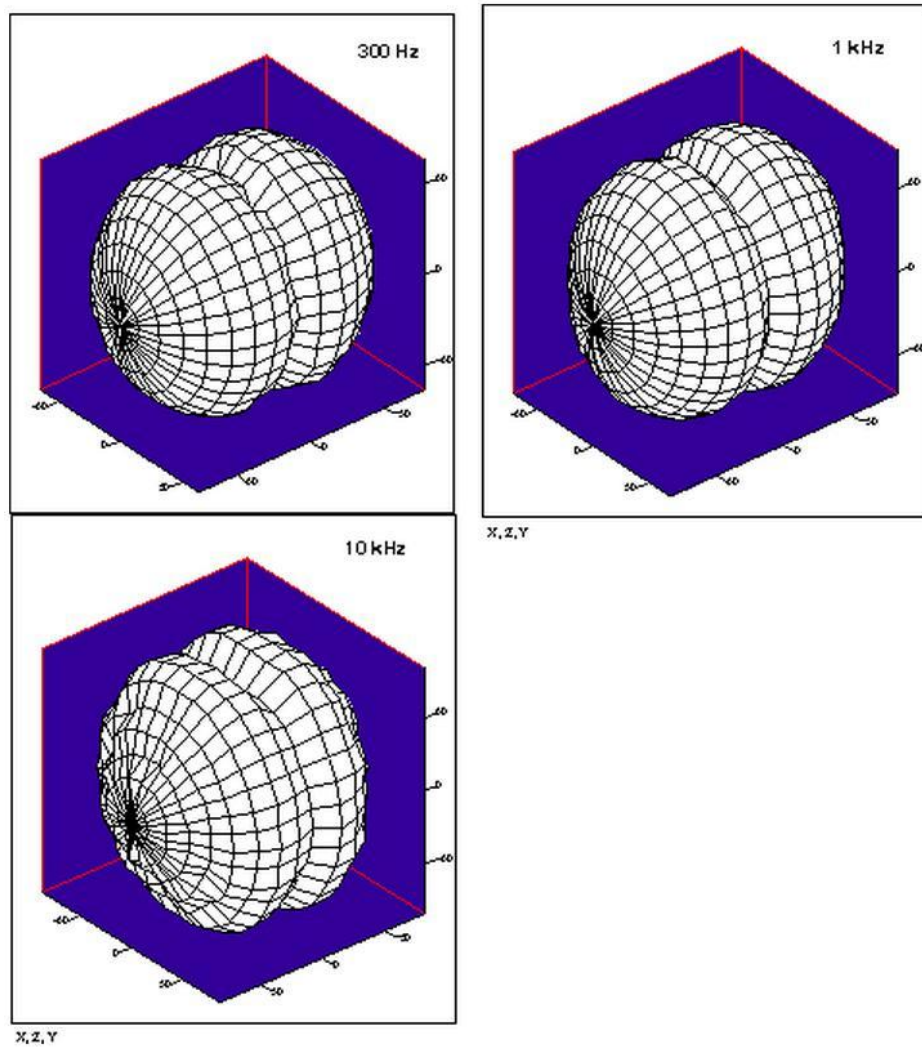
Fig. 1.9 3-D Polar response of a DML panel (0.09 m^2) at various frequencies [14]

The main advantages of a DML transducer are:

a) temporal and spatial diffusivity;

b) radiation over a broad frequency range;

c) a wide directivity spectrum;

d) improved room interaction flat power with no hotspots;

e) insensitivity to room conditions;

f) bi-polar radiation [16] [17].

Despite of many advantages, the main disadvantages of the DML transducer are:

a) poor sensitivity;

b) poor efficiency at low frequency range;

c) a woofer is required to complete a sound system by using the DML transducer;

d) Furthermore, the specific size and type of panels only can be adopted as a DML panel [18].

1.2.2 Electrostatic transducer

An electrostatic transducer consists of a diaphragm made of two pieces of metallic foil (or stator) separated by a sheet of dielectric diaphragm as shown in Figure 1.10 (a). The simplest form of the electrostatic transducer uses an equal signal applied to each plate to produce an audio output resulting from the like-charge attraction and repulsion as described in Figure 1.10 (b).

The force produced by this arrangement varies with the square of the applied voltage and of the distance between the two diaphragms. Audio frequency voltages are superimposed on the polarizing voltage and may either add to or subtract from the polarizing voltage, thus causing the foils to move in accordance with the waveforms of the applied audio frequency voltage [20] [21].
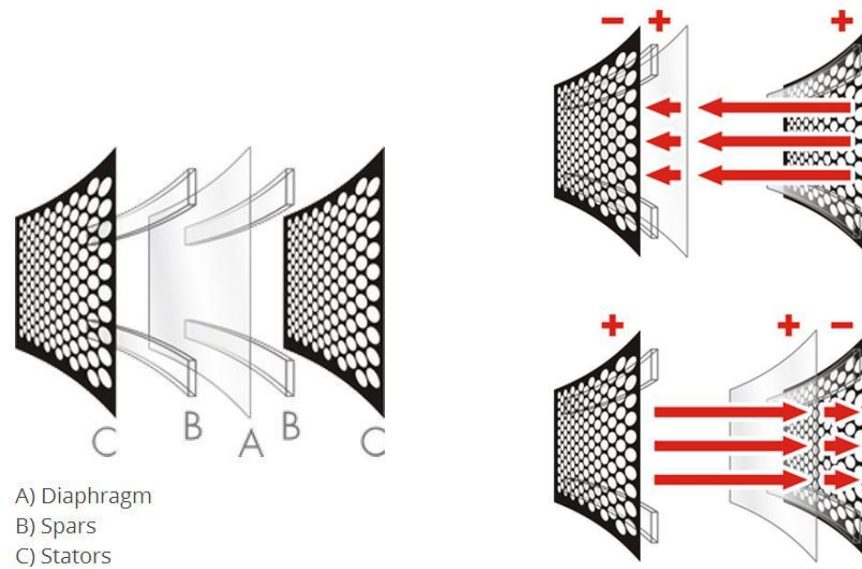
(a) Parts of an electrostatic transducer   (b) Electrostatic forces at work

Fig. 1.10 Electrostatic transducer [19]

It is claimed by the designers of electrostatic transducers that certain basic disadvantages of cone-type loudspeakers, particularly with respect to the propagation of acoustic energy at the high frequencies, are overcome because cone-type loudspeakers driven by a voice coil attached to the centre of the diaphragm fail to act as a piston at the middle and high frequencies. Because of this breakup at the higher frequencies, the voice coil does not control the diaphragm motion, and the result is a lack of correspondence between the electrical input and the acoustic output. Because the electrostatic transducer has a diaphragm that is driven more or less equally at all points on its surface, breakup is said to be eliminated, and harmonic distortion and phase differences are reduced. Because of the design, the diaphragm can be made effectively mass-less when compared to the air load on the diaphragm. This permits the loudspeaker to have good high-frequency and transient response.

An electrostatic transducer is designed to couple directly with the acoustic resistance of air, the mass of the diaphragm is quite small and can be neglected with

little effect on the accuracy of a predictive model. The maximum power output from an electrostatic transducer of a given diaphragm area is determined by the strength of the electrostatic field that can be produced between the diaphragm and the electrodes [22].

Advantages of electrostatic transducers are:

a) levels of distortion one to two orders of magnitude lower than conventional cone drivers in a box;

b) the extremely light weight of the diaphragm which is driven across it's whole surface;

c) exemplary frequency response (both in amplitude and phase) because the principle of generating force and pressure is almost free from resonances unlike the more common electro-dynamic transducer. The sound equipment does not colour or change the sound. Consequently, more details of the sound can be heard by a listener when compared to electro-dynamic speakers, because the radiating surface has much less mass than most other speakers and is therefore far less capable of storing energy to be released later. Electrostatics can also be executed as full-range designs, lacking the usual crossover filters and enclosures that could colour or distort the sound [23].

Many electrostatic speakers are tall and thin designs without an enclosure, and they act as a vertical-dipole line source. This makes for rather different acoustic behaviour in rooms compared to conventional electro-dynamic transducers.

Disadvantages include:

a) lack of bass response due to phase cancellation from a lack of enclosure and the difficult physical challenge of reproducing low frequencies with a vibrating taut film with little excursion amplitude. Phase cancellation can be somewhat compensated for by electronic equalisation (a so-called **shelving circuit** that boosts the region inside the audio band where the generated sound pressure drops because of phase cancellation). Nevertheless *maximum* bass levels cannot be augmented because they are ultimately limited by the membrane's maximum permissible excursion before it comes too close to the high-voltage stators, which may produce electrical arcing and burn holes through it. Thus this relative lack of loud bass is often remedied with a hybrid design using a dynamic loudspeaker - e.g. a woofer, to handle lower frequencies with the electrostatic diaphragm handling middle and high frequencies;

b) directionality of electrostatics can also be a disadvantage. It means the 'sweet spot' where proper stereo imaging can be heard is relatively small, limiting the number of people who can fully enjoy the advantages of the speakers simultaneously;

c) Because of their tendency to attract dust, insects, conductive particles, and moisture, electrostatic speaker diaphragms will gradually deteriorate and need periodic replacement. They also need protection measures to physically isolate their high voltage parts from accidental contact with humans and pets. Cost-effective repair and restoration service is available for virtually every current and discontinued electrostatic loudspeaker model.

1.2.3 Piezoelectric transducer

Piezoelectricity was discovered in the 1880s by French physicists Jacques and Pierre Curie. In a piezoelectric material, a voltage applied to the material will result in a mechanical strain or deflection. The reverse is also true, and piezoelectric elements can be used in microphones. To date, piezoelectric speakers have been developed using various piezoelectric materials such as quartz, $BaTiO_3$, ZnO, $Pb(Zr,Ti)O_3$ (PZT) (lead zirconate titanate), PMN-PT (lead magnesium niobate-lead titanate), PZN-PT (lead zinc niobate-lead titanate), and so on [24] [25] [26]. One of the most widely used types of piezoelectric materials is PZT which has an ABO_3-type complex perovskite structure. PZT piezoelectric materials have higher piezoelectric charge constants and electromechanical coupling coefficients. The piezoelectric charge constants quantify the volume change when a piezoelectric material is subject to an electric field. Thus, a piezoelectric material with a higher piezoelectric charge constant and electromechanical coupling coefficient produces a higher efficiency in a piezoelectric speaker. A piezoelectric material with a higher piezoelectric and electromechanical coefficient can offer a higher output sound pressure in a piezoelectric speaker.
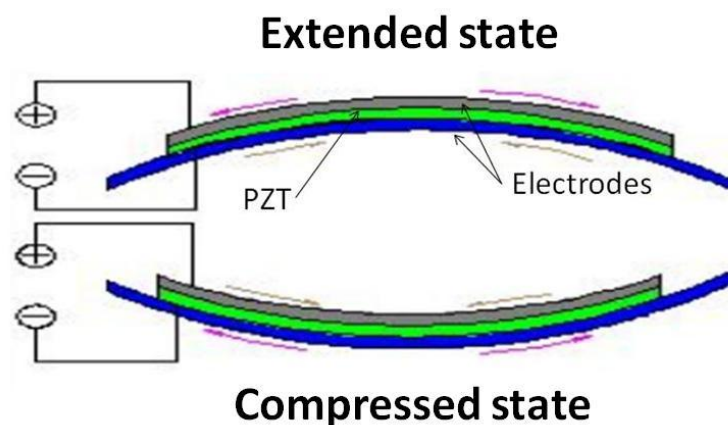
Fig. 1.11 Basic configuration of a piezoelectric speaker

Figure 1.11 shows a basic configuration of a piezoelectric speaker. When electricity is applied to the piezoelectric speaker, it makes the plates attract and repel, generating quick vibration which in turn will project the sound.

Advantages of piezoelectric speakers are:

a) Ultra-thin and ultra-light weight. Figure 1.12 presents the thinnest piezoelectric speaker [0.9 mm] developed by Murata manufacturing Co., Ltd. [27];

b) Rectangular shape of the speaker shape gives flat sound pressure-frequency characteristics. With the conventional round diaphragms, the basic resonance to be determined by a diameter of a disc and its odd-order resonance are used. There occurs an area where the sound pressure declines between different resonant frequencies. A rectangular diaphragm of a piezoelectric speaker generates the oscillation mode resulting from the long and short sides to optimally place as many resonances on the frequency axis as possible. As a result, a flat frequency response can be achieved as shown in Figure 1.13 when compared to a cone-type speaker;
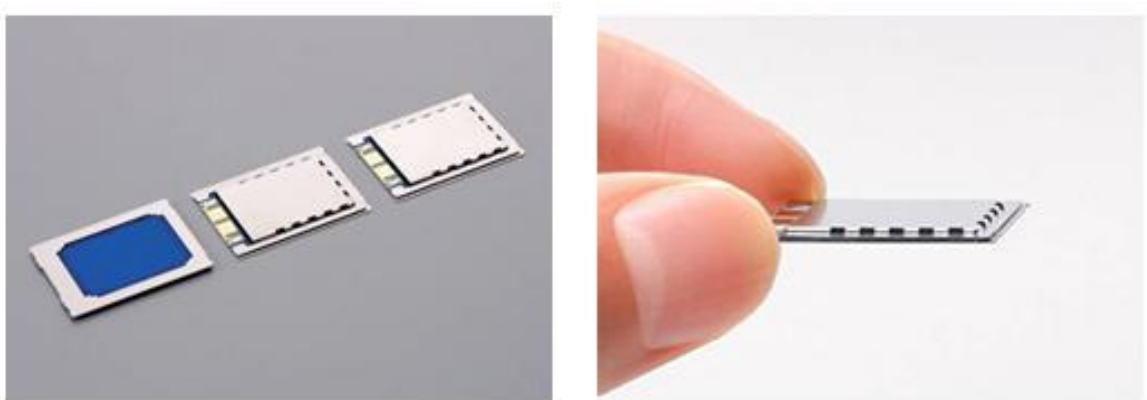
Fig. 1.12 The piezoelectric speaker by Murata manufacturing Co., Ltd [27]
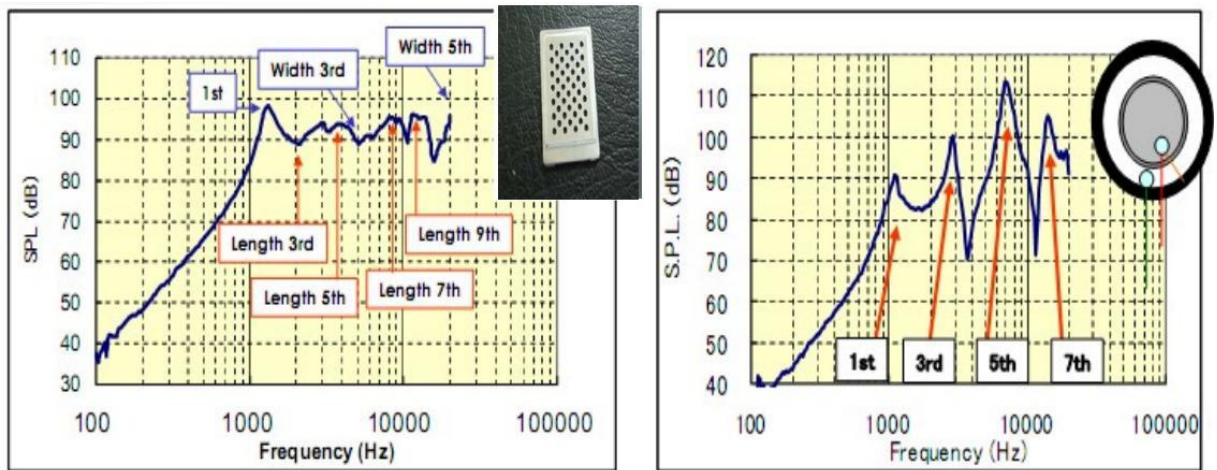
(a) Piezoelectric speaker (rectangular shape)   (b) Conventional speaker (disc shape)

Fig. 1.13 SPL of a piezoelectric speaker and conventional speaker [28]

c) Waterproof performance;

d) There is no magnet used. Therefore it is free from troubles caused by absorbing iron sand and there is no electromagnetic noise that may affect magnetic components.

However disadvantages are:

a) Large drive voltage required. Amplifier circuits that drive piezoelectric speakers have different output-drive requirements than those that drive conventional dynamic speakers. The structure of the piezoelectric speaker requires the amplifier to drive a large capacitive load and supply increasingly larger currents at higher frequencies while maintaining a high output voltage;

b) Restricted low-frequency response as shown in Figure 1.13 (a). The piezoelectric speaker is considered most efficient at producing high SPLs above its self-resonant frequency. But due to high rigidity of the device and little excursion amplitude of the piezoelectric film, its inherent resonant frequency is relatively high. Therefore a

piezoelectric speaker also requires an additional speaker to reinforce low-frequency response.

1.3 A gel-type audio transducer

The gel-type audio transducer was initially developed as a flat panel (or plate) speaker, which is similar to that of the DML transducer, discussed in section 1.2.1. So this transducer also produces high quality sound when placed against a wide range of flat panels.
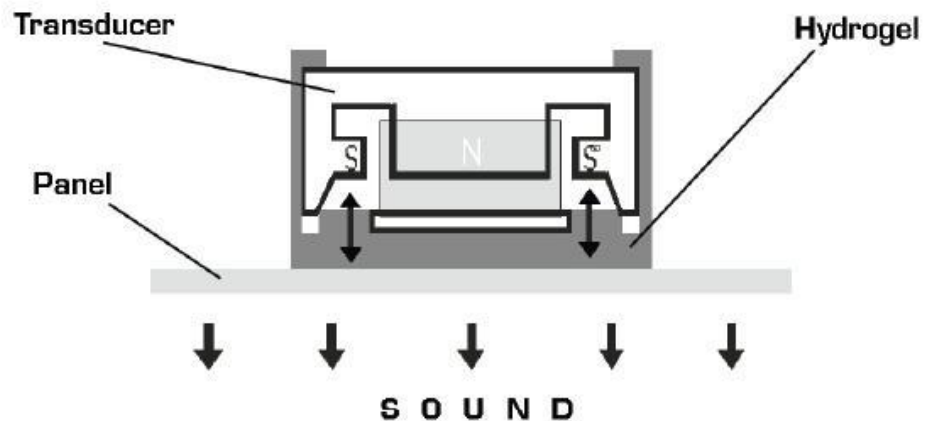
Fig. 1.14 An initial concept of the gel-type audio transducer

The main difference between the gel-type audio transducer and the DML transducer in their mechanical structure is that the hydrogel encloses the mechanical part of the gel-type audio transducer as shown in Figure 1.14, while a spider is used in the DML transducer to connect a voice-coil to a magnetic assembly [29].

In general, spiders are used to connect a rigid basket or a magnetic assembly via a flexible suspension that constrains a voice-coil to move axially through a cylindrical

magnetic gap. It was believed that the hydrogel enclosure adopted in the gel-type audio transducer not only allows a voice-coil to move axially but also this helps couple the panel with the transducer without constraining any parts resulting in the increased efficiency of energy transmission [30].

The panel when excited by the transducer contains the inherent mode frequencies (or natural frequencies) of vibration. At each of these mode frequencies, the structural deformation takes on a very definite pattern. This is called a mode shape (or simply the mode).

An enhanced acoustical performance of the gel-type audio transducer coupled with the panel can be achieved by either (a) the high density and even distribution of the modes on the panel or (b) the high output driving force (causing greater displacements of the panel) of the transducer or combination of both. Characteristics of the modes on the vibrating panel are mainly dominated by materials' properties, size, and boundary conditions of the panel.

Materials' properties of the panel: The bending wave velocity $v_B(\omega)$ as described in equation (2.40) affects the modes of the panel as the bending waves deform the panel. The $v_B(\omega)$ is determined by the ratio of the bending stiffness B to mass per unit area μ (= density ρ × thickness h), and higher $v_B(\omega)$ contributes to higher density of the modes and a more even distribution. As a result, panels with the high B (stiff) and low μ (light) are usually selected as a sound-radiating panel for flat panel speakers such as the DML and gel-type audio transducers, whereas high density and relatively less stiff panels are not desirable.

Size of the panel: The mode frequency of a given mode shape of order (*m,n*) is,

$$f_m = \sqrt{B/\mu}\left[(m\pi/l_x)^2 + (n\pi/l_y)^2\right] \tag{1.1}$$

where l_x and l_y are a length and width of the panel [31].

The mode frequencies of the specific ratios (0.4, 0.6, 0.8, 0.94, 0.99, and 1) of the l_x to the l_y of the panels (the boundary condition is clamped) versus the numbers of the modes created, are presented in Figure 1.15.
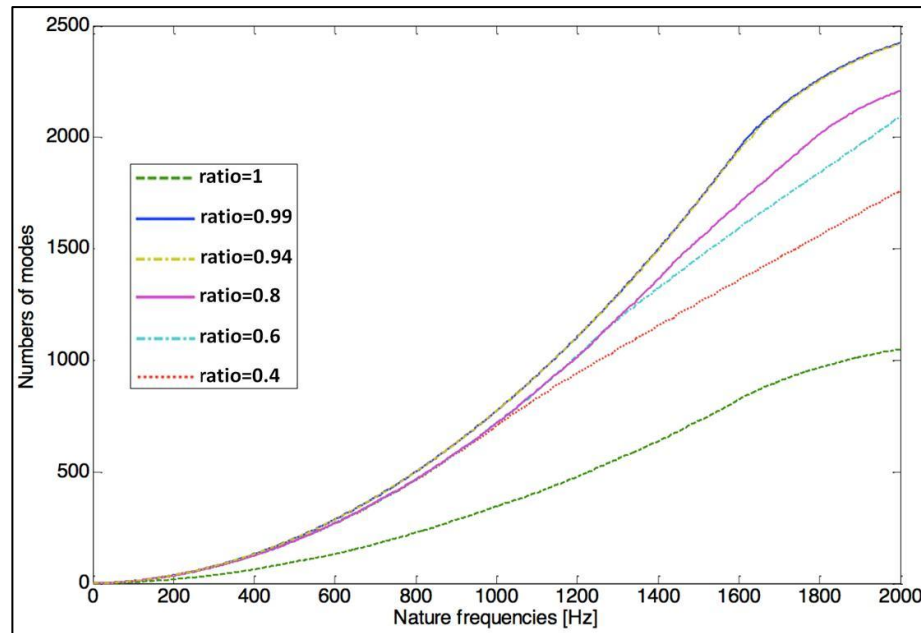
Fig. 1.15 Mode frequencies vs the number of modes on the panel [32]

It is observed that the numbers of modes increase for all the ratios as the mode frequencies increase. But for the higher ratio of the l_x to the l_y of the panel (except the ratio = 1), higher numbers of modes are formed on the panel as the mode frequency rises. The difference in the number of modes for the panels with the ratios in the range 0.4 to 0.99 is not great up to 1,000 Hz. Also it is noticed that the difference in size

between the ratios of 0.99 and 1 is not significant for a small-sized panel but the difference in the numbers of modes on the panel is great. So a rectangular panel with high a ratio of the l_x to the l_y is more suitable as a sound radiator than a square panel (ratio = 1). It is demonstrated in Figure 1.16 that the steel *rectangular* panel (the ratio = 0.66) forms a higher density and even distribution of the modes (visualised by a glass beads across the panel) than the steel *square* panel (ratio = 1) at their mode frequencies.

(a) Mode of the square panel at 340 Hz (left) and 800 Hz (right)
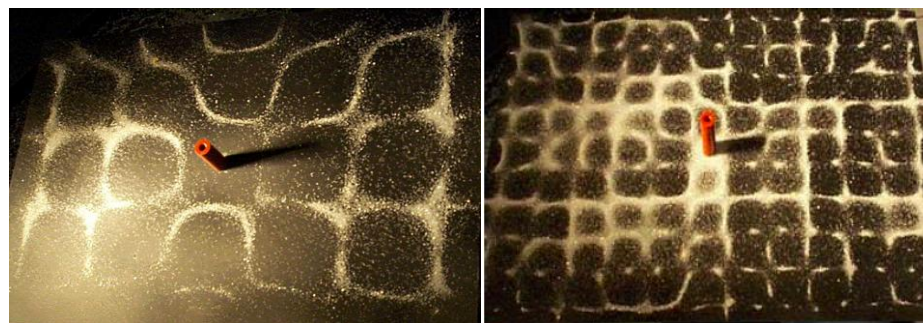
(b) Mode of the rectangular panel at 612 Hz (left) and 1,700 Hz (right)

Fig. 1.16 Modes of the panels (the boundary condition is free) [33]

The ratios of 0.94 and 0.99 presented in Figure 1.15 exhibit almost identical curves over the measured mode frequencies. The ratio of 0.99 is very close to 1 so it is

difficult to produce panels with that ratio due to inaccuracy of cutting. Therefore rectangular panels with the ratio of 0.94 are typically adopted in the production of sound-radiating panels. This ratio is the so-called "golden ratio". However the use of this ratio has been patented by NXT Ltd (a developer of DML transducers) and is therefore protected.

In general, for the bigger panels (under the same ratio of the l_x to the l_y, thickness, and material type), the higher density of the modes can be formed as more areas are engaged in creation of the modes. As a result, the bigger panels radiate higher SPL. Figure 1.17 shows the measured average SPL radiated from various sizes of the ABS panels (boundaries are clamped) excited by the gel-type audio transducer. The ratio of the l_x to the l_y of all panels is 0.7 and the thickness is 2 mm.

Within the low frequency range, as the panel's area increases from 312.5 cm^2 to 5000 cm^2, the average SPL also rises from 72 dB to 84 dB. The average SPL at medium frequency range also shows similar tendency with an increase of 6 dB (from 81 dB to 87 dB) from the smallest to the biggest panel. However within the high frequency range, the effective moving area of the panel becomes localised on the position of the transducer as reported in section 4.3.3.2. So the panel's area does not affect the mode of the panel within this frequency range and thereby, as shown in the graph, the average SPL radiated from the panels is less affected by the panel's area when compared to other frequency ranges. Areas, sizes, and ratio of the l_x to the l_y of the plastic panels (ABS for evaluation of the gel-type audio transducer and, PMMA, PC, and PVC for evaluation of a TV application) and the transducer used for experiments in the thesis, are shown in Table 1.1.

	Area	Size	Ratio of l_x to the l_y
ABS (Acrylonitrile butadiene styrene)	1,344 cm²	420 mm × 320 mm × 2 mm	0.76
PMMA (Poly(methyl methacrylate))	3,444 cm²	757 mm × 455 mm × 2 mm	0.7
PC (polycarbonate)	3,444 cm²	757 mm × 455 mm × 2 mm	0.7
PVC (Polyvinyl chloride)	3,444 cm²	757 mm × 455 mm × 2 mm	0.7
Gel-type audio transducer	15.4 cm²	D44.4 mm × 18 mm	-

Table 1.1 Area, size and ratio of the l_x to the l_y of the plastic panels and gel-type audio transducer
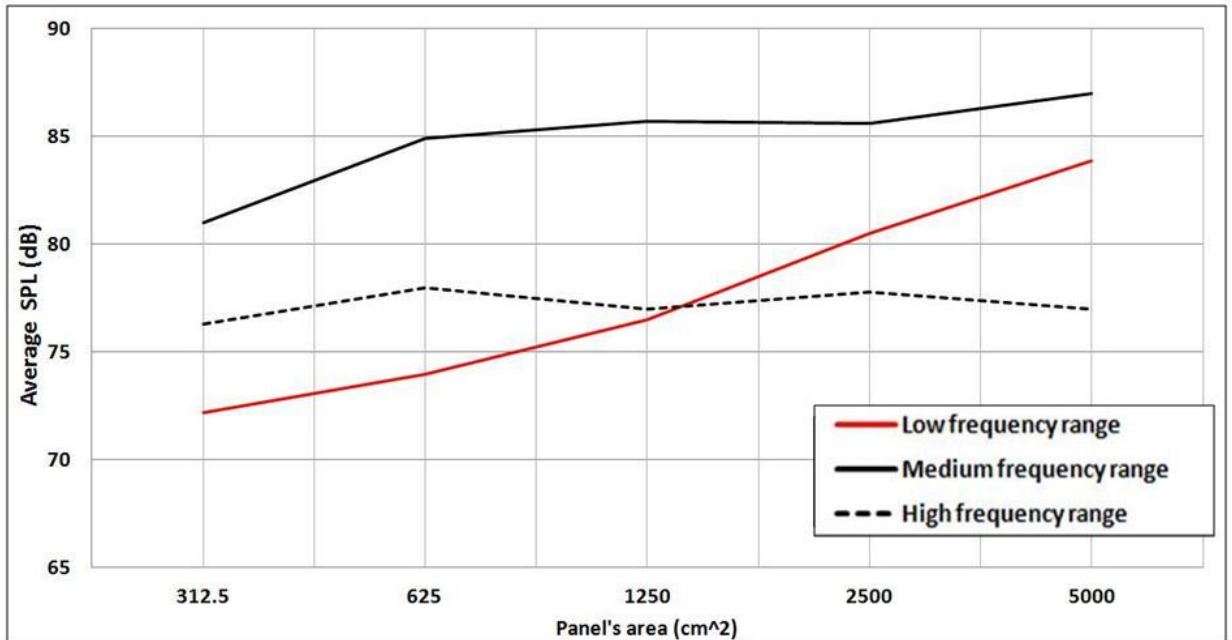
Fig. 1.17 Panel size vs average SPL

Other panel shapes (e.g. circular, elliptical, and polygonal) of panels also impact on the mode shapes and its density, affecting the acoustic performance. For example, as

shown in Figure 1.13, the SPL of the rectangular-shape sound radiator against the circular shape of the diaphragm was compared. Some shapes of panels might be more useful than rectangular panels as a sound radiator but due to lack of relevant references and testing equipment, a rectangular panel only will be considered in this thesis.

Boundary conditions of the panel: The boundary conditions of the panel affect the modes on the panel. The boundary conditions, that are usually considered, are clamped, free, and simply supported. Figure 1.18 shows the simulated result of the SPL of the panel excited by the gel-type audio transducer (R 22 mm $\times$ 18 mm) with these boundary conditions at frequencies in the range 30 Hz to 500 Hz. The size of the panel used for this simulation is 210 mm $\times$ 160 mm $\times$ 2 mm (ratio of the l_x to the l_y is 0.76) and the panel is made of an ABS (Acrylonitrile butadiene styrene) material. The transducer was attached to the centre of the panel.
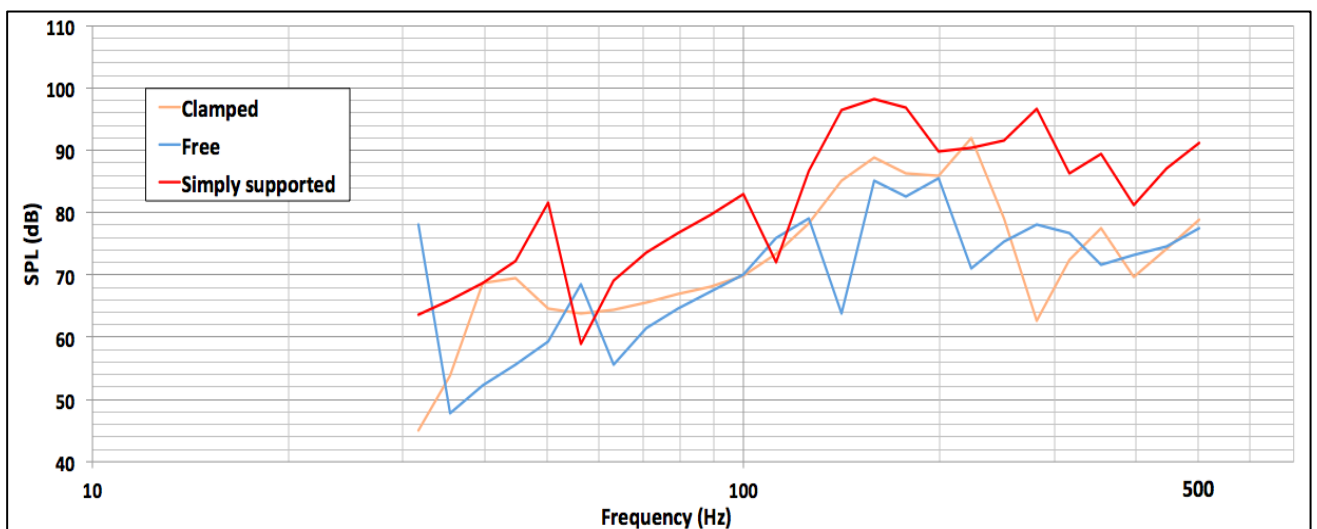
Fig. 1.18 Simulated result of the SPL with the different boundary conditions

According to the Fig. 1.18, the simply supported panel shows greater SPL than the free and clamped panels over the measured frequency range. The free and clamped

panels exhibit the similar shape of the SPL curves although there are a few different peaks. So a panel with a simply supported boundary condition seems ideal for a sound radiator at low frequencies.

However this boundary condition is not practical in the real world and this can also cause a measurement error due to the vibrations occurring at the boundaries of the panel. Furthermore most of the reference SPL data of conventional flat panel speakers such as DML transducers were measured with the clamped boundary condition. Thus, the boundary condition of the panel adopted in this thesis will be the "clamped" condition.

For the experiments described in Chapter 4, a thin ABS plastic panel that is relatively stiff, light, easy to handle and commercially available, was used. As presented in Table 1.1, the length and width of the ABS panel is 420 mm × 320 mm and the ratio of the l_x to the l_y of the panel is 0.76. This ratio was chosen because the use of the golden ratio (0.94) has been restricted by NXT Ltd and also there is not much difference in the number of modes created between 0.4 and 0.99 of the panel ratio at frequencies up to 1,000 Hz according to Figure 1.15.

Furthermore, due to the small size of the anechoic chamber built for this research, use of a large size of panel was not possible. As a focus of the current research is the development of next-generation gel-type audio transducers with an enhanced output driving force at low frequencies, the experiments will be carried out on the ABS panel referred to in the previous paragraph. However, other types of plastic panels (PMMA, PC, and PVC) were used for evaluation of the TV application incorporating the gel-type audio transducers and the results are reported in Chapter 5.
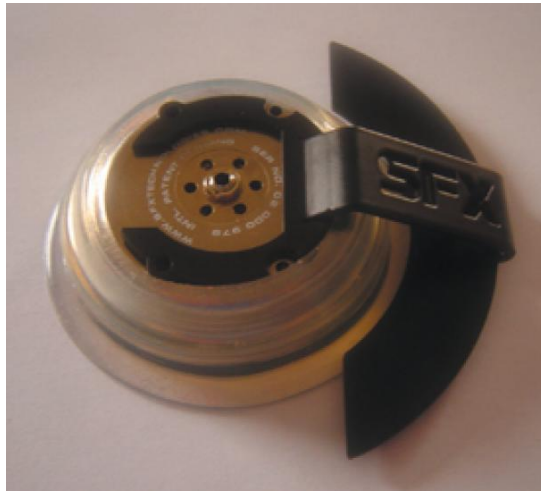
Fig. 1.19 Gel-type audio transducer with the hydrogel enclosure

Figure 1.19 and 1.20 show the gel-type audio transducer with the hydrogel enclosure and the measured SPL at 25 cm/1 W. The size of the testing panel is 420 × 320 × 2 mm.
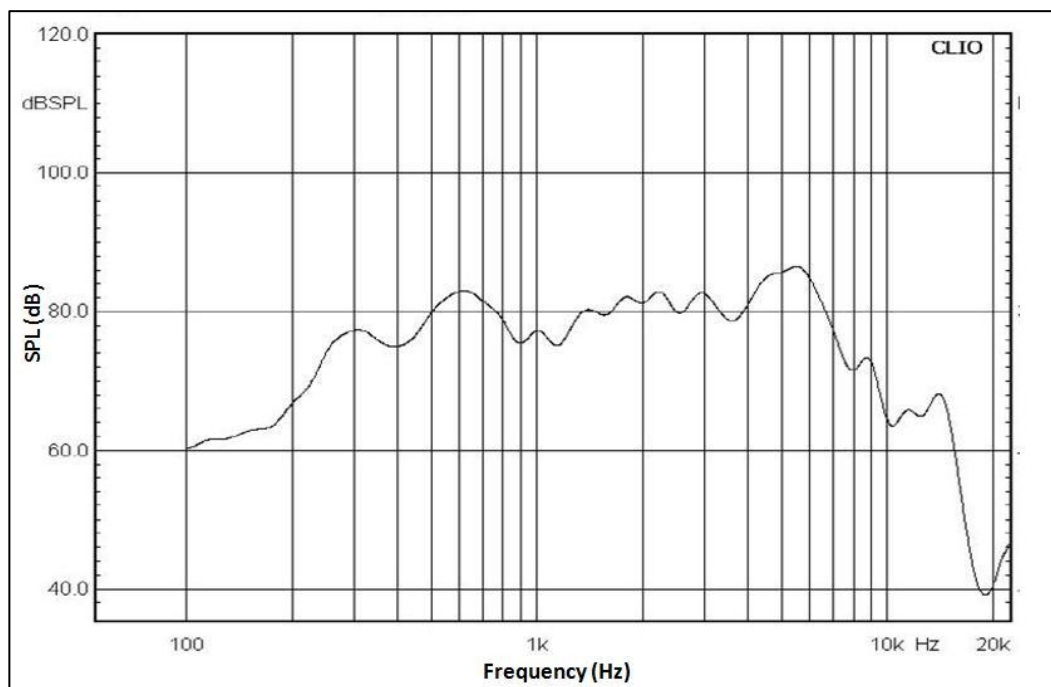
Fig. 1.20 SPL of the gel-type audio transducer with the hydrogel enclosure

The measured SPL shows a flat frequency response at frequencies in the range 300 Hz to 6000 Hz. However the transducer still has a poor frequency response at low frequencies below 300 Hz (the SPL drops down from 76 dB at 300 Hz to 60 dB at 100 Hz) in a similar manner to the alternative audio transducers that were considered in previous sections.

Main advantages of the transducer are quite similar to the DML transducer's. But easy installation process and low manufacturing cost, due to a simple construction of the transducer, make the gel-type audio transducer more attractive in the market but this transducer is still not distinguished from other speakers due to a poor performance at low frequency range.

1.4 Conclusions

Due to the remarkable advancement of technology in recent years, lighter, thinner and more compact loudspeaker design for woofers have been greatly required. Thus enormous research work were conducted in previous years and three promising examples of alternatives to dynamic cone speakers, which are the DML transducer, electrostatic transducer, and the piezoelectric transducer, were discussed in section 1.2. However these audio transducers also suffer from poor efficiency at low frequency range so they still require a standard woofer (big and heavy) to complete a sound system.

The concept of the gel-type audio transducer was proposed by SFX Technologies Ltd in 2004. This transducer is similar to that of the DML transducer and

it was briefly described in section 1.3. Although this transducer is not distinguished from other audio transducers, its unique operating principle showed a possibility to deliver a solution required in the market – that is, miniaturization of a woofer device.

In this thesis, therefore, investigation and development of next-generation gel-type audio transducers will be carried out, in order to overcome the current problems for loudspeaker design, and thereby, satisfy the market's need. Specific aims of the thesis were discussed in section 1.1.4.

As explained in section 1.1.5, following chapters will start with the literature review (Chapter 2), and thereafter, with the methodology adopted for the study (Chapter 3), discuss theoretical problems of the gel-type audio transducer including experiments and simulations (Chapter 4). Applications incorporating the gel-type audio transducer developed throughout the research will be presented with the commercial values (Chapter 5). Summary of the thesis including the main findings and future work will be presented in the end (Chapter 6).

CHAPTER 2 – LITERATURE REVIEW

2.1 Introduction

The mechanism of the sound reproduction of the gel-type audio transducer can be explained with three combined mechanisms - (a) generation of an output driving force of the transducer by means of the gel surround, (b) vibration of a panel (or plate) and (c) sound radiation from the panel. To understand background knowledge of these mechanisms, the review of following three sections will be discussed: "Characteristics of elastomers in energy transmission", "vibration of plates" and "principles of sound and its emission from the plates".

2.2 Characteristics of an elastomer in energy transmission

2.2.1 Background of an elastomer

An elastomer is defined by the American Society for Testing and Materials (ASTM) as "a material that, at room temperature, can be stretched repeatedly to at least twice its original length, and, upon immediate release of the stretch, will return with force to its approximate original length". Such large deformability with complete recoverability requires three molecular characteristics; (i) the material must consist of polymeric chains, (ii) the chains must have a high degree of flexibility and mobility, and (iii) the chains must be joined into a network structure [34] [35].

Elastomers have viscoelastic properties and some phenomena in viscoelastic materials are:

a. if the stress is held constant, the strain increases with time (creep);

b. if the strain is held constant, the stress decreases with time (relaxation);

c. the effective stiffness depends on the rate of application of the load;

d. if cyclic loading is applied, hysteresis (a phase lag) occurs, leading to a dissipation of mechanical energy;

e. acoustic waves experience attenuation;

f. rebound of an object following an impact is less than 100 percent; and

g. during rolling, frictional resistance occurs.

Elastomers consist of many simple molecules that are repeating monomer units. Each of the monomers is usually made of carbon, hydrogen and silicon. Those monomers are cross-linked each other during the vulcanising process so the molecular structure of an elastomer has long three-dimensional chains. In a general molecular structure, a backbone chain that links other monomers is the series of covalently bonded atoms and it is usually hydrocarbon atom. But atoms such as the oxygen, nitrogen, sulphur and silicon can take place of the carbon atom within the backbone chain [36].

2.2.2 Effect of chemical structures on mechanical properties

The Young's modulus E and shear modulus G which are the important mechanical properties are represented by the equation (2.1):

$$E = t_s/\varepsilon \cong 3N_c k_f T = 3\text{G} \tag{2.1}$$

where t_s is the true tensile stress per unit strained cross-sectional area, and ε is the strain. And N_c is the number of network chains per unit volume and k_f is the force constant applied on a network chain. T is absolute temperature. Both E and G are proportional to the N_c, K_f, and T.

Also properties such as elongation and resilience are closely related to a bond angle, length of bonded atoms, type of cross-linking mechanism, and the N_c [37]. For example, each atom is bonded one another at specific angle (e.g. polyethylene's bond is at $109°$ to the next). This bond angle causes the chain to twist and rotate into a variety of three-dimensional configurations, resulting in a resilient property. These movements have been studied by Heijboer [38].

Some elastomers such as natural rubber, Neoprene, and butyl rubber have high regularity in their backbone structure. They will align and crystallise when a strain is applied, with resulting high tensile properties. Other elastomers do not strain-crystallise and require the addition of reinforcing fillers to obtain adequate tensile strength [39]. The mechanism of the reinforcement is believed to be both chemical and physical in nature [40]. For example, Carbon black is the most widely used material for reinforcement. Its primary properties are surface area and structure. Smaller particle-size blacks having a higher surface area give a greater reinforcing effect. Increased surface area gives increased tensile, modulus, hardness, abrasion resistance, tear strength, electrical conductivity, decreased resilience, and flex-fatigue life. The same effects are also found with increased levels of carbon black, but peak values occur at different levels. Structure refers to the high-temperature fusing together of particles into

grape-like aggregates during manufacture. Increased structure will increase modulus, hardness, and electrical conductivity but it will have little effect on tensile, abrasion resistance, and tear strength.

2.2.3 Static physical properties of an elastomer

An elastomer has properties that are drastically different from other engineering materials. Consequently, it has physical testing procedures that are unique. Following sub-headings describe static physical properties of an elastomer with the testing conditions.

Hardness

Hardness is defined as the resistance to indentation. A durometer is an instrument that measures the penetration of a stress-loaded metal sphere into an elastomeric sample. Hardness measurement in an elastomer is expressed in Shore 00, Shore A or Shore D units according to ASTM test procedures. Because of the viscoelastic nature of an elastomer, a durometer reading reaches a maximum value as soon as the metal sphere reaches maximum penetration into the specimen and then decreases the next 5 to 15 sec. Hand-held spring-loaded durometers are commonly used but are very subject to operator error. Bench-top dead-weight-loaded instruments reduce the error to a minimum.

Stress – strain

An elastomer is an incompressible material that deflects by changing shape rather than changing volume. It has a Poisson's ratio of approximately 0.5. At very low strains the ratio of the resulting stress to the applied strain is a constant. This value is the

same whether the strain is applied in tension or compression. Hooke's law is therefore valid within this proportionality limit. However, as the strain increases, the linearity ceases, and Hooke's law is no longer applicable. Also the compression, shear, torsion, buckling and tension stresses are then different.

The stress-strain properties of an elastomer are usually measured under tension as per ASTM procedures. Either moulded rings or die-cut "dumbbell"-shaped specimens are used in testing. Stress measurements are made at a specified percentage of elongation and reported as *modulus* values. For example, 300 percent modulus is defined as the stress per unit cross- sectional area (in psi or MPa units) at an elongation of 300 percent. Also measured are the stress at failure (tensile) and maximum percentage elongation.

The stiffness (spring rate) is the ratio of stress to strain expressed in newtons per millimetre. It is dependent not only on an elastomer's modulus but also on the shape of the specimen or part being tested.

Shape factor

When a load is applied to an elastomer, the elastomer deflects or undergoes a change in shape and the shape of the elastomer affect the way the elastomer deforms as an elastomer is an incompressible material. For example, there are two blocks cut from the same piece of an elastomer. One is a cylinder shape and the other is a block of the same height and cross-sectional area but rectangular in shape. If equal weights are placed on the blocks, subjecting them to the same compressive stress, the rectangular block will deflect more than the cylinder. Since the blocks will not change in volume, the reduction in height is caused by the freedom of the sides to bulge. So the rectangular block deflects more than the cylindrical one because the sides of the rectangular block

provide a greater area free to bulge. The designer of elastomeric parts allows for this behaviour by using a concept called *shape factor*. Shape factor describes the role of the shape in determining how a part with parallel load faces will behave under compressive forces. Thus if the elastomeric part does not deflect enough, the shape factor can be reduced by increasing the thickness of the elastomeric part.

The shape factor is given by,

$$\text{Shape factor} = Area\ under\ Load/Area\ free\ to\ bulge \qquad (2.2).$$
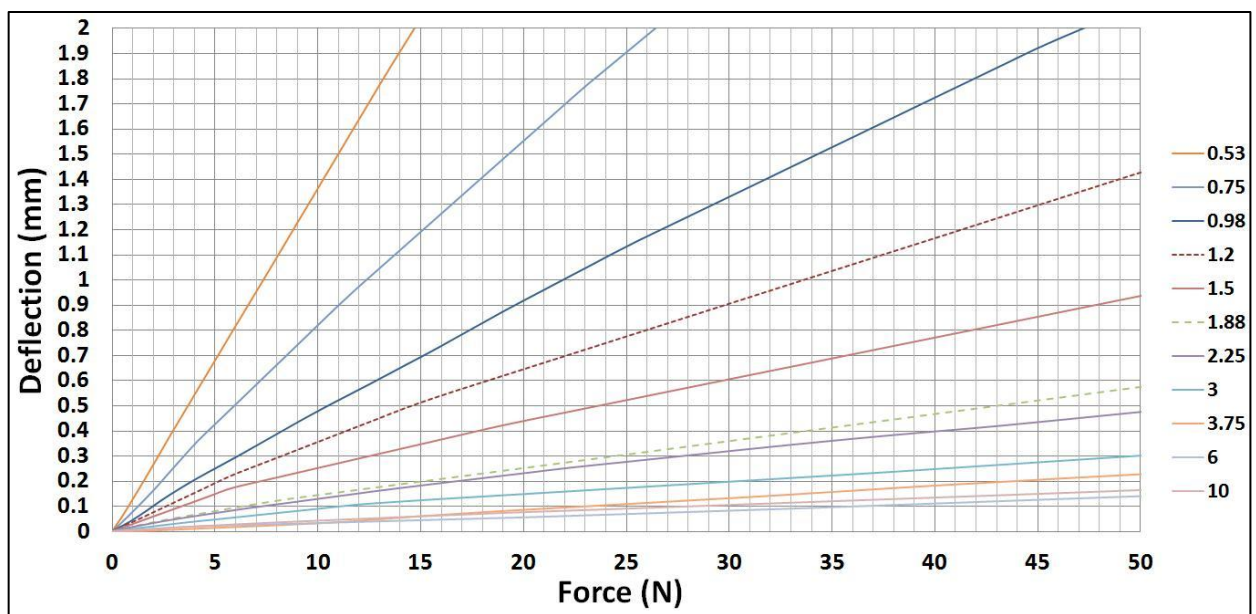
Fig. 2.1 Force vs deflection as a function of the shape factor for the 35 Shore 00 silicone sample

Figure 2.1 shows deflection curves of the 11 cylindrical samples made of 35 Shore 00 RTV silicone elastomer with various shape factors from 0.53 to 10. These curves reveal that the samples made of the same hardness of the silicone elastomer

exhibits different values of deflection according to the shape factor. The lower shape factor the sample has, the greater deflection is obtained.

Tear

Vibration isolators and dampers that are subjected to cyclical loads frequently fail due to a fracturing of an elastomeric component. A fracture may initiate in an area where stress concentration is at a maximum. After initiation, the fracture increases in size and progresses into a tearing action. Tear properties are therefore important in some applications. Tensile tests are run on dumbbell-shaped samples containing no flaws. The stress is therefore evenly distributed across the sample. Tear-testing procedures concentrate the stress in one area, either through sample design or by cutting a nick in the sample. The peak force and sample thickness are recorded. Tear values are reported in units of pounds per inch or kilo-newtons per meter.

Mechanical properties and temperature

Mechanical properties of the elastomers are affected significantly by temperature. Typically elastomers become harder, stiffer, and less resilient with decreasing temperature (Resilience in this context is the ratio of energy input to energy output in a rapid full recovery of a deformed specimen). These changes are brought about by a reduction in the "free volume" between neighbouring molecules and a subsequent reduction in the mobility of the elastomer molecules due to low temperature. As might be expected, when the temperature rises so "free volume" increases. Thus properties of elastomers can be notably different when measured at a higher temperature (compared to room temperature for example), even if no aging has occurred. A case in point is butyl rubber, which exhibits limited resilience at room temperature but has

significantly higher resilience at 80 ℃. The tensile strength of many elastomers drops as soon as a higher temperature is reached. A cured NR (natural rubber) compound has a tensile strength of 30 MPa at 23 ℃, reducing to 23 MPa at 80 ℃, and 5 MPa at 140 ℃ [41].

Visco-elastic properties of elastomers such as the storage and loss modulus, and the loss tangent, also change with temperature variations. This will be discussed in section 2.2.4.

Some vibration isolators and dampers function in high temperature environments (e.g. 180 ℃). The elastomeric compounds used in these applications must therefore be resistant to high temperature degradation. This is particularly important as degradation accelerates with temperature. The stability at high temperature is related to the chemical structure of the elastomer and the chemical cross-linking bonds are formed during vulcanization. Elastomers containing no unsaturation (chemical double-bonds) in the backbone have better high-temperature properties. Elastomers containing EPDM (ethylene propylene diene monomer), for example, have better high-temperature resistance than ones containing natural rubber or SBR (styrene-butadiene rubber). In a sulphur cure, mono or disulfide cross-linking bonds have better high-temperature stability than polysulfide bonds. Cure system modifications are therefore used to improve high temperature stability. The high temperature resistance of elastomers is determined by measuring the percentage of change in tensile strength, tensile stress at a given elongation, and ultimate elongation after aging in a high temperature oven as per ASTM procedure.

2.2.4 Dynamic physical properties of an elastomer

One of the unique characteristics of viscoelastic materials is that their properties are influenced by many parameters. They can include: frequency, temperature, dynamic strain rate, static pre-load, time effects such as creep and relaxation, aging, and other irreversible effects. Most important of these include temperature and frequency effects.

Viscoelasticity

Viscoelastic materials like elastomers have the properties of both viscous and elastic properties. These viscoelastic properties allow an elastomer to maintain a constant shape after deformation, while simultaneously absorbing mechanical energy. The viscosity increases with reduced temperature. The elasticity follows Hooke's law and increases with increased strain, while the viscosity follows Newton's law and increases with increased strain rate. Therefore, when applying a strain, the resulting stress will increase with increasing strain rate.

Springs or dashpots are frequently used to make theoretical models which illustrate the interaction of the elastic and viscous components of an elastomer [42]. Connecting a spring and damper in series yields a model of a Maxwell material while connecting a spring and damper in parallel yields a Kelvin-Voigt material. The Maxwell model is good at predicting the stress relaxation while the Kelvin-Voigt model is good at predicting creep. The most accurate model is the Standard Linear Solid model which combines the characteristics of both the Maxwell and Voigt models [43].

Effect of temperature

Viscoelastic materials exist in various unique states or "phases" over the broad temperature and frequency ranges in which they are used. These regions are typically

referred to as the Glassy, Transition, Rubbery, and the Flow Regions as shown in Figure 2.2. Elastomers behave differently based on which region they exist in for a specific application. In the glassy region, the polymer chains are rigidly ordered and crystalline in nature, possessing glass-like behaviour. Storage modulus is at its highest for the material in this region, and damping levels are typically low.
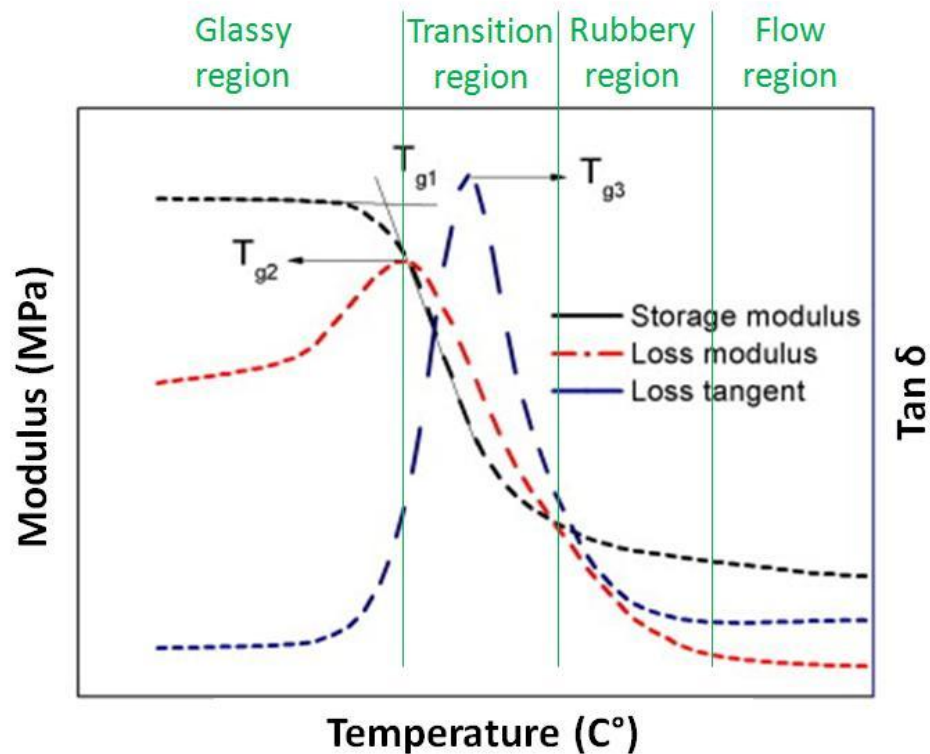
Fig. 2.2 Variation of complex modulus with temperature for a typical elastomer [44]

The glass transition temperature T_g of an elastomer refers to the elbow of the storage modulus curve at the edge of the glassy region as it enters into the transition region. T_g also defines the peak of the loss modulus E'' curve. The transition region is so named because the material is transitioning from the glassy to the rubbery region. In this area, the viscoelastic material goes through its most rapid rate of change in stiffness and possesses its highest level of damping performance. In this region, the long molecular chains of the polymer are in a semi-rigid and semi-flow state, and are able to rub against

adjacent chains. These frictional effects result in the mechanical damping characteristic of viscoelastic materials. In the rubbery region, the material reaches a lower plateau in stiffness. Damping is at a lower, but reasonable level. An elastomer selected to exist in this region is ideally suited for such devices as isolators or tuned mass dampers because the modulus varies only slightly with changes in temperature and frequency [45].

Creep

Creep strain is time-dependent elongation due to the viscoelastic property of elastomers. So the total strain is expressed as:

$$\hat{\varepsilon} = \varepsilon_e + \varepsilon_c \tag{2.3}$$

where ε_e is the elastic strain and ε_c is the creep strain. These strains are proportional to the applied stress.

The *J(t)* is creep compliance and it can be written as,

$$J(t) = \varepsilon_c(t)/\sigma \tag{2.4}$$

where σ is a constant stress.

$J(t)$ provides a means to quantify the capacity of a material to flow in response to a sudden applied stress [46].

Figure 2.3 and 2.4 schematically illustrates the linear viscoelastic creep response at various applied stresses. The doubling of the instantaneous and constant applied

stress σ exactly doubles the strain $\varepsilon(t)$ for any time t during creep for linear viscoelastic materials as presented in Figure 2.3.
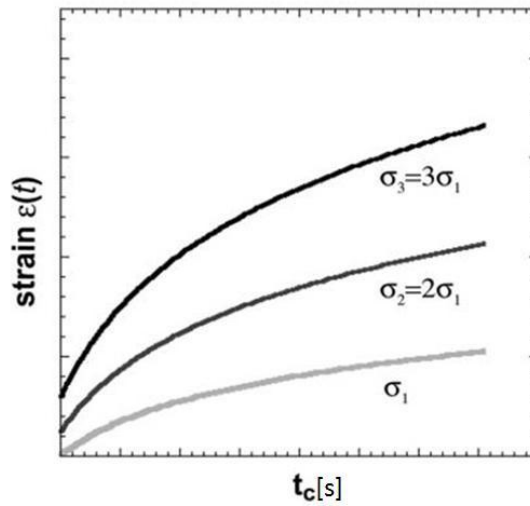
Fig. 2.3 Ideal linear viscoelastic behaviour is illustrated as strain, ε as a function of time during creep, t_c for three instantaneous and constant levels of applied stress, σ [47]

It is well-established as shown in Figure 2.4 that the $J(t)$ for a linear viscoelastic material is invariant with applied stress due to the linear relationship between stress and strain at any time point for such materials.
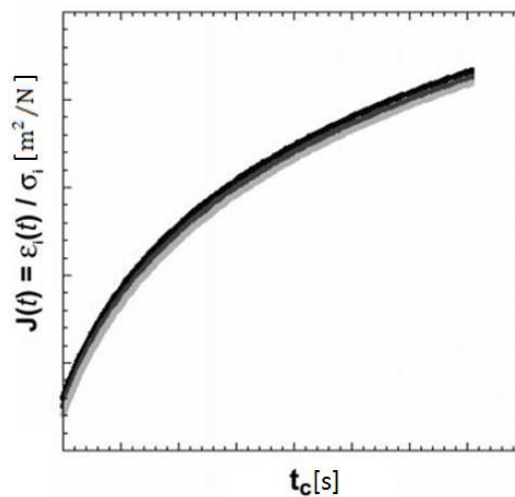
Fig. 2.4 Creep compliance $J(t)$ for a linear viscoelastic material is characteristic of that material and independent of σ [47]

However, polymers including elastomers generally exhibit linear viscoelastic property at low stresses such as that the corresponding strain is below $\sim 0.5 \times 10^{-2}$. At higher stress levels, the material will assume nonlinear viscoelastic behaviour which will not obey the linear relation between stress and strain.

Stress relaxation

The classical theory of elasticity describes the elastic solid where stress is proportional to strain in small deformations and the response of stress is independent of the strain rate. However elastomers exhibit the properties of viscous fluid, for which the response of stress is dependent upon the strain rate. The strain lags the stress by the phase angle, δ that needs the time lags for the molecular rearrangements. These properties are studied by the DMA (dynamic mechanical analysis) where a sinusoidal force (stress, $\bar{\sigma}$) is applied to a specimen material and the resulting displacement (strain, $\bar{\varepsilon}$) is measured [48].

$$\bar{\sigma} = \sigma_0 \, exp \, (i\omega t) \tag{2.5}$$

$$\bar{\varepsilon} = \varepsilon_0 \, exp \, (i\omega t - \delta) \tag{2.6}$$

where σ_0 is the stress amplitude. ε_0 is the strain amplitude and ω is the angular frequency. δ is the phase angle.

The stress-strain relationship is defined as equation (2.7).

$$\bar{\sigma} = (E' + iE'')\,\bar{\varepsilon} \tag{2.7}$$

where E' is the elastic modulus and E'' is the loss modulus of the system during one cycle. i is the imaginary unit.

Such moduli are defined as follows:

$$E' = \frac{\sigma_0}{\varepsilon_0} \cos\delta, \qquad E'' = \frac{\sigma_0}{\varepsilon_0} \sin\delta \tag{2.8}$$

Therefore the complex modulus E^* is $E^* = E' + iE''$. From a graph of the sinusoidal strain and resultant stress as a function of time or angle, measured by the DMA shown in Figure 2.5, the E^* can be calculated by dividing the resultant maximum stress amplitude by the maximum imposed strain amplitude. Also both the maximum elastic stress amplitude and the maximum viscous stress amplitude are calculated from the measured stress amplitude and the phase angle δ using simple trigonometric functions. Dividing these stress values by the strain gives the E' and E''.

Expressions for the stored modulus E' and loss modulus E'' can be rearranged by using the stiffness k and compliance C in the Kelvin model.

$$E' = \frac{K\sqrt{\pi}}{2\sqrt{A}}, \qquad E'' = \frac{\omega C\sqrt{\pi}}{2\sqrt{A}} \tag{2.9}$$

where A is the cross-sectional area. Equation (2.9) shows that the elastic modulus and loss modulus are related to the stiffness and compliance respectively in the system.

The phase angle δ in equation (2.8) is given as:

$$tan\,\delta = \frac{E''}{E'} \qquad\qquad (2.10)$$

The $tan\,\delta$ is the ratio of the loss modulus to storage modulus during one cycle vibration of an elastomer [50]. δ should be between 0° and 90°. If δ approaches 0°, a material approaches a purely elastic behaviour. As δ approaches 90°, the material approaches a purely viscous behaviour [51]. The value of $tan\,\delta$ is a measurement of damping or hysteresis.
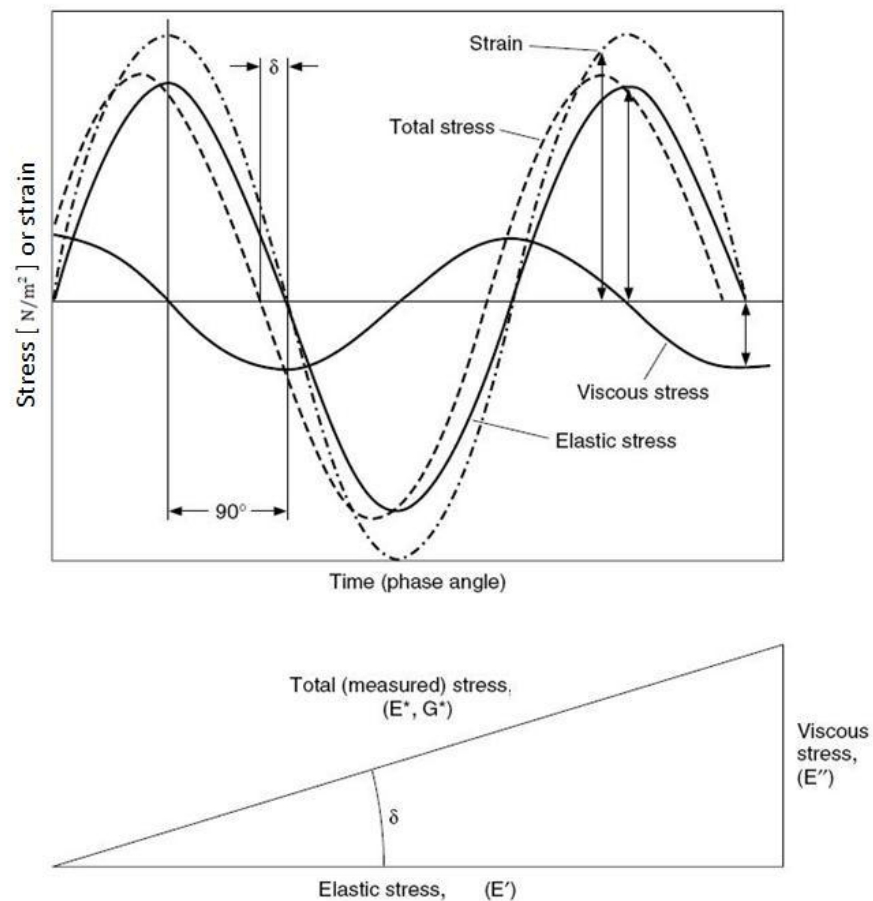
Fig. 2.5 The applied sinusoidal strain and the resultant stress plotted stress as a function of time or phase angle [49]
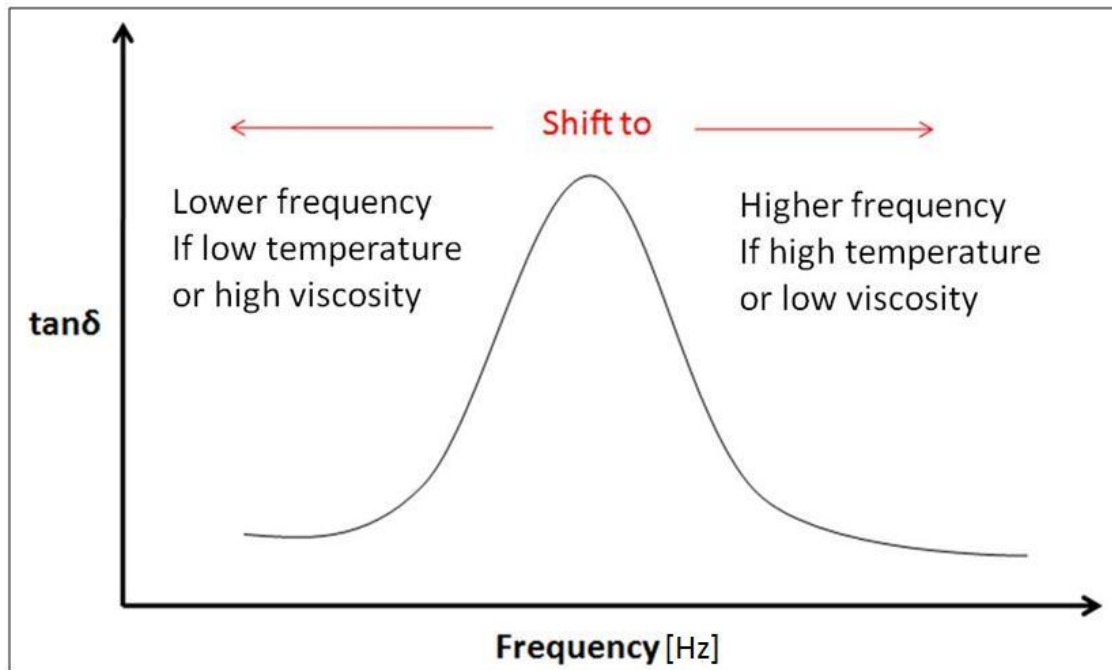
Fig. 2.6 $\tan\delta$ curve against frequency

In general, the $\tan\delta$ of a viscoelastic material passes through at least one peak as a function of frequency as shown in Figure 2.6. A peak of the $\tan\delta$ shifts to lower or higher frequency depending on the temperature and a level of viscosity of an elastomer. Also the width and amplitude are important as the usual aim in damping applications is to realise high damping over as wide a frequency range as possible [52].

The effect of damping can be also expressed through the mechanical quality factor, Q_m [53],

$$Q_m = 2\pi \times (Energy\ stored\ /Energy\ lost\ per\ cycle) \qquad (2.11)$$

The dynamic mechanical analyser (DMA) is mostly used to calculate the $\tan\delta$ recently. But this can be also measured by the logarithmic decrement δ method [54]. One of oldest methods is to calculate the ratio of the average energy dissipated per cycle

to the total energy (the sum of kinetic energy and potential energy) of the system developed by Ungar and Kerwin [55].

Damped system – forced oscillations

The simplified single-degree-of-freedom (SDOF) model shown in Figure 2.7 can represent many real world structures. In this analytical system, this is represented using a Kelvin-Voigt model in which the damping element (shown as a dashpot) is proportional to velocity dx/dt.
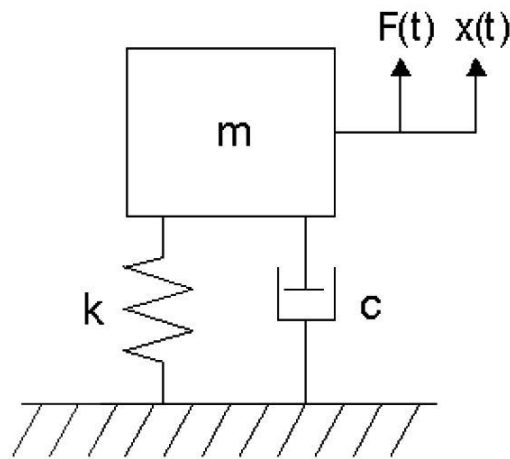
Fig. 2.7 Single-degree-of-freedom damping model

The classic complimentary solution to the transient, free vibration response of the system of Figure 2.7 yields the analytical representation of viscous damping as the damping ratio, ζ, shown in the following equation:

$$\zeta = C/C_c = C/2\sqrt{km} = C/2m\omega_0 \qquad (2.12)$$

where C_c is the critical damping coefficient. m is the mass and ω_0 is the natural angular frequency.

The critical damping for a system is defined as the smallest level of viscous damping in which the mass of Figure 2.7 will exhibit no oscillation when displaced from equilibrium. The damping ratio is often presented as a percentage of the fraction of critical damping or percent critical damping. A system is classified as *underdamped* if ζ < 1, *critically damped* if ζ = 1, and *overdamped* if ζ > 1. Vibratory motion will only exist for an underdamped system. In all the cases above, the response of a system set into motion will eventually decay to zero with time, except when $\zeta = 0$ [56].

When a sinusoidal driving force acts on a damped harmonic oscillator of the system shown in Figure 2.7, the equation of motion is:

$$m(d^2x/dt^2) + R_m(dx/dt) + kx = F_0 \cos \omega t \qquad (2.13)$$

$$\text{or } \ddot{x} + 2\gamma_c \dot{x} + \omega_0^2 x = (F_0/m) \cos \omega t$$

where x is the displacement, R_m is the mechanical resistance or the strength of the damping force, and ω_0 is the natural angular frequency that is equal to $\sqrt{k/m}$, t is time. γ_c is a constant and this is equal to $R_m/2m$. ω is the driving angular frequency. F_0 is the magnitude of the driving force [53].

By substituting the displacement $x = A'\cos(\omega t + \varphi)$ where A' and φ are constants to be determined , it is found to satisfy that equation only when,

$$A' = (F_0/m)/\sqrt{(\omega_0^2 - \omega^2)^2 + (2\gamma_c\omega)^2} \, , tan \, \varphi = 2\gamma_c\omega/(\omega_0^2 - \omega^2) \qquad (2.14)$$

The angle φ represents the phase of the driving force relative to the forced oscillation in equation (2.14). The tangent of this angle is the ratio of imaginary to real part of the solution.

If the complex velocity is given by $V^* = V_0 e^{i(\omega t + \varphi)}$ where V_0 is the magnitude of the velocity, the complex mechanical impedance of the system Z_s is as follows:

$$Z_s = F_0 e^{i\omega t} / V^* \qquad (2.15)$$

The mechanical impedances of damping (a dashpot) Z_c, spring Z_k and mass Z_m are given by,

$$Z_c = c \qquad (2.16)$$

$$Z_k = -ik/\omega \qquad (2.17)$$

$$Z_m = i\omega m \qquad (2.18)$$

So the total Z_s is,

$$Z_s = c + i(\omega m - k/\omega) \qquad (2.19)$$

At low frequencies, ω is very small and Z_s equals $c - i(k/\omega)$ as $i\omega m$ can be neglected. At high frequencies, ω is large and Z_s equals $c - i\omega m$ [18].

72

2.2.5 Energy dissipation of an elastomer

The elliptical plot of stress versus strain in dynamic loading of a linear material encloses some area as shown in Figure 2.8.

The mechanical energy of the system, W in the quarter cycle, or $t = \pi/2\omega$ is given by,

$$W = \int_0^{\pi/2\omega} \sigma (d\varepsilon/dt) dt \tag{2.20}$$

If making the substitution $\sigma = \sigma_0 \sin \omega t$ and $\varepsilon = \varepsilon_0 \sin(\omega t - \delta)$, the equation (2.20) is rearranged as:

$$W = \omega \varepsilon_0 \sigma_0 \int_0^{\pi/2\omega 0} (\cos \omega t \sin \omega t \cos \delta + \sin^2 \omega t \sin \delta) dt \tag{2.21}$$

$$= \varepsilon_0 \sigma_0 \left[\frac{\cos \delta}{2} + \frac{\pi \sin \delta}{4} \right]$$

The first term represents the stored energy and second term (which vanishes for $\delta = 0$) represents dissipated energy. Thus the energy stored elastically, W_s in the material is:

$$W_s = \int_0^{\varepsilon_0} E'\varepsilon \, d\varepsilon = 1/2 \cdot E'\varepsilon_0^2 \tag{2.22}$$
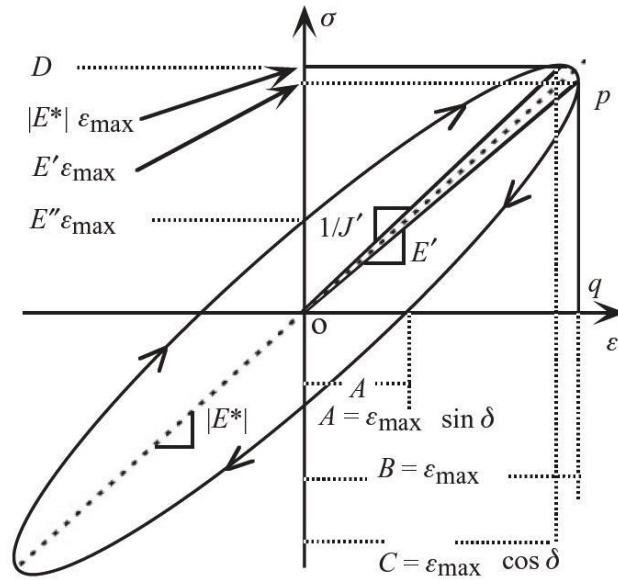
Fig. 2.8 Stress versus strain for a linearly viscoelastic material under oscillatory loading

[57]

This stored energy corresponds to the area in the triangle *opq* in Figure 2.8. The stored energy is calculated for a quarter cycle rather than a full cycle since the material returns to its original condition after a full cycle. The dissipated energy for a full cycle is proportional to the area within the ellipse in Figure 2.8. The dissipated energy, W_d over a quarter cycle is determined by taking one-quarter of the integral over a full cycle.

$$W_d = 1/4 \cdot \int_0^{2\pi/\omega} \sigma(d\varepsilon/dt)\, dt = 1/4 \cdot E^{"} \varepsilon_0^2 \tag{2.23}$$

Therefore,

$$W_d/W_s = \pi/2 \cdot tan\, \delta \tag{2.24}$$

The physical meaning of the $tan\,\delta$ is associated with the ratio of energy dissipated to the energy stored in dynamic loading [58].

2.3 Vibrations of plate

Several mathematical models have been developed to cover the behaviour of vibrating plates. In this subsection, the rectangular Kirchhoff plate, which is for thin plates with small deflections but negligible shear energy and uncoupled membrane-bending action, is discussed as this is most commonly used in vibrations.

The Kirchhoff model satisfies the following conditions [59];

a) The plate is thin in the sense that the thickness h is small compared to the characteristic length(s), but not so thin that the lateral deflection becomes comparable to h.

b) The plate thickness is either uniform or varies slowly so that three-dimensional stress effects are ignored.

c) The plate is symmetric in fabrication about the mid-surface.

d) Applied transverse loads are distributed over plate surface areas of dimension h or greater

e) The support conditions are such that no significant extension of the mid-surface develops.

The boundary conditions of the plate significantly affect the behaviour of vibrating plates. Those boundary conditions are; a) simply supported, b) clamped, and c) free. The clamped boundary condition only will be reviewed here as other boundary conditions are not applicable to this research. More details about solutions for a clamped rectangular thin plate subjected to uniform loading have been presented by many authors [60] [61] [62] [63].

2.3.1 Fundamental equations of plate bending

In classical plate theory, it is common to let the plate stretch in the x-y directions, and to let the z-axis point downwards. This custom is adopted in Figure 2.9, where the stresses and stress resultants for a plate element is shown.
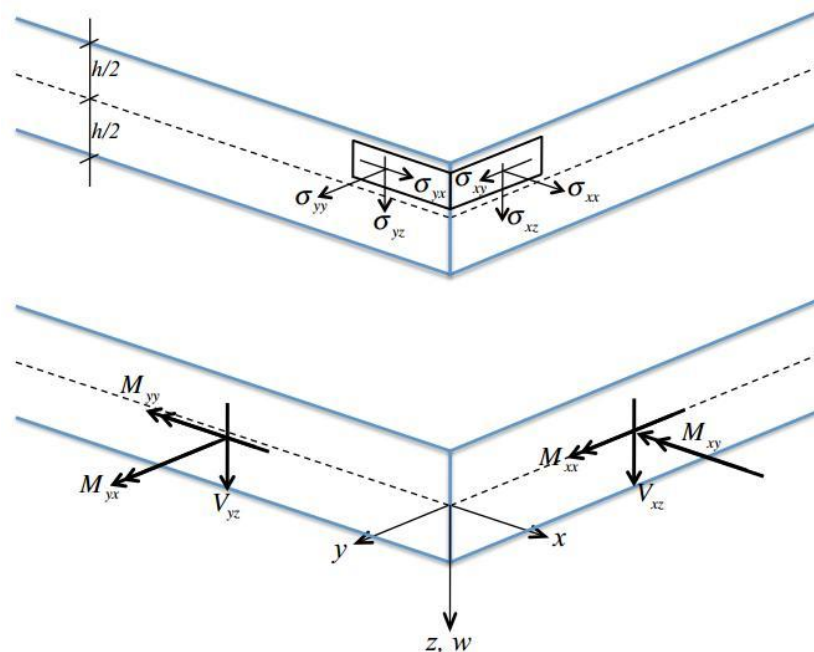
Fig. 2.9 Stresses and stress resultant in a plate element

The first index of the stress components is named after the surface that the component acts on. The second index identifies the direction of the stress component. For example, bending moments with two equal indices, M_{xx} and M_{yy} act on the surface with normal vector equal to that index. And M_{xy} and M_{yx} are twisting moments which act on the surface of the first index. The second index simply indicates the other direction to identify that it is a twisting moment.

Section integration

Letting the z-axis have its origin at the neutral plane of the plate, the stress resultants are defined by the integrals,

$$M_{xx} = \int_{-h/2}^{h/2} z\sigma_{xx} \, dz$$

$$M_{yy} = \int_{-h/2}^{h/2} z\sigma_{yy} \, dz$$

$$M_{xy} = \int_{-h/2}^{h/2} z\sigma_{xy} \, dz$$

$$M_{yx} = \int_{-h/2}^{h/2} z\sigma_{yx} \, dz \tag{2.25}$$

From solid mechanics, it is known that the bending moments are equal: $M_{xy} = M_{yx}$.

Equilibrium

Considering the infinitesimal plate element shown in Figure 2.10, it extends dx in x-direction and dy in y-direction. Its thickness is h and it is subjected to a distributed load of intensity q in the z-direction.
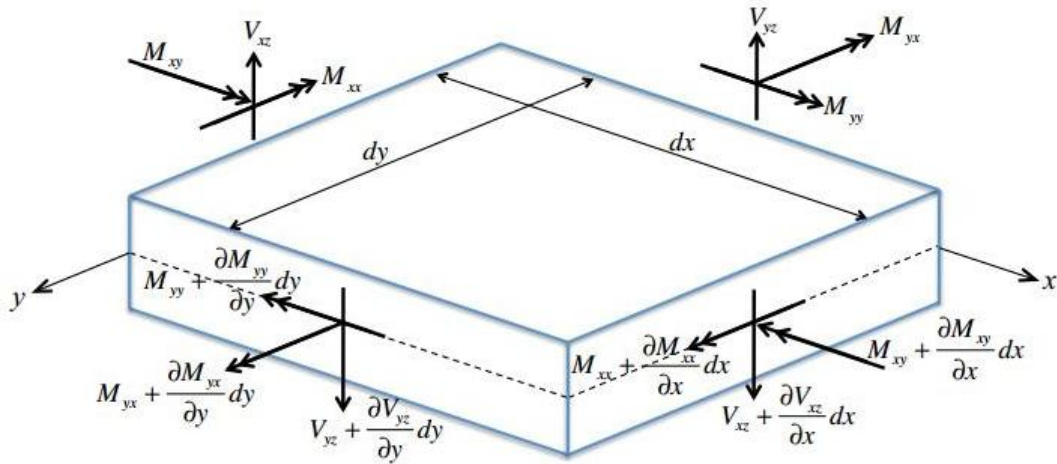
Fig. 2.10 Infinitesimal plate element

Equilibrium in the z-direction yields

$$q + \partial V_{yz}/\partial y + \partial V_{xz}/\partial x = 0 \tag{2.26}$$

Moment equilibrium about the y-axis yields

$$\partial M_{xx}/\partial x + \partial M_{yz}/\partial y = V_{xz} \tag{2.27}$$

Moment equilibrium about the x-axis yields

$$\partial M_{yy}/\partial y + \partial M_{xy}/\partial x = V_{yz} \tag{2.28}$$

where V is the shear force.

The three equilibrium equations can be combined into one. Partial differentiation of equation (2.27) with respect to x and partial differentiation of equation (2.28) with respect to y, followed but substitution of those equations into equation (2.26) yields,

$$q + \partial^2 M_{xx}/\partial x^2 + \partial^2 M_{yy}/\partial y^2 + 2 \cdot \partial^2 M_{xy}/\partial x \partial y = 0 \qquad (2.29)$$

Differential equation

Differential equation of vibration for an anisotropic plate with transverse displacement of the plate w is defined as;

$$D_{xx}[\partial^4 w/\partial x^4] + 2H \,[\partial^4 w/\partial x^2 \,\partial y^2] + D_{yy}[\partial^4 w/\partial y^4] = q \qquad (2.30)$$

where $H = D_1 + 2D_{xy}$, $D_{xx} = \frac{E_x\, h^3}{12}$, $D_{yy} = \frac{E_Y h^3}{12}$, $D_1 = \frac{E_1\, h^3}{12}$, $D_{xy} = \frac{G\, h^3}{12}$, h is thickness of the plate, D is the flexural rigidity and q is given by $-\rho\, h \frac{\partial^2 w}{\partial t^2}$ where ρ is the density of the material of the plate and t is time. E and G are the Young's modulus and shear modulus [64].

When the plate is made up of isotropic material,

$$E_x = E_y = (E/1 - v^2), \qquad E_1 = vE/(1 - v^2), \qquad G = E/2(1 + v) \qquad (2.31)$$

where v is the Poisson's ratio. Hence,

$$D_{xx} = D_{yy} = D = [E\,h^3/12(1-v^2)], \qquad H = D_1 + 2\,D_{xy} = D \qquad (2.32)$$

Equation (2.30) is rearranged as follows;

$$D\,\{[\partial^4 w/\partial x^4] + 2\,[\partial^4 w/\partial x^2\,\partial y^2] + [\partial^4 w/\partial y^4]\} = q \qquad (2.33)$$

The bending moments M_{xx}, M_{yy} and M_{xy} (the rotational moment) associated with displacement are:

$$M_{xx} = -D\{v[\partial^2 w/\partial y^2] + [\partial^2 w/\partial x^2]\}$$

$$M_{yy} = -D\{[\partial^2 w/\partial y^2] + v[\partial^2 w/\partial x^2]\}$$

$$M_{xy} = -D(1-v)(\partial^2 w/\partial x \partial y) \qquad (2.34)$$

Kirchhoff's Shear force

When a square plate is bending under uniform downward loading then the corners will experience uplift. This is due to the net unbalanced concentrated force equal to $2M_{xy}$ at the corner. This shear force is known as Kirhhoff's shear force and the corner uplift is referred to as the Kirchhoff effect.

$$V_{xz} + \partial M_{xy}/\partial y = -D[\partial^3 w/\partial x^3 + (2-v) \cdot (\partial^3 w/\partial x \partial y^2)]$$

$$V_{yz} + \partial M_{yx}/\partial y = -D[\partial^3 w/\partial y^3 + (2-v) \cdot (\partial^3 w/\partial x^2 \partial y)] \qquad (2.35)$$

For a clamped rectangular plate, the deflexion and the slope are both zero at the edge,

$$w = 0 = \partial w / \partial n \qquad (2.36)$$

where n denotes the normal to the edge.

2.3.2 Bending waves in plates

The motion of an elemental section of a beam has been studied initially by authors [65] [66] [67]. Fahy, one of authors has shown:

$$B(\partial^4 w / \partial x^4) = -m(\partial^2 w / \partial t^2) \qquad (2.37)$$

where B is the bending stiffness that is given by,

$$B = Eh^3 / 12(1 - v^2) \qquad (2.38)$$

where m is the mass per unit length and t is time.

This equation can be extended to describe a thin plate lying in the x-y plate in rectangular Cartesian coordinates;

$$B(\partial^4 w / \partial x^4 + 2(\partial^4 w / \partial x^2 z^2) + \partial^4 w / \partial z^4) = -\mu(\partial^2 w / \partial t^2) \qquad (2.39)$$

81

where μ is the mass per area of plate. A solution that satisfies equation (2.39) is;

$$v_B(\omega) = \sqrt[4]{B/\mu} \ \sqrt{\omega} \qquad\qquad (2.40)$$

where $v_B(\omega)$ is the bending wave velocity.

$v_B(\omega)$ is the rate at which the phase of the wave propagates in the panel. Hence the bending wave is dispersive with a phase velocity given in equation (2.40) [68] [69]. As $v_B(\omega)$ is proportionally related to the ratio of B ($\approx E$) to μ of the panel that the wave passes through, the higher the ratio of B to μ results in a bending wave with increased speed and longer wavelength.

The bending waves enable the plate to displace transversely at the $v_B(\omega)$ so the bending modes are formed across the panel at the mode frequencies (natural frequencies) as shown in equation 1.1. Typically the panel moves as a rigid piston at low frequencies where the sound wavelength is much greater than the panel's dimensions. As frequency increases, the panel's movement breaks up and different mode shapes appear at the mode frequencies. These mode shapes on the panel can be observed by using finite element analysis (FEA) and laser scanner (see section 4.3).

The bending waves are closely related to the sound radiation from the plate. The sound radiation of plate will be discussed further in section 2.4. The sound radiation intensity from the plate depends on $\sqrt{v_B(\omega)}$. The requirement for constant velocity is that the mechanical impedance of the plate Z_p must be resistive.

$$Z_p = 8\sqrt{B\mu}, \qquad K_b(\omega) = \sqrt{\omega\sqrt{\mu/B}} \qquad\qquad (2.41)$$

where K_b is the wave number of the bending wave [70].

2.4 Principles of sound and its emission from a plate

2.4.1 Acoustic wave equations

Acoustic waves are small changes in the physical properties of the air which propagate through the medium at a finite speed. That is, the initial air pressure change causes the air in contact with it to move by compressing it (the longitudinal wave). The air has a mass and hence inertia so the speed of sound takes a finite time to propagate through the different materials.

The speed of sound in the air:

The speed of sound c in air depends on a number of factors such as temperature, pressure, and density. The equation of the speed of sound in the air is as follows;

$$c = 331.4[^m/_s] + 0.6[^m/_s]/°C \times T \qquad\qquad (2.42)$$

where T is the temperature. This equation gives the speed of sound, 343.2m/s in dry air at 20℃.

The speed of sound in solids:

Sound waves in solids propagate as two different types – a longitudinal wave and transverse wave as shown in Figure 2.11. These waves have a different wave speed at the same frequency.

$$c_l = \sqrt{[E(1-\mathrm{v})/\rho(1+\mathrm{v})(1-2\mathrm{v})]}, \quad c_t = \sqrt{G/\rho} = \sqrt{E/\rho 2(1+\mathrm{v})} \qquad (2.43)$$

where c_l is the longitudinal wave speed, c_t is the transverse wave speed, and ρ is the density. Typically the longitudinal waves are faster than the transverse waves as E is usually greater than G [71].
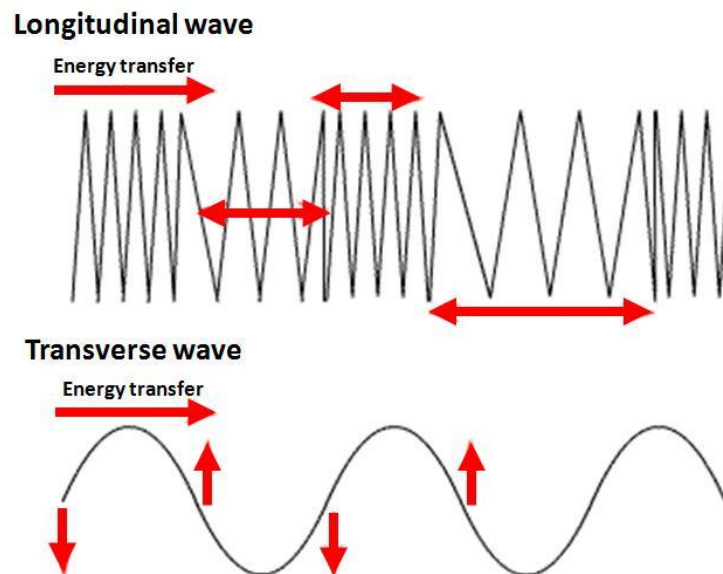
Fig. 2.11 Longitudinal and transverse wave

The speed of these waves in solids is usually determined by E (or G) and ρ. The larger the elastic constants and the lower ρ the material has, the faster sound waves travel due to the stronger interactions between molecules. Table 2.1 shows the speed of

the transverse wave c_t with a relevant wavelength λ in the panels used for the experiments.

Materials		E [N/m^2]	ρ [Kg/m^3]	c_t [m/s]	λ at 100 Hz [m]
Plastic	PMMA (Poly(methyl methacrylate))	4.2×10^9	1150	1163	11.6
	PVC (Poly(vinyl chloride))	3.2×10^9	1100	1037	10.3
	ABS (Acrylonitrile butadiene styrene)	2.7×10^9	1200	912	9.1
	Polycarbonate	2.3×10^9	1190	846	8.4

Table 2.1. Properties of materials used in the experimental panel

Wave number

Wave number k_n is the number of alternate positive and negative cycles that occur in a given distance.

$$k_n = \omega/c \tag{2.44}$$

Wave length

Wavelength λ is the distance occupied by one cycle of a single frequency wave [49].

$$\lambda = c/f \tag{2.45}$$

where f is the frequency.

The standing wave

When multiple acoustic waves propagate through a given point at the same time, an interference field is set up. Waves remain unchanged when being interfered with each other, but the pressures in each of the waves can be summed positively or negatively to yield the total sound field known as the standing wave field. If the pressure $\hat{p}$ of a plane wave at any point in time t and at any position x is defined as $\hat{p}(x,f) = \hat{P}\, e^{-jk_n x}$, the standing wave is given by:

$$\hat{p}(x,f) = \hat{P}\, e^{-jk_n x} + \hat{Q}\, e^{-jk_n x} \tag{2.46}$$

where $\hat{P}$ and $\hat{Q}$ are the magnitude of high and low pressure respectively [20].

Sound intensity and power

Sound waves carry energy in two energy forms – kinetic energy (acoustic particle velocity) and potential energy (acoustic pressure). The acoustic particle velocity $\hat{u}(x,f)$ is defined as:

$$\hat{u}(x,f) = \hat{p}(x,f)/\rho c \tag{2.47}$$

The sound intensity I is the product of the pressure and that proportion of particle velocity that is in phase with pressure, averaged in time over one cycle.

$$\hat{I} = \hat{p}(x,f) \times \hat{u}(x,f) = \hat{p}(x,f) \times [\hat{p}(x,f)/\rho c] = |\hat{p}|^2/2\rho c \tag{2.48}$$

where $|\hat{p}|$ is the root-mean-square (RMS) pressure.

The sound power W_p is the sound intensity per unit area S.

$$W_p = \int I\, dS \qquad (2.49)$$

Acoustic impedance

The ratio of acoustic pressure to particle velocity at any point in a sound field is the acoustic impedance Z_a.

$$\widehat{Z_a}(f) = \hat{p}(f)/\hat{u}(f) \qquad (2.50)$$

Acoustic impedance is the complex number, $\widehat{Z_a} = R_a + iX_a$ where R_a and X_a are the real part and imaginary part of the Z_a. Equation (2.50) gives the rearrangement of equation (2.49) as follows;

$$\hat{I} = Re\{\hat{Z}(x,f)\} \times \hat{u}(x,f)^2 \qquad (2.51)$$

where $Re\{\hat{Z}(x,f)\}$ is equal to R. The particle velocity next to a vibrating surface is equal to the velocity of the surface and that sound power W_p is the integral of intensity over the area of surface so the sound power radiated by a vibrating surface can be calculated. The specific acoustic impedance evaluated on a vibrating surface is also known as the acoustic radiation impedance [20]. Therefore the higher the acoustic radiation impedance is given, the higher sound power is radiated and directivity of the sound field becomes narrow. When the imaginary part of the radiation increases, this gives higher the reactive loading which does not contribute the total sound power.

Sound pressure level:

The sound pressure level (SPL) in dB is given by

$$\text{SPL(dB)} = 20 \, log_{10}(P/P_0) \tag{2.52}$$

where P is the acoustic pressure of interest and P_0 is the reference pressure (20 µPa).

2.4.2 Sound radiation from acoustic sources

The sources of sound - the point monopole source in the free-field and the plate, and the sound radiation from the plate will be also considered in this subsection.

The point monopole in the free-field:

This source is omnidirectional and consists of spherical waves propagating away from the source. The spherical sound field radiated by a point monopole at a single radial frequency is given by:

$$\hat{p}(r_a, f) \propto e^{-jk_n r_a}/r \tag{2.53}$$

where r_a is the radius from the source. By defining the volume velocity, $\hat{q}$, $\hat{q} = \hat{u}S$ where S is radiation area, equation (2.53) is rewritten as,

$$\hat{p}(r_a, f) = j\rho c k_n \hat{q} \, e^{-jk_n r_a}/4\pi \tag{2.54}$$

The sound intensity at any radius r_a becomes $I(r_a) = \frac{|\hat{p}|^2}{2\rho c}$ so it gives the sound power of the monopole W_{sp} as [53]:

$$W_{sp} = \int (|\hat{p}|^2/2\rho c)\, dS = \rho c k_n{}^2 |\hat{q}|^2/8\pi \tag{2.55}$$

The point monopole from the plate:

The sound radiated by a point monopole on the plate has the volume velocity that is constrained to radiate the sound into a hemisphere.

$$\hat{p}(r_a, f) = j\rho c k_n \hat{q}\, e^{-jk_n r_a}/2\pi \tag{2.56}$$

The monopole source on the plate radiates twice the sound pressure into half of the space. The sound power is also twice the free-field sound power output as follows,

$$W_{sp} = \int (|\hat{p}|^2/2\rho c)\, dS = \rho c k_n{}^2 |\hat{q}|^2/4\pi \tag{2.57}$$

The sound radiation from the panel:

The sound radiation of the panel can be the sum of all of the equivalent monopoles;

$$\hat{p}(R_o, f) = \sum_N \hat{p}_n(R_o, f) = (j\rho c k_n/2\pi) \sum_{N_m} \left[\hat{q}_n \times \left(e^{-jk_n r_n}/r_n \right) \right] \tag{2.58}$$

where R_o is the observation point, N_m is the total number of monopoles, $\hat{q}_n$ is the volume velocity of monopole n and r_n is the distance from that monopole to R.

By assuming that (1) the total volume velocity of the panel is $\hat{q}_p$ $(= \hat{u}_p \, \hat{S}_p)$, where $\hat{u}_p$ and $\hat{S}_p$ are the velocity and radiating area of the panel respectively, (2) R_o is sufficiently far from the panel when compared to the radius of the panel, and (3) there are an infinite number of monopoles in the panel, equation (2.58) can be simplified as:

$$\hat{p}(R_o, f) = (j\rho c k_n \hat{q}_p / 2\pi R_o) \int e^{-jk_n r_n} \, dS_p \qquad (2.59)$$

Equation (2.59) can be used to predict the sound pressure radiated from a vibrating panel over the full range of audible frequencies between 20 Hz and 20,000 Hz. But in practice there can be differences between predicted and measured data of the sound pressure at some frequencies where the panel's movement breaks up. At these frequencies, both the in-phase and anti-phase regions of the modes form across the panel, resulting in the acoustical cancellation of the sound waves (This was discussed more fully in section 4.4.1). At other frequencies where the panel moves as a rigid piston or only the in-phase region of the modes on the panel appears, prediction of the sound pressure by using equation (2.59) is satisfactory.

The sound power with the volume velocity of the plate W_{pp} is given by,

$$W_{pp} = \int (|\hat{p}|^2 / 2\rho c) \, dS = \rho c k_n^{\,2} |\hat{q}_p|^2 / 4\pi \qquad (2.60)$$

The sound power of the plate is proportional to the square of the volume velocity of the plate.

2.5 Conclusions

The aim of this Chapter was to review the research previously carried out that will be also useful to identify problems of the current research and establish a theoretical background on a mechanism of the sound reproduction from the panel (or plate) excited by the gel-type audio transducer. Hence the background of an elastomer with the static and dynamic (temperature, time, and frequency dependent) characteristics was discussed to understand the dynamic behaviour of the gel surround in a vibratory condition. Also theories including the fundamental equations on vibration of plates and the sound radiation were reviewed to comprehend the mechanism of the sound reproduction of the vibrating plate. Theoretical and experimental investigation for the gel-type audio transducer will be considered in Chapter 4.

CHAPTER 3 – METHODOLOGY

3.1 Introduction

In this Chapter, the fabrication of the gel-type audio transducer and testing methods were discussed. In section 3.2, the design of each part – a magnetic assembly, coil-drive plate assembly, and the gel surround – was described in detail. This includes a part drawing, materials used, and an assembly process. Especially manufacturing techniques for gel surrounds with three different types of elastomers are introduced in section 3.2.3. Testing machines and conditions adopted for this research are presented from section 3.4 to section 3.9. The summary of this Chapter was presented in section 3.10. External contributions to the work reported in this Chapter are indicated in the relevant section.

3.2 Fabrication of the gel-type audio transducer

The gel-type audio transducer consists of three main parts – the magnetic assembly, coil-drive plate assembly, and the gel surround as shown in Figure 3.1. Thus, design features of each part and manufacturing process will be considered at the separate section.

The gel-type audio transducer is attached to any solid surface such as a rigid panel and excites it to create the sound. So a bracket, that holds the transducer and gives

a firm contact with the surface, is required. This bracket was also designed for testing and it was presented in section 3.2.5.

The size of the gel-type audio transducer can vary depending on target nominal impedance and "maximum output power". For example, the nominal impedance of the voice coil of the transducer used for the experiments was chosen at 8 Ω as this value is the most commonly adopted for many applications. At this stage, the wire diameter, length, and the coil layer were selected. A high number of coil turns are also required to give the transducer a greater "maximum output power". As a result, the optimised specification of the voice coil generated a coil assembly with an outer diameter of 30.58 mm and a wind width of 4 mm. Thereafter the magnetic flux density and mass of the magnetic assembly were calculated with the given dimensions of the coil assembly, in order to increase the force factor influencing the output power of the transducer. And finally the gel surround was designed to couple those two assemblies. Thus the external dimensions of the transducer used for the experiments became 44.4 mm in diameter and 18 mm in thickness.
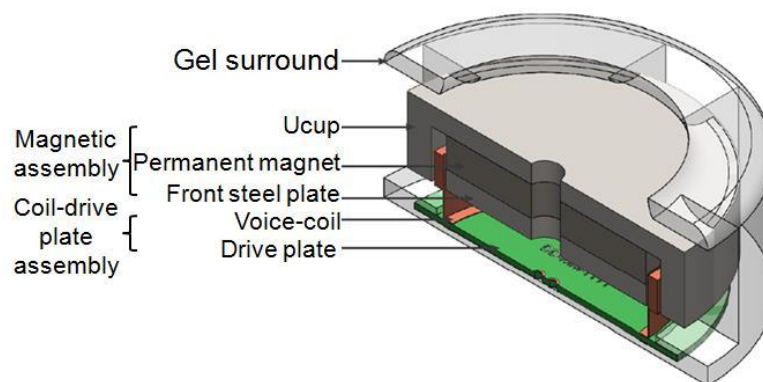
Fig. 3.1 Configuration of the gel-type audio transducer

3.2.1 Magnetic assembly

The magnetic assembly of the gel-type audio transducer comprises a permanent magnet, front steel plate, and an Ucup. Electrical parameters, such as the magnetic flux density, were predicted and investigated by using the simulation software - COMSOL Multiphysics (FEA: Finite element analysis) by the author. All Best Tech Ltd, China produced the sample prototypes for the experiments according to the drawings provided. For a permanent magnet, a neodymium magnet made from an alloy of neodymium, iron and boron ($Nd_2Fe_{14}B$) was used and magnet grade is N48. Table 3.1 shows a remanent magnetic flux density B_r.

Magnet grade	B_r (Gauss, **G**/ Tesla, **T**)
N48	14200/1.42

Table 3.1 Remanent magnetic flux density, B_r
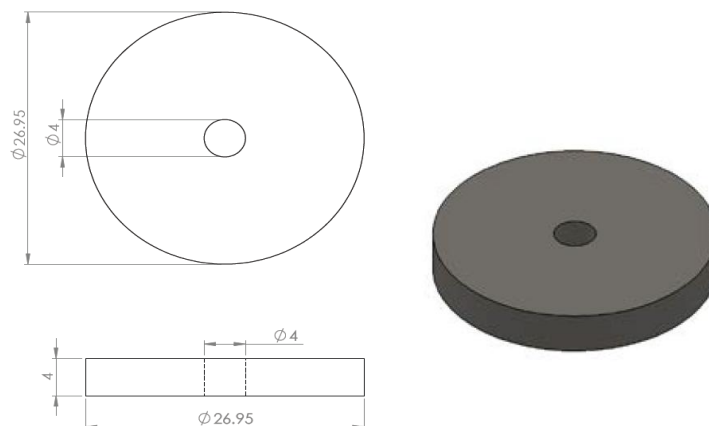
Fig. 3.2 Drawing of the permanent magnet

Drawing of the magnet including dimensions was presented in Figure 3.2.

The front plate and Ucup of the magnetic assembly were made of mild steel and their dimensions were shown in Figure 3.3.
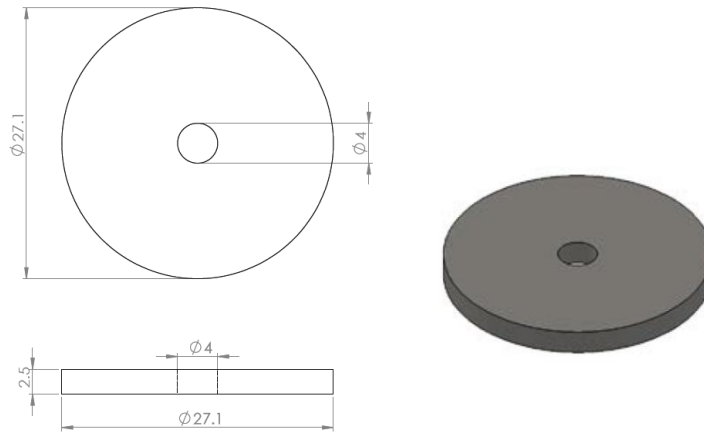
(a) Drawing of the front plate
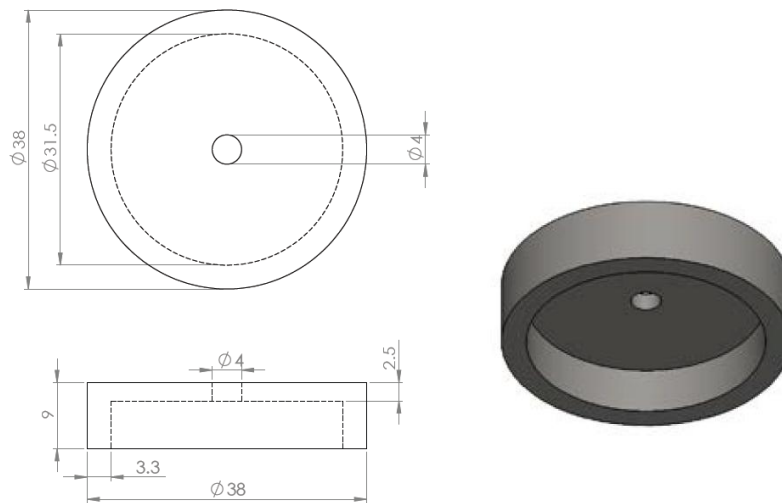
(b) Drawing of the Ucup

Fig. 3.3 Drawing of the front plate and Ucup

The magnet was magnetised first and thereby, this was glued to the front plate followed by the Ucup by using a Jig to align them as described in Figure 3.4. The glue used is a LOCITE 480 adhesive.
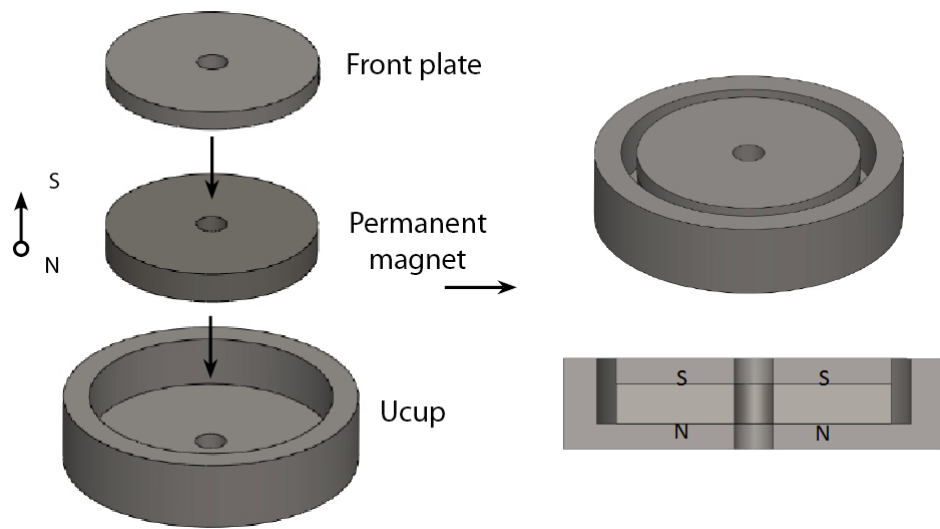
Fig. 3.4 Assembly of the magnetic assembly

3.2.2 Coil-drive plate assembly

Inner diameter	28 mm	DC Resistance	8 Ω
Outer diameter	30.58 mm	Inductance	0.498 mH
Wire diameter	0.17 mm	Total length	9.661 m
Wind width	4 mm	Former thickness	0.1 mm
Layers	6	Former height	7.5 mm
Tinned length	10 mm	Upper free end	0.2 mm
No. of turns	105	Lower free end	3.3 mm

Table 3.2 Specification of the voice-coil (000) and former (000)

The coil-drive plate assembly consists of a voice-coil bonded onto a drive plate. The voice-coil is wound on a former made of polyamide film as presented in Figure 3.5. The drive plate was made of a prepreg material, FR-4, that is composed of woven fibre-

glass cloth with an epoxy resin binder. Table 3.2 shows a specification of the voice-coil and former.
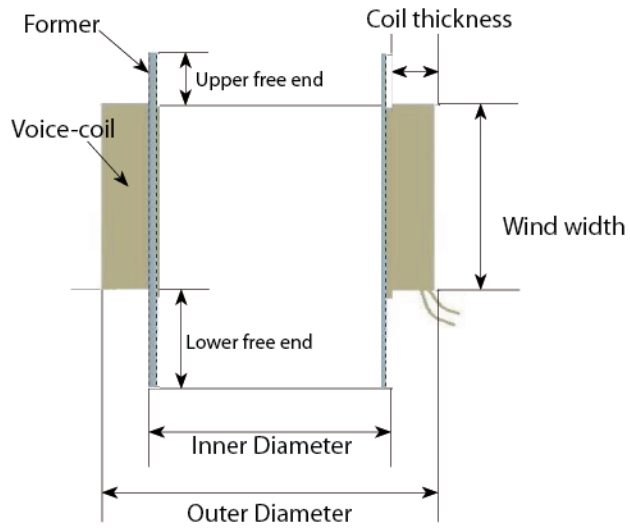
Fig. 3.5 Construction of the former and voice-coil

Dimensions of the drive plate were shown in Figure 3.6.
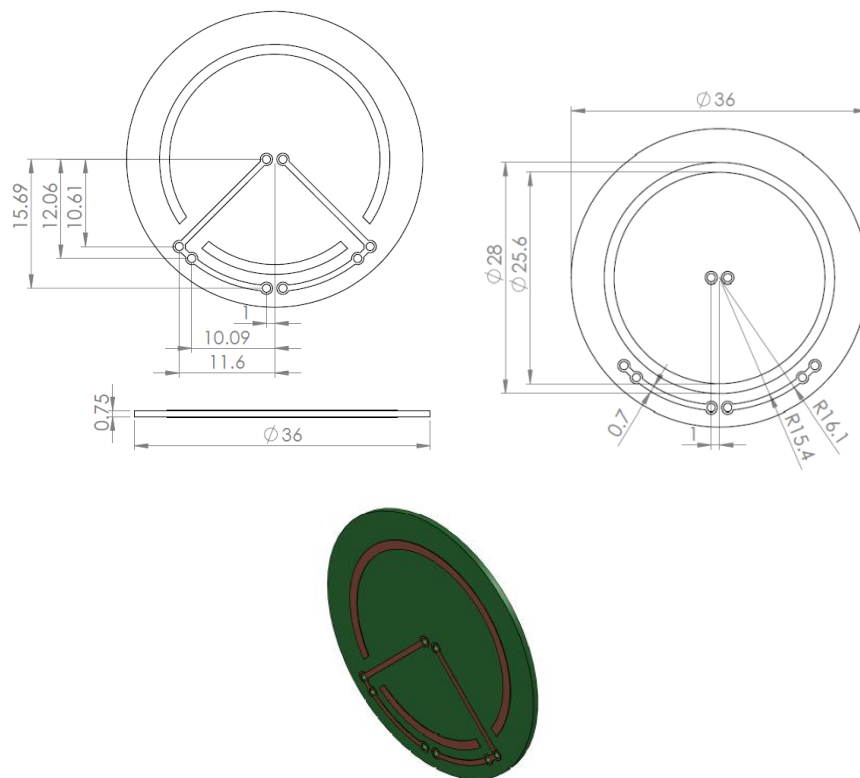
Fig. 3.6 Drawing of the drive plate
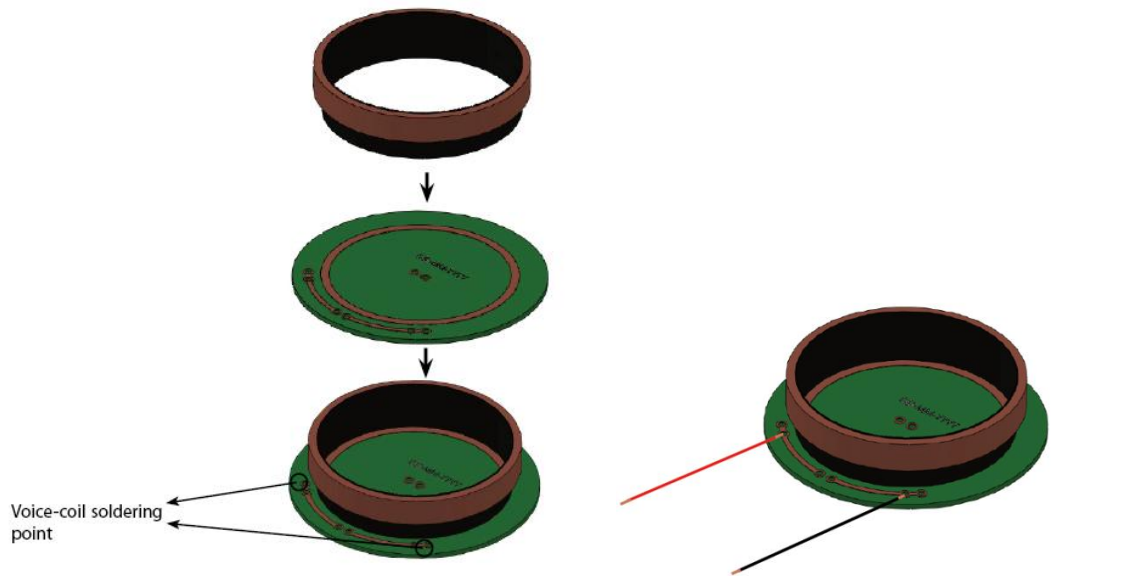
(a) Bonding process of the coil and drive plate   (b) Complete assembly with wires

soldered

Fig. 3.7 Assembly of the coil-drive plate assembly

The voice-coil was mounted directly onto the top surface of the drive plate using an alignment jig. Wires were also connected to the drive-plate. These are described in Figure 3.7. The voice-coil calculator and simulation software - COMSOL Multiphysics (FEA) were used to find optimised set of properties (i.e. the blocked coil impedance, electrical resistance, and force factor) for the voice coil and drive plate. The majority of this work was carried out by the author with support from his colleagues at SFX Technologies. The prototypes based on this specification were subsequently manufactured by Wanstonic electronics Ltd, China.

3.2.3 Gel surround

The gel surround must be made of low-hardness elastomers. Figure 3.8 shows the drawing of the gel surround.
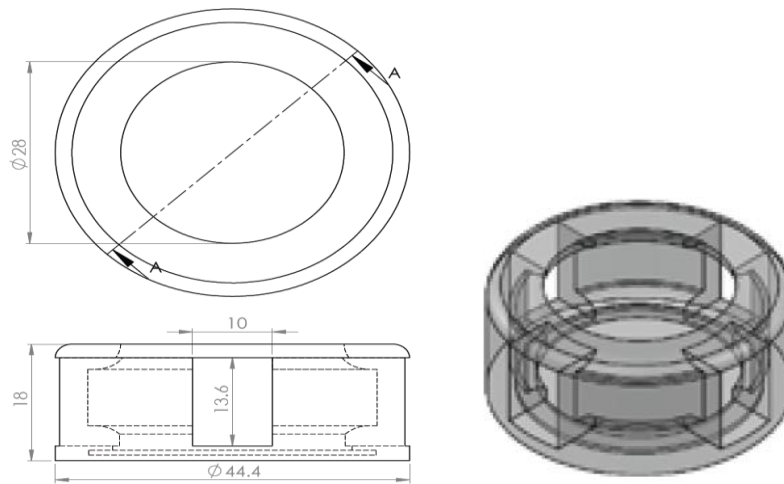
Fig. 3.8 Drawing of the gel surround

For this research, three different types of elastomers, covering a range of the hardness, were used to produce testing samples. This enabled the effect of varying the compliance C of the gel surround on the acoustical performance of the transducer. In this case, C is the property that characterises the damping ability of a material. A more detailed discussion of this topic is presented in section 4.2.1. The elastomers selected for this part of the investigation included a **RTV (room-temperature vulcanising) silicone elastomer; thermoplastic elastomer (TPE)** based on the styrenic block copolymer; and a **silicone foam elastomer**.

These materials were chosen for a variety of reasons. RTV silicone elastomers are widely used in a range of applications among the ***thermoset polymer family*** and they are available commercially in many different hardness. RTV silicones, with varying properties, can also be manufactured relatively easily in the laboratory by simply changing the mixing ratio of the raw materials. Block-based styrene thermoplastic elastomers (TPEs), are also readily available commercially, are comparatively cheap to manufacture and exhibit useful and suitable physical characteristics among the ***thermoplastic elastomer family***. Silicone foam elastomers are

particularly applicable in the acoustic engineering field, because of their unique mechanical performance. The material is highly compressible (Poisson's ratio is less than 0.3) but maintains many of the other useful properties found in silicone elastomers. Furthermore, all three classes of materials can be relatively easily processed using standard polymer moulding techniques, enabling products to be manufactured on equipment available at Edinburgh Napier University or elsewhere.

Two processing techniques – namely injection and compression moulding - were employed to manufacture the test samples, depending on the type of material used. The aluminium moulds were built by Alumould Ltd UK, and the sample gel surrounds were produced by the author in the the Polymer Processing Laboratory at Edinburgh Napier University.

To manufacture a range of the hardness, a **_RTV silicone elastomer_** was used. _PlatSil_[®] _Gel-10_ (55 Shore 00) and _PlastSil_[®] _7120_ (70 Shore 00) were used as shown in Figure 3.9. They consist a two-component system (A: silicone elastomer, B: vulcanising agent – platinum catalyst). The mixing ratio is 1:1 by volume with 5 and 20 minute working time that cures in 30 minutes and 120 minutes for _PlatSil_[®] _Gel-10_ and _PlastSil_[®] _7120_ respectively. A softener, _Smith's Prosthetic Deadener_ was added to lower the hardness, in order to achieve the target hardness. Figure 3.10 (a) and (b) present aluminium moulds used to cure the RTV silicone gel surrounds.

Figure 3.9 RTV raw silicone materials

(a) Aluminium moulds   (b) 70 Shore 00 (purple) and 35 Shore 00 (white)

Figure 3.10 Aluminium moulds and silicone gel surrounds

For samples made of ***thermoplastic elastomer (TPE),*** styrenic block based copolymers were used and these include Versaflex® CL2003X (35 Shore 00) and UN-2005® (70 Shore 00) developed by "GLS" and "Tekner Apex" respectively. Figure 3.11 (a) and (b) show the Battenfeld injection machine chosen to use and the TPE samples respectively.

(a) Battenfeld injection moulding machine
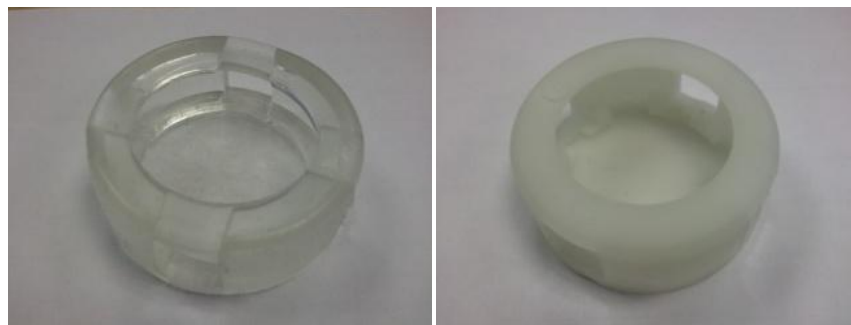
(b) TPE sample, 35 Shore 00 (clear) and 70 Shore 00 (white)

Figure 3.11 Battenfeld injection moulding machine and TPE samples

WACKER ELASTOSIL series for the *silicone foam elastomer* was used to manufacture 35 and 70 Shore 00 silicone foam samples. This product is a thixotropic, addition-curing forming a closed cell silicone foam. To produce samples, a compression moulding machine was employed. The transducer assembled with the foam gel surround is shown in Figure 3.12.

Fig 3.12 Complete assembly with the silicone foam gel surround

3.2.4 Assembly of the gel-type audio transducer

Figure 3.13 shows the assembly procedure and cross-section view of the transducer. The prototypes of each component in the transducer, namely the magnetic, coil-drive plate assembly, and the gel surround were constructed into a complete unit. Figure 3.14 illustrates each part of the transducer as well as the completed assembly.

1) Insert the PCB into the gel surround

2) Insert the magnetic assembly
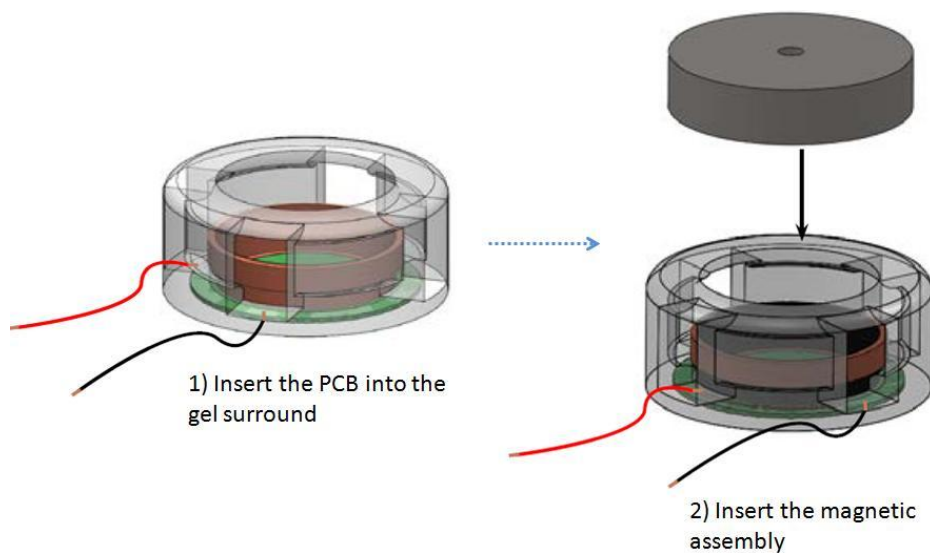
(a) Assembly procedure
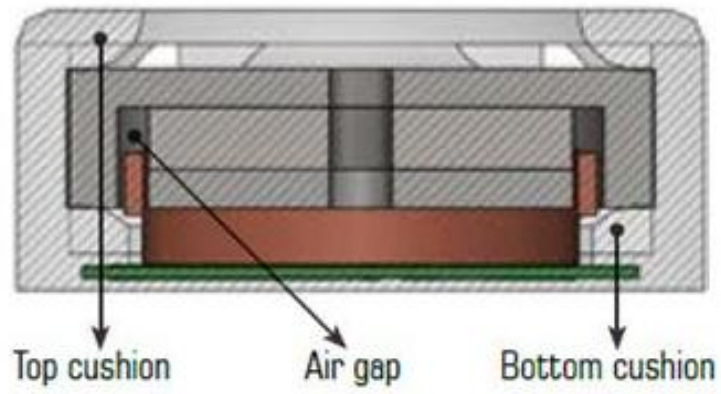
(b) Cross-section view

Fig 3.13 Assembly procedure and cross-sectional view of the transducer
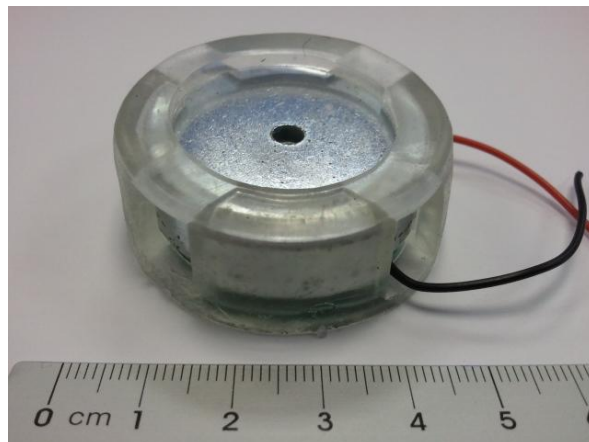
Fig 3.14 The magnetic, coil-drive plate and gel surround assembly (from left to right)

and the completed unit

104

3.2.5 Bracket

Figure 3.15 shows the drawing of a bracket base and cap.
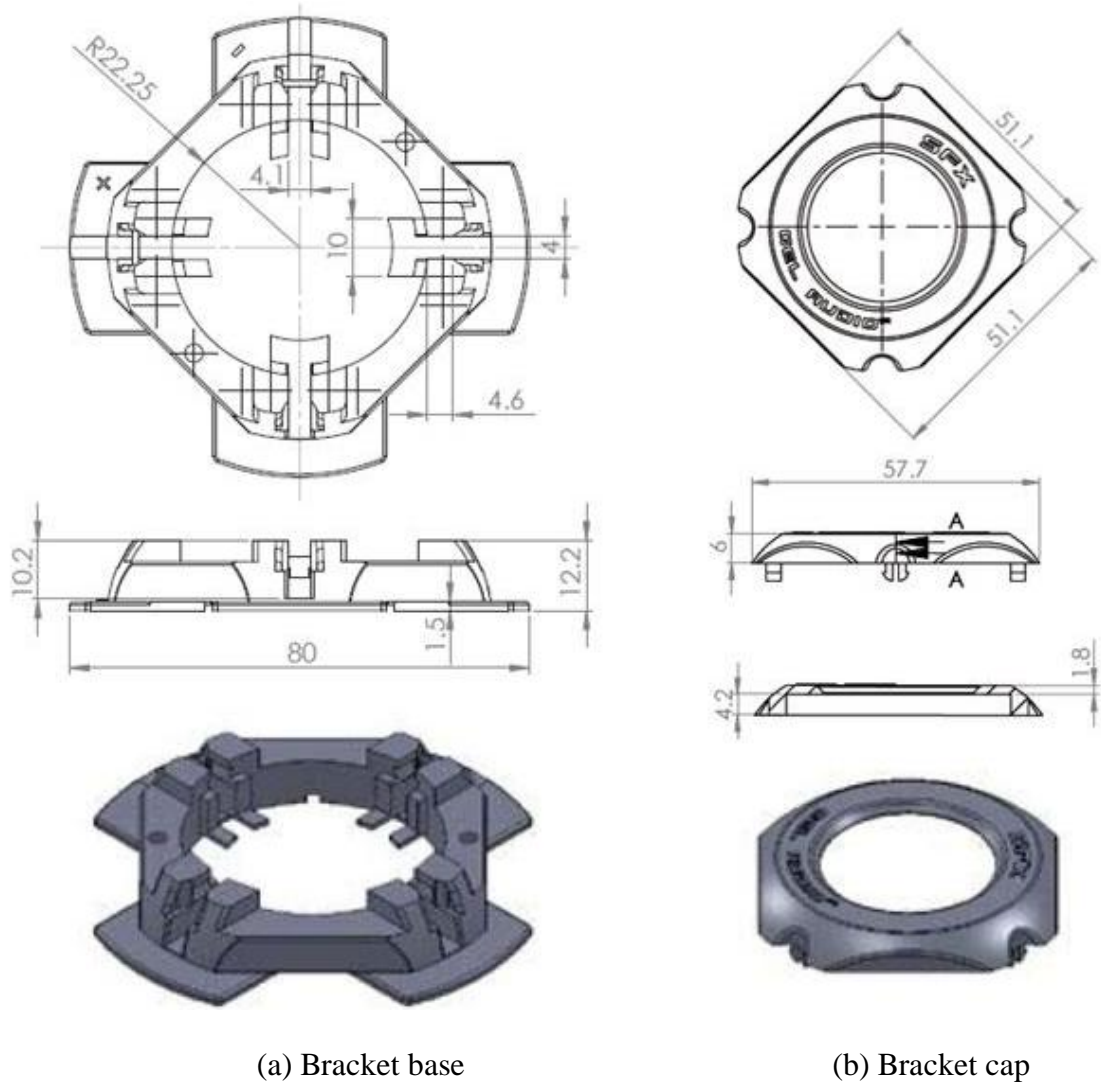
(a) Bracket base   (b) Bracket cap

Fig. 3.15 Drawing of the bracket

The gel-type audio transducer is assembled with the bracket base and cap as illustrated in Figure 3.16. Wires of the transducer were connected to terminal blocks in the bracket. This bracket is bonded to any flat surface by using a double sided foam tape.

The bracket was made of ABS. This component was designed by the author and other staff members at SFX Technologies, and subsequently manufactured by All Best Tech Ltd., in China.
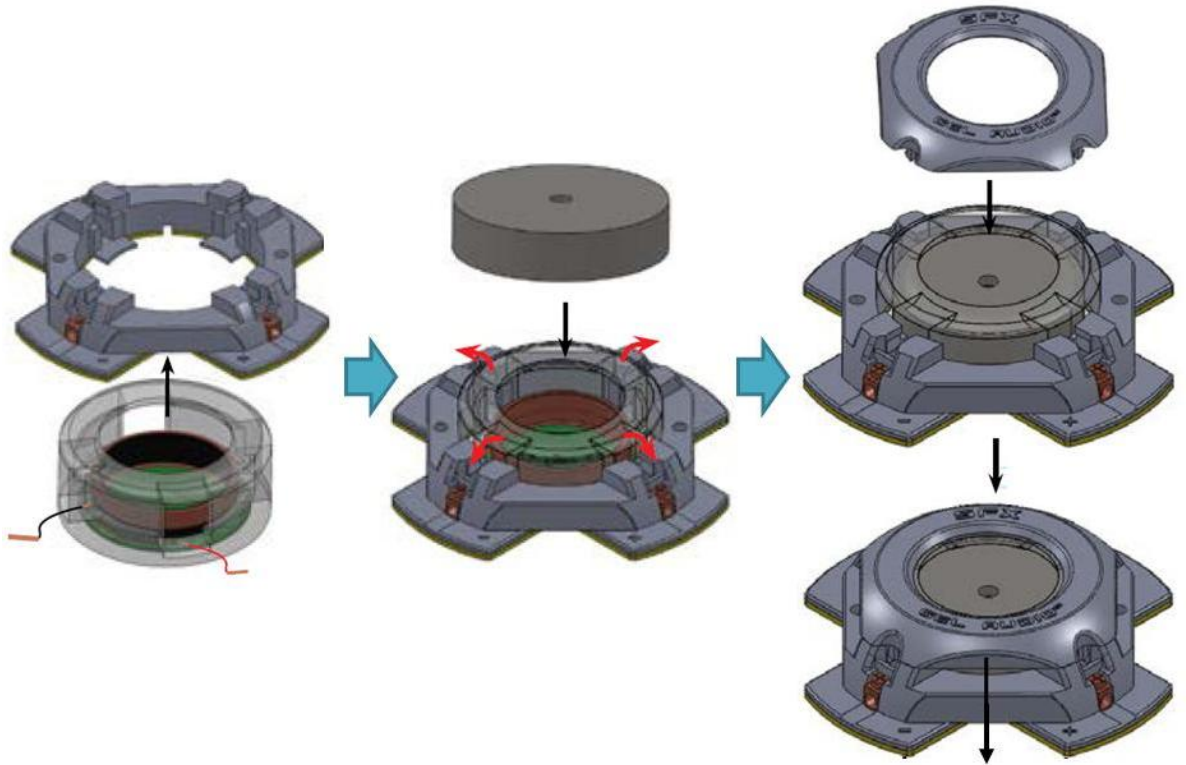
Fig. 3.16 Picture of the complete assembly

3.3 Finite element analysis

For this thesis, COMSOL multiphysics - FE analysis was used for various engineering problems, especially coupled phenomena. Models described in the following Chapter employ magnetic field physics from the AC/DC module in order to compute the force factor BL, electrical force F_e, and blocked coil impedance Z_b of the transducer as a function of frequency (20 Hz to 20,000 Hz). The stress-structure module was used to investigate the structural behaviour of a panel excited by the transducer. The COMSOL simulation models were all designed in-house by the author. The

acoustic module was also employed to predict the performance of the newly designed sample transducers. More details regarding COMSOL simulations will be presented in Chapter 4.

3.4 Acoustic measurement

For acoustic testing, an aluminium testing Jig was used. After the size and panel type were chosen and designed as described in section 1.3, the jig was built by All Best Tech Ltd. The aluminium testing Jig (size: 456mm x 356mm) consists of the four aluminium bars and frame base. A testing panel (size: 420mm x 320mm x 2mm) that is made of ABS, was clamped by using the bolts and nuts as shown in Figure 3.17 (a). Figure 3.17 (b) presents the testing set-up in the anechoic chamber. The chamber was originally built at SFX Technologies, UK.
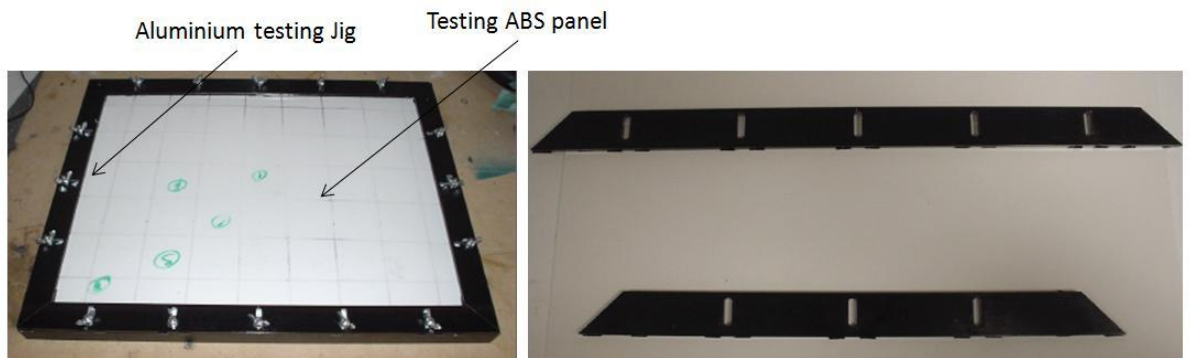
(a) The complete aluminium testing Jig and clamp plates
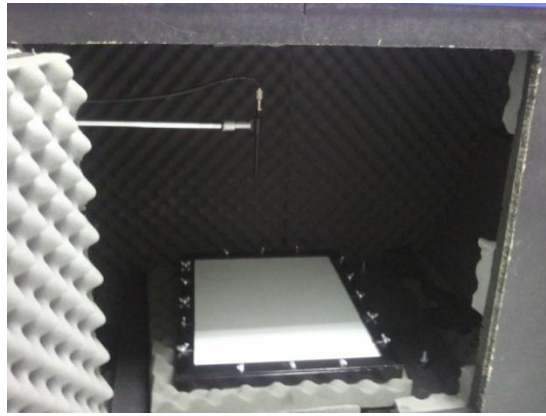
(b) Testing Jig in the anechoic chamber

Fig. 3.17 Testing Jig in the anechoic chamber

A testing transducer was positioned in the centre of the testing panel for measurement. The panel was placed 3cm high from the floor in the anechoic chamber. A microphone was set up at 25cm above the centre of the panel on axis as shown in Figure 3.18.
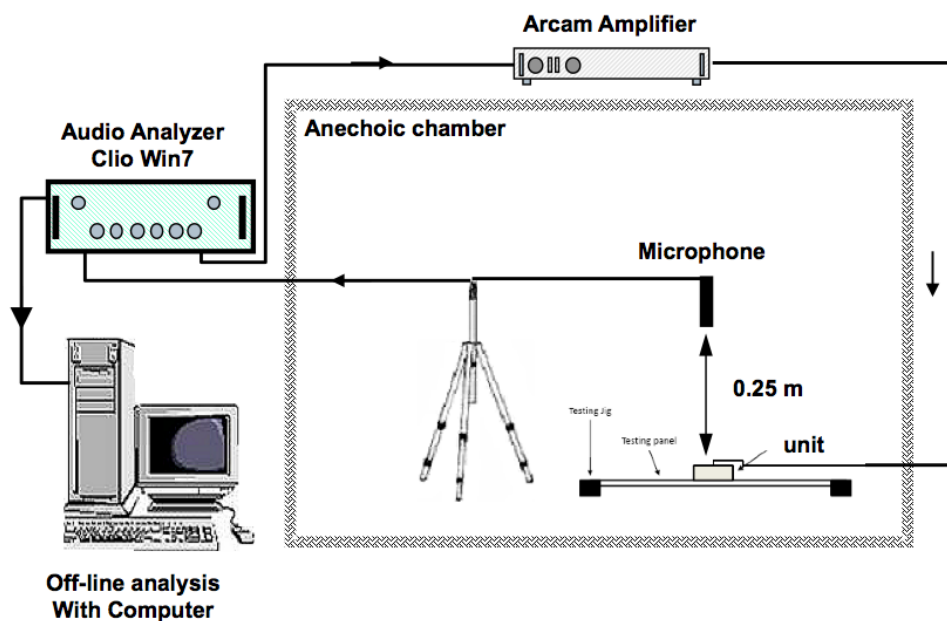
Fig. 3.18 Schematic diagram of the acoustic testing set-ups

A sinusoidal sine sweep at 1 W was driven from 20 Hz from 20,000 Hz. Audio analyser, Clio Win7 was used to measure the sound pressure level and an Arcam amplifier was employed to amplify the signal.

3.5 Laser scanning measurement

The vibrating mode, displacement, and acceleration of the panel excited by the gel-type audio transducer were observed as a function of frequency (20 Hz to 20,000 Hz) by a laser Doppler vibrometer (LDV) - model PSV_400_B manufactured by Polytek. The LDV measures the frequency shift of backscattered laser light from a vibrating panel. A periodic chirp signal (20 Hz to 20,000 Hz) at 1 W with a resolution of 5 Hz was fed into the transducer attached to the panel. The measurements were conducted by the author at SFX Technologies. For measurements, 200 points were chosen along the panel. The testing set-up was described in Figure 3.19 and Figure 3.20 shows each step of the scanning procedure.
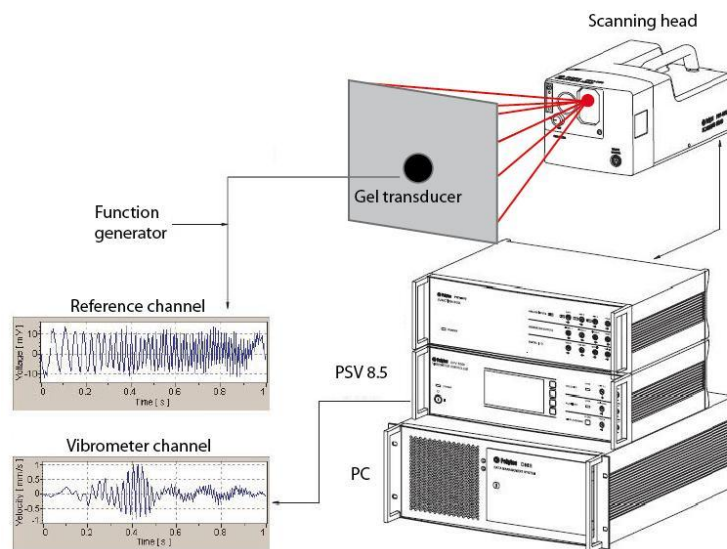
Fig 3.19 LDV measurement
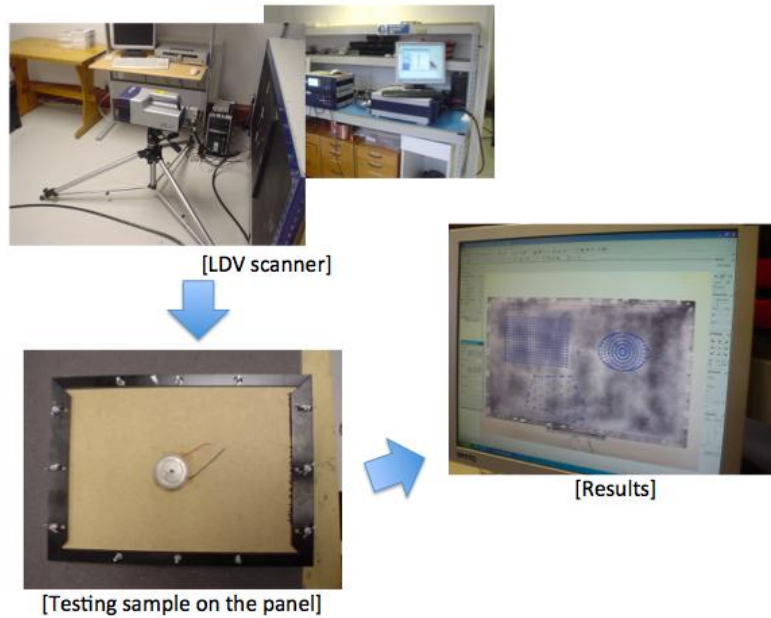
Fig 3.20 Testing procedure of the LDV scanning

3.6 Tensile and compression measurement

The mechanical properties of the elastomeric samples, in particular tensile and compressive performance, were investigated by the author at Edinburgh Napier University's Advanced Materials Centre.
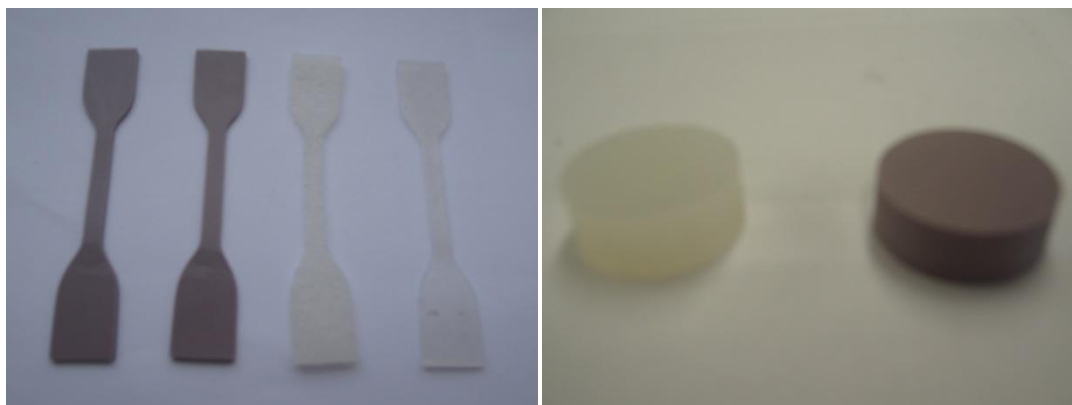
(a) Dumbbell shape of silicone sample   (b) Round shape of silicone sample

(c) Tensile test   (d) Compression test

Fig 3.21 Elastomeric samples and testing pictures

Dumbbell and round shape of silicone samples were made for the tensile and compression test respectively as shown in Figure 3.21. A JJ Lloyd single column tester with a 100 and 50 N load cell for the tensile and compression test was used. The testing speed was set at 8.33 ms^{-1}.

3.7 Hardness measurement

A Shore 00 digital durometer was used to measure the hardness of elastomeric samples. On this instrument, the indentor has a round tip and is pressed onto the test piece for 3 seconds (the dwell time). The test piece is 6.35 mm thick and a measurement is taken after averaging values of three meter readings. Figure 3.22 shows the type of durometer used. All hardness tests were conducted by the author at Edinburgh Napier University.

Fig. 3.22 The Shore 00 digital durometer

3.8 Tesla measurement

The magnetic flux density along the "air gap" in the magnetic assembly was measured by a Gauss meter. An average of 4 values was used to determine the flux density in accordance with the procedure outlined in Figure 3.23. Once again these tests were carried out by the author at Edinburgh Napier University.

Gauss meter prove must be placed where the coil is meant to be.

Measurement points
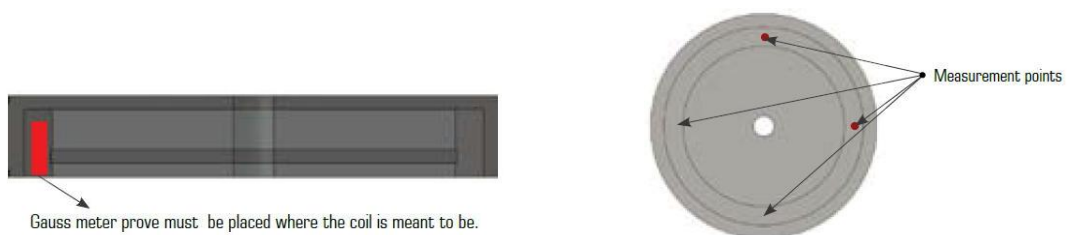
(a) Position of the Gauss meter in the magnetic assembly   (b) 4 measurement points

(c) Gauss meter measuring the magnetic flux density

Fig 3.23 Tesla measurement

3.9 DMA (dynamic mechanical analysis) measurement

The $tan\,\delta$ of the 35 and 70 Shore 00 gel surrounds as a function of frequency was measured by the DMA technique [the model is PE DMA 8000 manufactured by Perkin-Elmer] as shown in Figure 3.24. Measured data were imported into the simulation to predict the structural and acoustical behaviours of transducers. Testing was performed in shear mode using 3.1 mm thick and 5.6 mm diameter test pieces.

Fig 3.24 DMA tester [PE DMA 8000]

The DSA (peak to peak dynamic strain amplitude) was set at 0.066 % over the frequency range 1 to 500 Hz. Seven repeated sweeps were made and the mean was reported. Samples were bonded to the shear plates using cyanoacrylate adhesive. The shear head set-up of the DMA is shown in Figure 3.25. These measurements were carried out by Artis, UK.
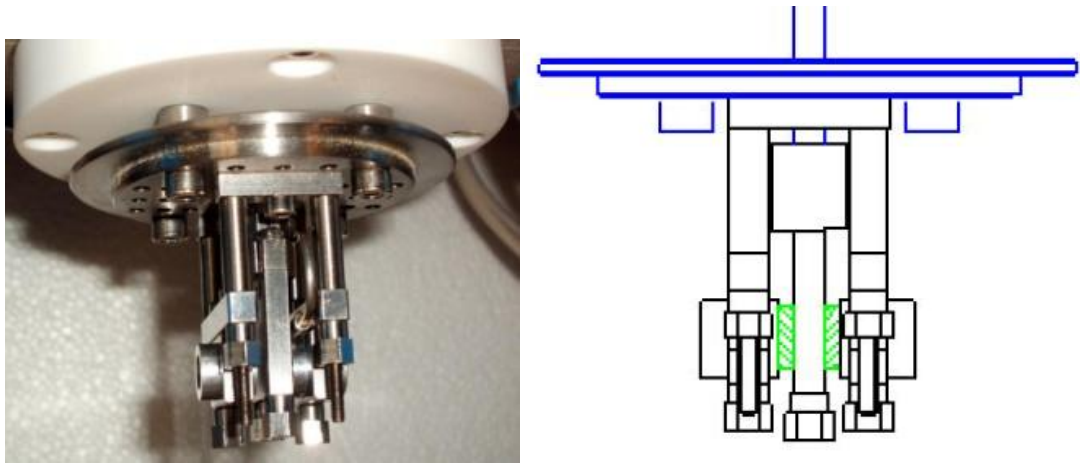
Fig. 3.25 Shear head set-up of DMA

3.10 Conclusions

In section 3.2, the gel-type audio transducer that will be used for experiments was discussed. Section 3.2.1, 3.2.2 and 3.2.3 described the production of each part – the magnetic assembly, coil-drive-plate assembly, and the gel surround. For materials used for the gel surround, a RTV silicone elastomer, TPE, and a silicone foam elastomer in a different hardness range were employed. Also FE analysis by using COMSOL multiphysics for the magnetic, stress-structure, and acoustic simulation was briefly introduced in this Chapter but more details will be discussed in Chapter 4. Mechanical testing methods including advanced techniques such as the LDV and DMA were

presented. Testing results, carried out by these methods, will be investigated in the following Chapter.

CHAPTER 4 – THEORETICAL AND EXPERIMENTAL INVESTIGATION

4.1 Introduction

The energy transfer process of the gel-type audio transducer can be distinguished to three stages: 1) generation of the output driving force, 2) mechanical energy transfer from the transducer to a solid surface (in this case, a panel) to which the transducer is attached, and 3) radiation of the transferred energy in the form of acoustic waves. The gel surround that is made of a soft elastomer, is a critical part of the gel-type audio transducer because this is directly involved in those three stages. The following sections from 4.2 to 4.4 will discuss the theoretical problems of each stage and experiments including the FE analysis. Conclusion of the Chapter will be summarised in section 4.5.

4.2 Effect of soft elastomers on output driving force of the gel-type audio transducer

In this section, the mechanism of the gel-type audio transducer is discussed. The impedance analogue model was developed to identify the factors affecting the performance of the transducer. The effect of these governing factors on a output driving force generated by the transducer was also investigated. The FE analysis was used to

simulate the problems, and thereafter, the experiments were carried out to validate the simulation results.

4.2.1 Theoretical problems

The schematic construction of the gel-type audio transducer is shown in Figure 4.1.
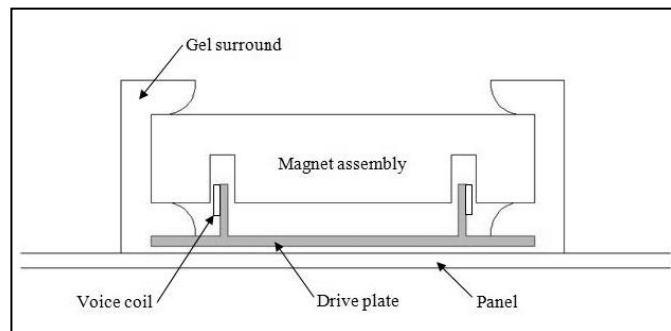
Fig. 4.1 Schematic construction of the gel-type audio transducer

The mechanism of the transducer can be considered as a coupling of two separate transducers as shown in Figure 4.2 - the actuator system (a) that converts the electrical energy to mechanical energy and the driving system (b) that converts the mechanical energy to acoustic energy. Those two independent mechanisms are coupled by means of the gel surround.

The device can be constructed as a mechanical element of two-mass-spring system that can be used to analyse complicated mechanical systems. In the actuator system (a) as shown in Figure 4.2, the electrical force F_e is generated as a product the magnetic flux density B, coil length L, and the total electric current I_e.

$$F_e = BLI_e \qquad (4.1)$$
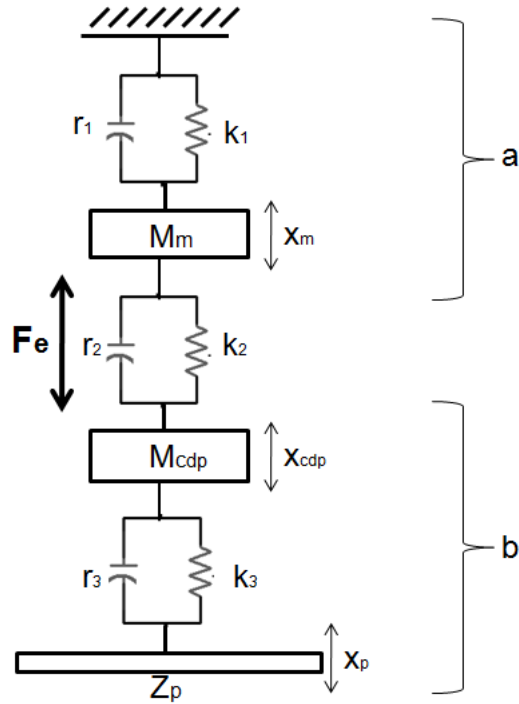
Fig. 4.2 Mechanical element of the gel-type audio transducer

The voice coil consists of a number of turns N, of thin copper wire and occupies a cross-sectional area A. Thus, F_e from the current on the coil hence becomes:

$$F_e = -I_e \, (2\pi N / A_c) \int r \, B_r dA_c \qquad (4.2)$$

$$BL = -\, (2\pi N / A_c) \int r \, B_r dA_c \qquad (4.3)$$

where the integral is taken over the coil domain.

BL is also known as the force factor that determines F_e.

$$I_e = (V_I - V_{emf})/Z_b \tag{4.4}$$

where V_I and Z_b are the input voltage and blocked coil impedance respectively. V_{emf} denotes the back Electro Magnetic Force (EMF) - the voltage induced in the voice coil due to its motion through the permanent magnetic field in the gap.

$$-V_{emf} = -v(2\pi N/A_c) \int r \, B_r dA_c \tag{4.5}$$

where v is a velocity travelling perpendicular to the wire. The wire gets an induced back *EMF* equal to $v\boldsymbol{BL}$.

In Figure 4.2, M_m, M_{cdp} and Z_p are the mass of the magnetic and coil-drive plate assembly as well as the mechanical impedance of the panel respectively. Displacement of the magnetic, coil-drive plate assembly and the panel are given as symbols, x_m, x_{cdp} and x_p respectively.

Finally r_1, r_2, r_3, k_1, k_2 and k_3 are the resistive damping and stiffness of the gel cushions and pad between M_m, M_{cdp} and Z_p.

The gel cushions and underneath pad of the gel surround form one part assembly moulded from a single grade of an elastomer material. Thus for the purpose of the model, the resistive damping and stiffness values of the elastomer are assumed to be the same at any position within the gel surround: $r_1, = r_2 = r_3$ and $k_1 = k_2 = k_3$.

The operation of the actuator system can be expressed by,

$$M_m \times d^2x_m/dt^2 - r\, dx_m/dt - kx_m = F_e(t) \tag{4.6}$$

This equation can be rewritten as:

$$j\omega\, M_m v_m - r v_m - kx_m = F_e(t) \tag{4.7}$$

where v_m is the velocity of the magnetic assembly.

The driving system (b) is given as:

$$Z_p \times dx_p/dt = M_{cdp}\, d^2x_{cdp}/dt^2 + F_e(t) \tag{4.8}$$

This equation can be rewritten as;

$$Z_p v_p + j\omega\, M_{cdp} v_{cdp} = F_e(t) \tag{4.9}$$

where v_p and v_{cdp} are the velocity of the panel and coil-drive plate assembly respectively.

The total output driving force F_{total} that is applied to the panel, is $Z_p v_p$ and it is expected to be converted to the acoustic energy. In this thesis, the acoustic energy is expressed as the sound pressure level (SPL).

$$F_{total} = j\omega\, M_m v_m - j\omega\, M_{cdp} v_{cdp} - (r v_m + (1/C)x_m) \tag{4.10}$$

where C and v_m is the compliance which is a reciprocal of k of the gel surround, and velocity of the magnetic assembly respectively.

Figure 4.3 shows the complete impedance analogue model of the gel-type audio transducer.
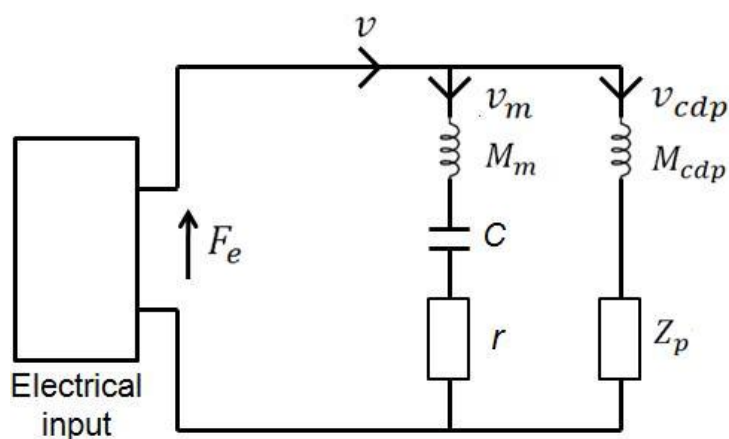
Fig. 4.3 Complete impedance analogue model of the gel-type audio transducer

This impedance analogue model demonstrates that the velocity of the panel excited by the gel-type audio transducer is governed by the values of either M_m or C (or both) which are acting as a high-pass filter at low frequency range and by the M_{cdp} at high frequencies. It means that if M_m or C (or both) increase, the total output driving force that is applied to the panel $Z_p v_p$ within this low frequency band also increases giving rise to greater panel displacement. This principle takes advantage of the inertial effect.

There is a phase shift occurred between the F_e and oscillation of the magnetic and coil-drive plate assembly due to the damping nature of the gel surround. The phase is given by the angle φ:

$$\varphi = tan^{-1}(2\zeta\gamma/(1 - \gamma^2)) \tag{4.11}$$

where ζ is the damping ratio of the gel surround and γ is the ratio of the harmonic force frequency ω to the natural frequency of the system ω_0.

Thus the phase of the F_e to the forced oscillation of the magnetic and coil-drive plate assembly are φ_m and φ_{cdp} respectively, thereby the phase shift between both assemblies can be expressed as $\varphi_{cdp} - \varphi_m$.
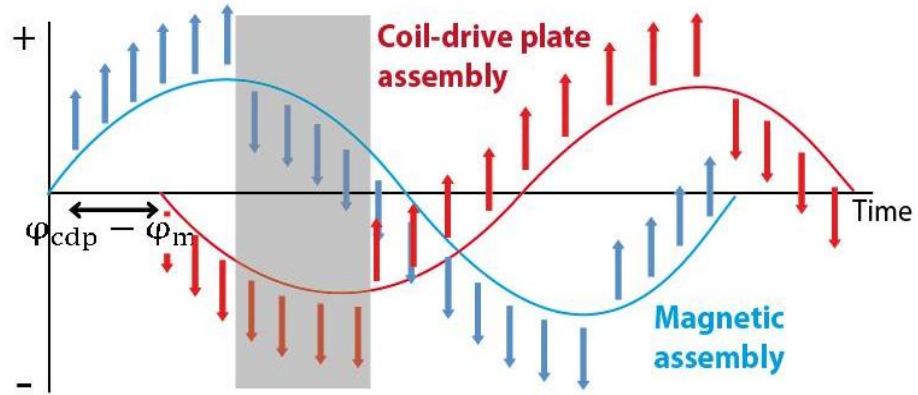
Fig. 4.4 Phase of the magnetic and coil-drive plate assembly

Figure 4.4 shows that the force transferred to the panel reaches a maximum, when the magnetic and coil-drive plate assembly accelerate towards the panel in phase. This is highlighted in the grey on Figure 4.4. As a result, the inertial force induced by the movement of the magnetic assembly is added to the coil-drive plate assembly, resulting in an amplified force.

The value of compliance C in an elastomer affects the compressibility of the gel surround manufactured from it: if the material with higher compliance, and, as the result, with lower hardness, is chosen, the gel surround becomes more compressible. As a result, this gel surround allows the magnetic and coil-drive plate assembly to oscillate with higher amplitude, so greater movement of these assemblies can be obtained, resulting in enhancement of the output driving force of the transducer. The same effect is also observed when larger value of M_m is used. The enhancement of the output driving force is clearly observed at low frequency where movement of the magnetic and coil-drive plate assembly is large.

The compliance C characterises the damping ability of materials in the expression of $tan\,\delta$ (tan delta or loss factor) [72]. The loss factor is a phase angle between the elastic modulus and loss modulus that represents a damping ability of a material measured by the DMA (see Chapter 3.9), which was used for the experiments.

Thus, the output driving force of the gel-type audio transducer can be enhanced by using the material with the large value of the C for the gel surround and greater mass of the magnetic assembly M_m at low frequency range. Furthermore, The relationship between the resonant frequency of the transducer f_0 and the characteristics of the material are shown in Helmholtz Resonance expression [51]:

$$f_0 = 1/(2\pi\,\sqrt{C} + M_m) \tag{4.12}$$

The equation (4.12) demonstrates that the increased values of C of M_m (or both) lowers f_0 of the transducer, that enables it to operate to lower frequency range.

4.2.2 Simulations and experiments

Four samples were manufactured for the series of testing to observe the effect of the change of the M_m and compliance C of the gel surround on the output driving force of the gel-type audio transducer. The force factor *BL,* electrical force F_e, and other parameters of sample transducers were simulated by using the COMSOL multiphysics.

The laser scanning measurement (for methodology refer to Chapter 3.5) and other mechanical tests were carried out to measure an output driving force of the sample transducers.

4.2.2.1 Test procedure

	Weight of M_m	Hardness of gel surround
Transducer A	80 g	35 Shore 00
Transducer B	40 g	35 Shore 00
Transducer C	40 g	35 Shore 00
Transducer D	40 g	70 Shore 00

Table 4.1 Four sample transducers

Four sample transducers were prepared for the experiments. The testing parameters of these transducers are shown in Table 4.1. The transducers A and B were used for the weight study, and the transducers C and D for the effect of the C on the output driving force of the transducer.

The mechanical properties of the RTV silicone samples used to produce the samples of the gel surround are shown in table 4.2.

	Hardness of gel surround	
	35 Shore 00	70 Shore 00
Density, ρ	1050 kg/m^3	1090 kg/m^3
Poisson's ratio, v	0.49	0.49
Young's modulus, E	7×10^{-2} MPa	6.2×10^{-1} MPa

Table 4.2 Properties of the RTV silicone samples

The DMA measurement technique was used to measure the compliance C of 35 and 70 Shore 00 in the form of $tan\ \delta$.

The laser scanning measurement was used to record the map of displacements of the panel excited by the transducer as a mean of measuring the output driving force of the transducer.

The FE analysis, using COMSOL multiphysics, was carried out to compute electrical parameters such as BL, Z_b and F_e.

4.2.2.2 FE analysis

For the FE analysis, the AC/DC module was used to simulate the B, L_b, and the F_e to calculate the BL, Z_b and inductance of the blocked coil (imaginary part of Z_b). Figure 4.5 shows a 2D CAD drawing of the transducer for the electromagnetic simulation. Although the voice coil consists of many turns of wire, it is for simplicity modelled as a homogenised domain.
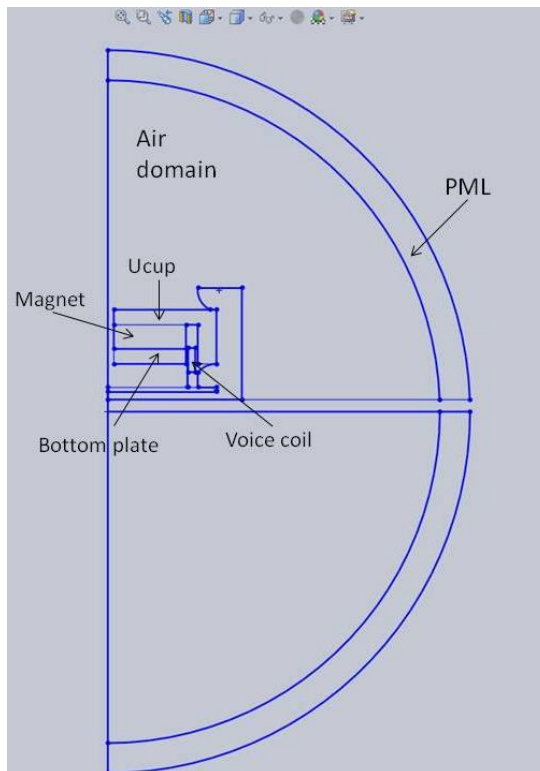
Fig. 4.5 CAD drawing of the model geometry

Figure 4.6 presents the domains (a) of the transducer and mesh of these domains (b) respectively in COMSOL software. The model is the axial-symmetric. Maximum and minimum element size of the mesh is 0.0402 m and $1.8e^{-4}$ m respectively; and maximum element growth rate is 1.3. Computed number of mesh elements for this model was 7311.
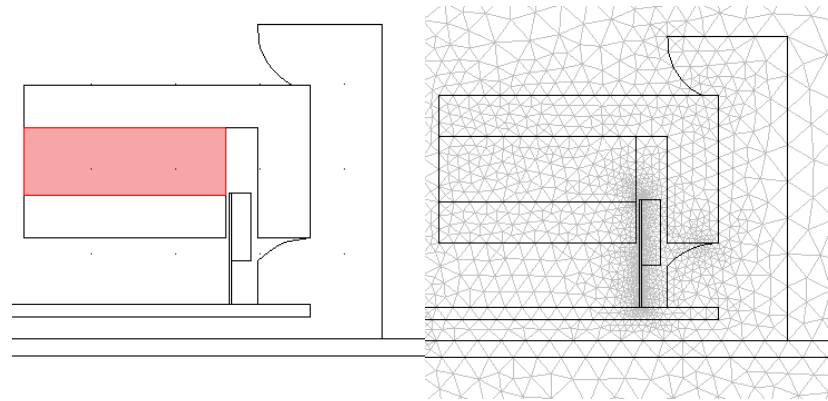
(a) Drawing of the domains   (b) Mesh of the domains

Fig. 4.6 Drawing of magnetic assembly

A permanent magnet used is a rare-earth magnet (NdFeB) with *B0* = 1.42 T. All input constant parameters required for the simulation are shown in Figure 4.7.

Name	Expression	Value	Description
V0	4[V]	4 V	Peak driving voltage
R0	7.34[ohm]	7.34 Ω	Blocked coil resistance
N	105	105	Number of turns in coil
B0	1.42[T]	1.42 T	Remnant magnet flux density
freq	0	0	Frequency for stationary analysis
omega0	2*pi*f0		Angular frequency at which loss factor is given

Fig. 4.7 Parameters for the electromagnetic simulation

For stationary analysis as required for electromagnetic simulation, the frequency variable was set as frequency = 0.

The variables required for the problem solution are listed in Figure 4.8.

Fig. 4.8 Variables for the electromagnetic simulation

The complex value Z_b was computed as a function of frequency between 20 Hz and 20 KHz.

4.2.3 Results and discussions

Electrical parameters of the sample transducers were computed and the results were shown in Figure 4.9. The simulation indicates that the average magnetic flux density in the air gap, where the coil is placed, is 0.95 T.
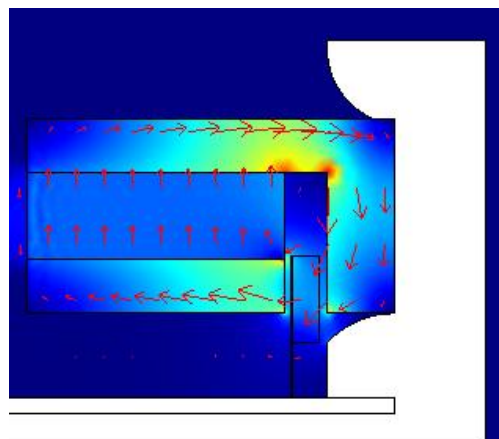
Fig 4.9 Predicted flow of magnetic flux within the magnetic assembly

The L_b, that is the imaginary part of the Z_b, is presented in Figure 4.10 and the real part of the Z_b, which is the electrical resistance R_b, is also shown in Figure 4.11. These values lead to the Z_b by the following expression;

$$Z_b = R_b(frequency) + j\omega\, L_b(frequency) \qquad (4.13)$$

The BL calculated is $7.5\ \text{T} \cdot \text{m}$ and the F_e for the four sample transducers as a function of frequencies in the range 10 Hz to 1000 Hz is given in Figure 4.12.
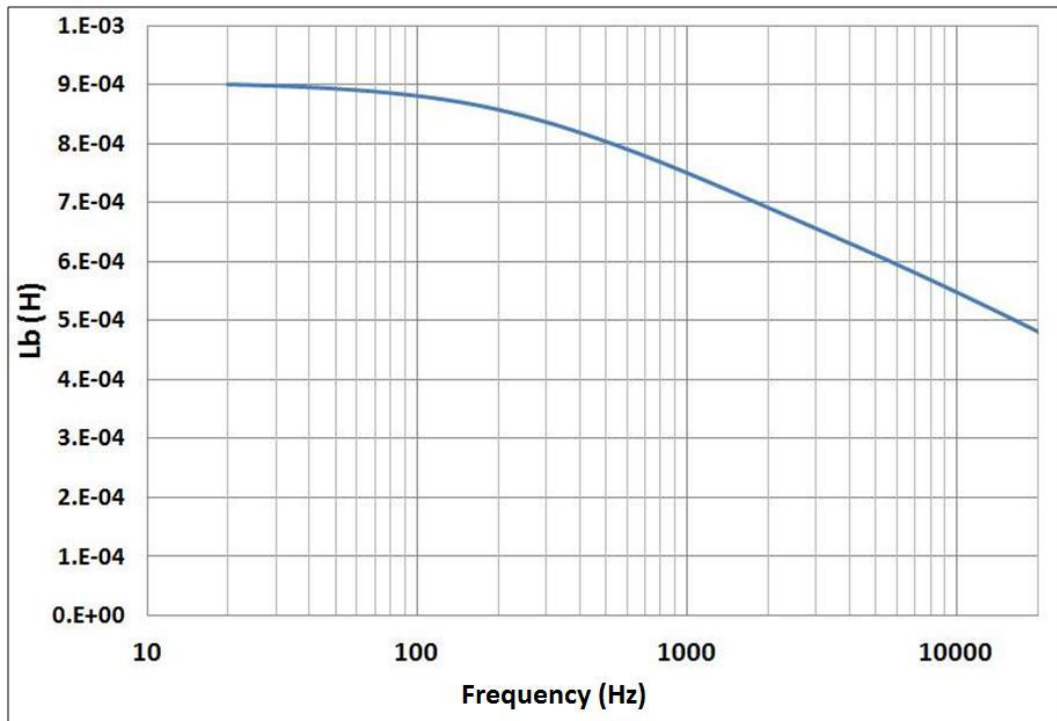
Fig. 4.10 The blocked coil inductance L_b
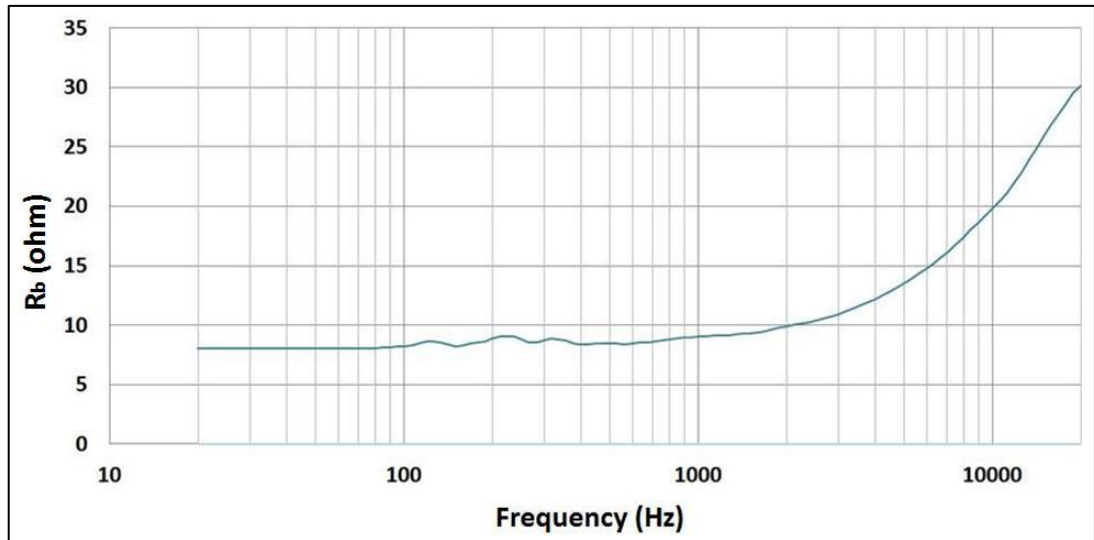
Fig. 4.11 The electrical resistance R_b
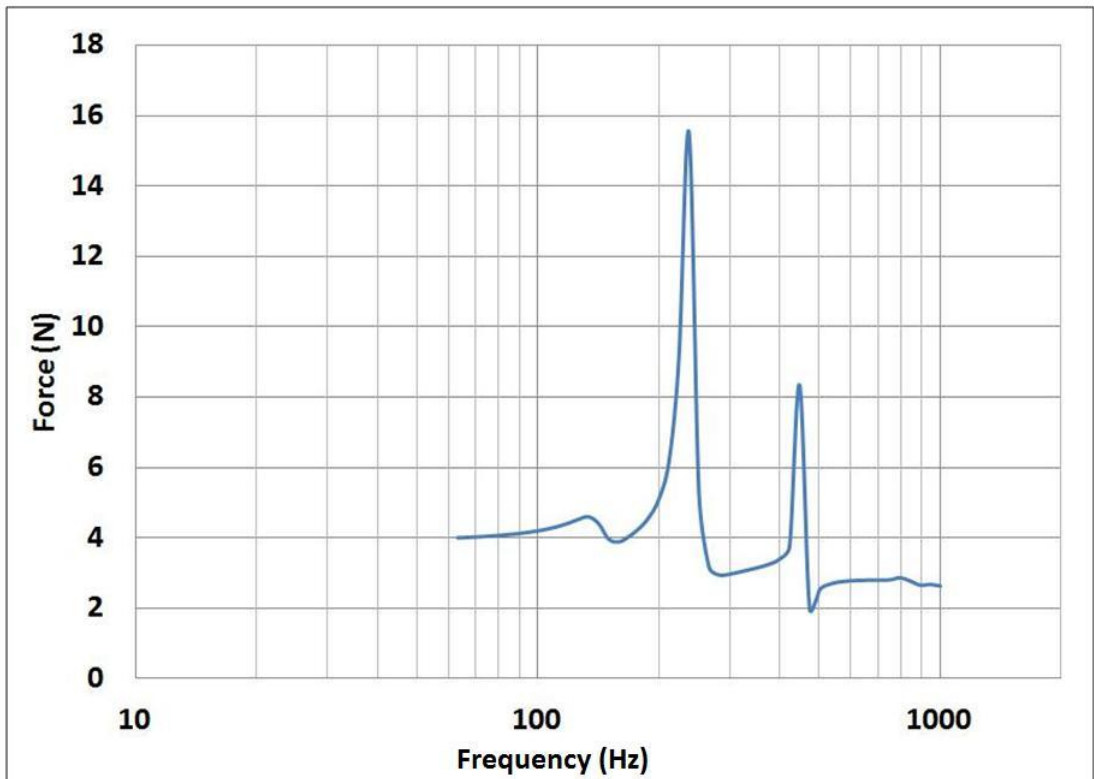
Fig. 4.12 The electrical force F_e

Thus the F_e of the four transducers generated as the product BL and Z_b changes

between 3 to 4 N between 10 and 1000 Hz with the electrical resonant peaks at 250 Hz

130

and 550 Hz. However the following experimental results show that the output driving force of the transducers change depending on the values of the M_m and C.

Figure 4.13 shows the average displacement of the panel excited by the transducer A and B where the M_m for the transducer A is 80 g and for transducer B is 40 g. The panel excited by the transducer A has the first resonant peak at 30 Hz with the magnitude of 3.5 µm, while for the transducer B the resonant frequency shifts to 60 Hz with the magnitude of 0.95 µm. The magnitude of the average displacement for the transducer A between 20 Hz and 200 Hz is between 0.5 µm and 3.5 µm; and for transducer B is between 0.05 µm and 1 µm. The results suggest that the increase of the mass of the magnetic assembly M_m enhances the output driving force applied to the panel. Also larger M_m results in the reduction of resonant frequency f_0 that extends a working frequency down to 30 Hz.
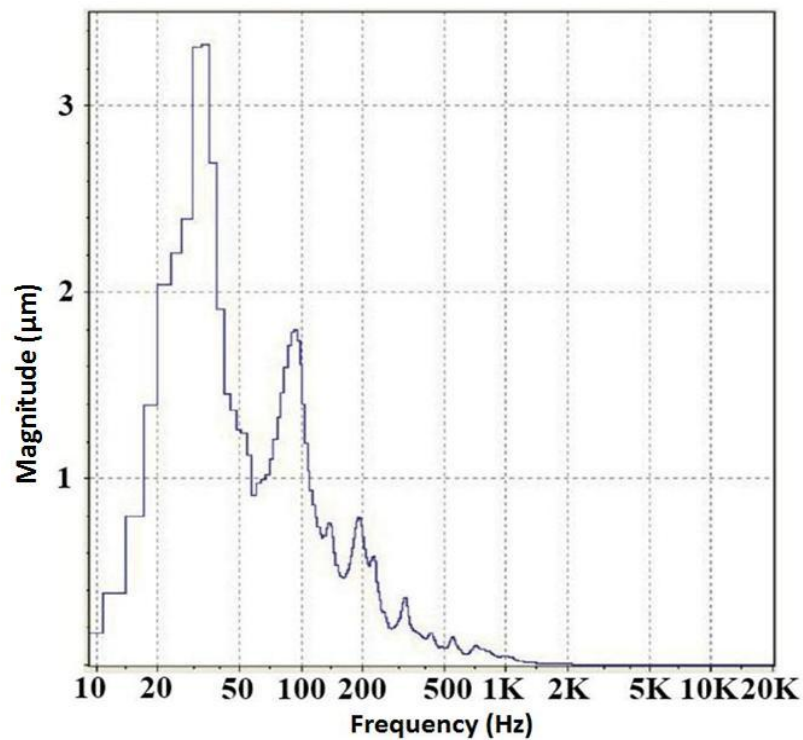
(a) Transducer A
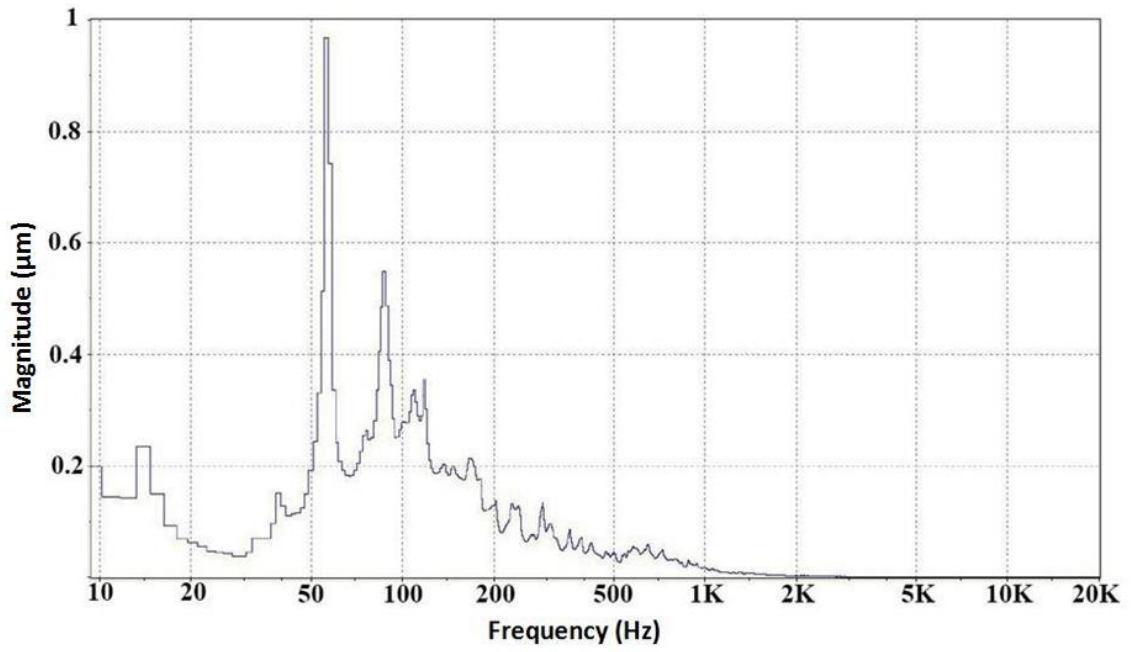
(b) Transducer B

Fig. 4.13 Average displacement of the transducer A and B
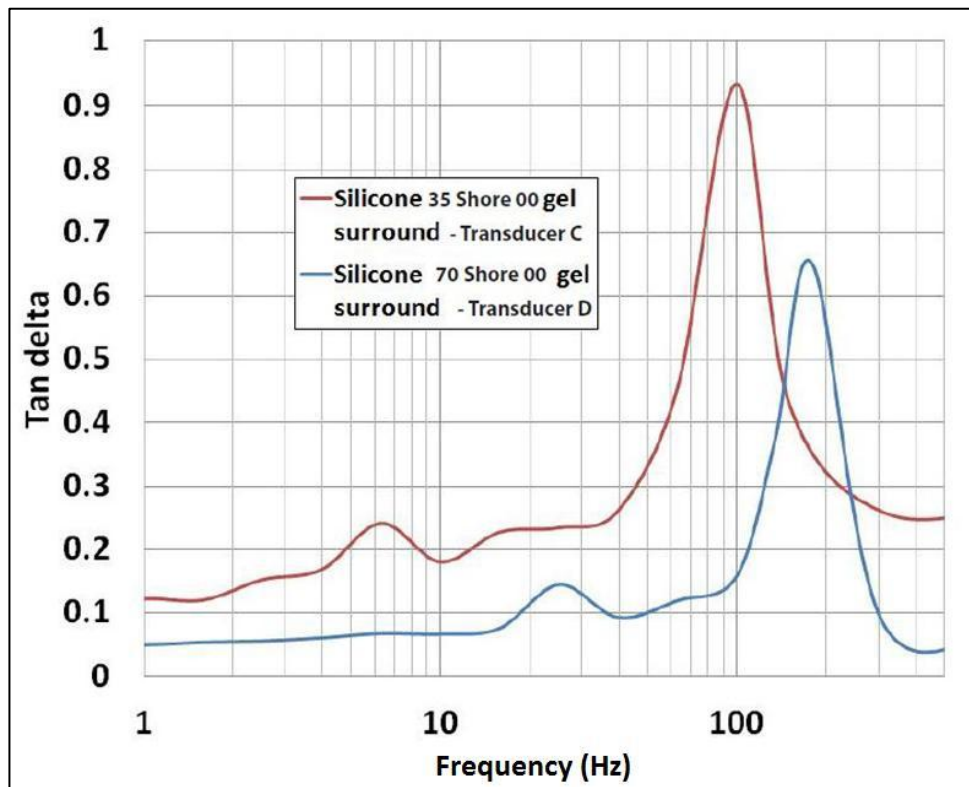
Fig. 4.14 The $tan\ \delta$ of 35 and 70 Shore 00 gel surrounds

Figure 4.14 shows $tan\,\delta$ of 35 and 70 Shore 00 gel surrounds measured at frequencies in the range 1 to 500 Hz (the measuring frequency was limited to 500 Hz due to instrument resonance occurring). When 35 Shore 00 material is used for gel surround, its loss factor $tan\,\delta$ changes between 0.1 and 0.25 over the chosen frequency range, with the resonant frequency at 100 Hz (0.9 of the peak $tan\,\delta$), whilst the gel surround made of 70 Shore 00 has $tan\,\delta$ under 0.1 over the same frequency range with the resonant frequency of 180 Hz (0.65 of the peak $tan\,\delta$). The results demonstrate that 35 Shore 00 elastomer has twice bigger the loss factor value than 70 Shore 00 elastomer.

Therefore, when the 35 Shore 00 material is used to produce the gel surround for the transducer C, the magnetic and coil-drive plate assemblies move with greater magnitude by the inertial force, comparing with the transducer D with the gel surround made of 70 Shore 00 elastomer. So the greater output driving force can be achieved by the transducer C with the 35 Shore 00 gel surround. The performance of the transducer C and D is shown in Figures 4.15 and 4.16 in terms of the panel's displacement, as function of frequencies in the range 10 Hz to 20,000 Hz, and the displacement of the longitudinal centre axis of the panel at 120 Hz and 180 Hz (the highest peak) respectively. The magnitude of the average displacement for the transducer C between 20 Hz and 200 Hz is between 0.25 µm and 1.5 µm; and for transducer D is between 0.08 µm and 0.6 µm. So the magnitude of the average displacement of the panel excited by the transducer C with the 35 Shore 00 gel surround is almost twice higher than the panel excited by the 70 Shore 00 gel surround transducer D. Figures 4.15 (b) and 4.16 (b) show that the peak displacement of the panel excited by the transducer C is 1.5 µm whereas the transducer D is 0.55 µm. Thus the enhanced output driving force of the transducer that causes the greater displacement of the panel was achieved by increasing the value of $tan\,\delta$ which represents C.
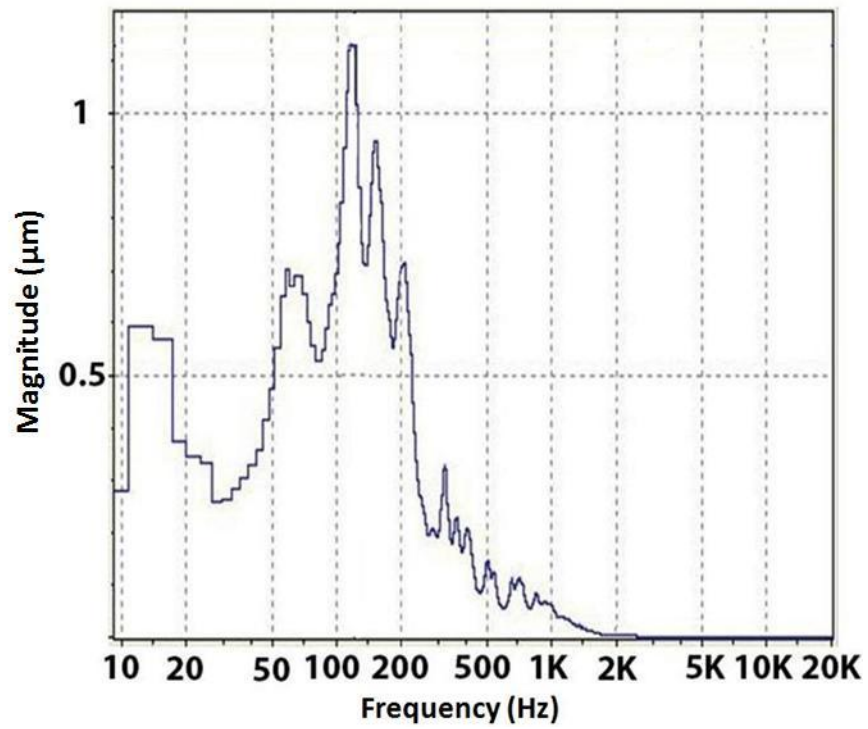
(a) Average displacement from 20 Hz to 20,000 Hz
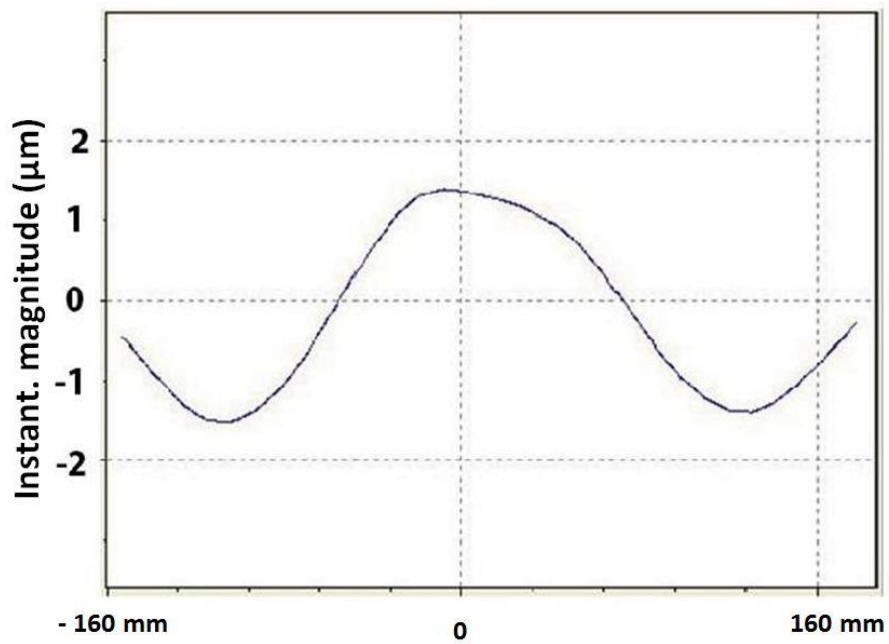
(b) Displacement of the profile of the panel at 120 Hz

Fig. 4.15. Displacement of the panel excited by 35 Shore 00 gel surround transducer C

The transducer C has its first resonance f_0 at around 70 Hz, as shown in Figure 4.15 (a). The first resonance f_0 for the transducer D presented in Figure 4.16 (a) is the first peak on the graph after the ambient vibration at 10 Hz. This was measured at 120 Hz.. Third resonance f_0 of the transducer C and D was observed with a highest amplitude at 120 Hz and 180 Hz respectively. Thus as indicated in equation (4.12), the larger the value of C of the gel surround (in this case, 35 Shore 00), the lower the resonance f_0 of the system, so it can extend its operating frequency range down to lower frequencies.
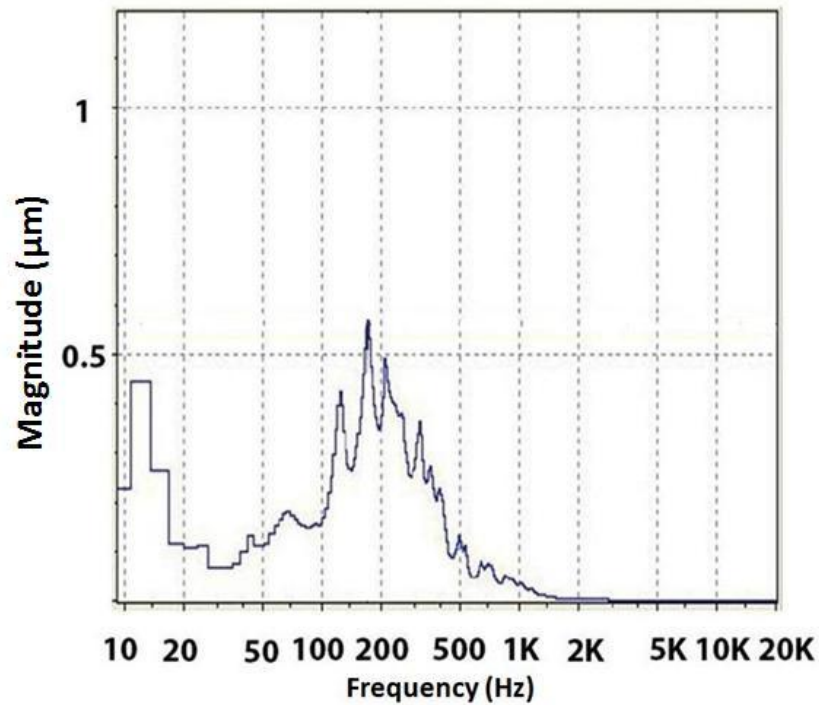
(a) Average displacement from 20 Hz to 20,000 Hz
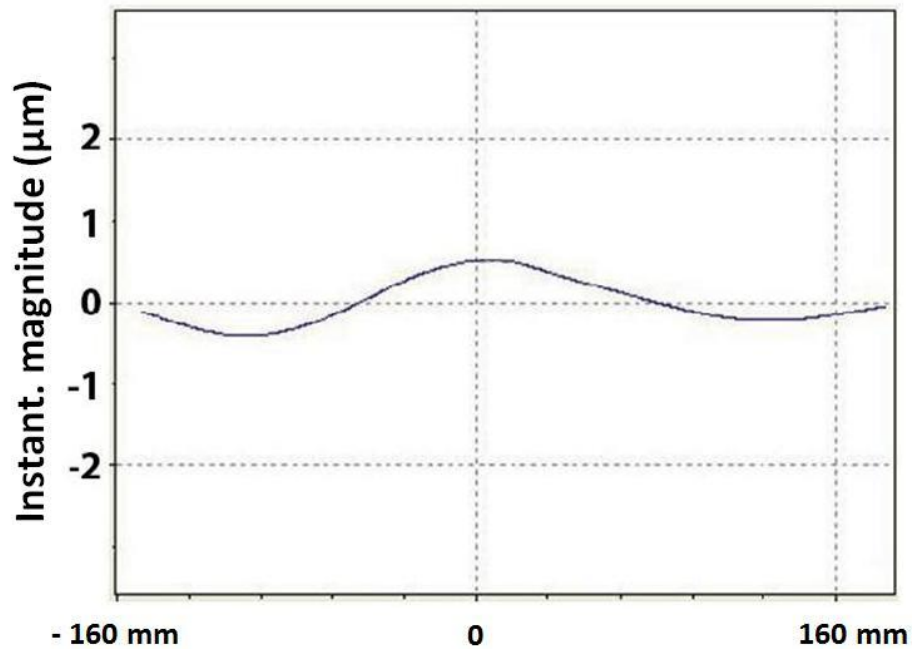
(b) Displacement of the profile of the panel at 180 Hz

Fig. 4.16. Displacement of the panel excited by 70 Shore 00 gel surround transducer D

4.2.4 Summary

The factors governing the performance of the gel-type audio transducer were theoretically identified and the effect of the M_m and C was investigated by COMSOL Multiphysics simulation software combined with physical experiments.

It was demonstrated that the total output driving force generated by the gel-type audio transducer was greatly enhanced at low frequency range when the larger M_m or C of the gel surround (or both) were used. This effect was noticeably observed at low frequencies where the movement of the magnetic and coil-drive plate assembly is large. For example, the panel excited by the transducer A (80 g of the M_m) and B (40 g of the M_m) has the first resonant peak at 30 Hz and 60 Hz with the magnitude of 3.5 μm and 0.95 μm of the displacement respectively. Also the magnitude of the average

136

displacement of the panel vibrated by the transducer A between 20 Hz and 200 Hz is between 0.5 μm and 3.5 μm whereas the transducer B's is between 0.05 μm and 1 μm. Thus the larger M_m increases the output driving force of the transducer. For the effect of the C, the displacement of the longitudinal centre axis of the panel, excited by the transducer C incorporating 35 Shore 00 gel surround, at 120 Hz (the highest peak) was measured at 1.5 μm whilst the 70 Shore 00 gel surround transducer D generated the displacement of 0.55 μm at 180 Hz (the highest peak). The first (third) resonance f_0 of the transducer C and D were also measured at 70 Hz (120 Hz), and 120 Hz (180 Hz) respectively.

Thus the larger M_m or C ($tan\,\delta$) (or both) of the gel surround increases the output driving force of the gel-type audio transducer and extends its operating frequency range to lower values by reduction of the f_0 of the system.

The increase of M_m means the enlargement of the magnet, which cannot be utilised for the gel-type audio transducers. The size of the magnet and its weight for the applications have to be kept minimal for miniaturisation of woofer devices. Therefore the focus of the remaining thesis will be on the effect of changing C ($tan\,\delta$) in the following Chapters.

4.3 Effect of soft elastomers on energy transfer

To work as a driving unit, the gel-type audio transducer should be attached to a solid panel. For this system the gel surround acts as a coupling medium between the transducer and panel. In this section the role of the gel surround in transferring the

energy to the panel and the behaviour of the vibrating panel excited by the transducer are discussed. The FE analysis was used to predict the panel's behaviour as a function of frequency. For experiments, the laser scanning and acoustic measurement were employed to observe vibrating modes of the panel, the mechanical distortion, and the sound pressure level radiated from the panel.

4.3.1 Theoretical problems

4.3.1.1 The role of gel surround in the energy transfer

The gel surround acts as a shock absorber and is illustrated in Figure 4.17. The figure describes the panel's deflection at 2nd mode frequency where the panel's movement starts to break up, and the reflected transverse waves travelling towards the transducer. In reality, more complex waves and mode shapes exist depending on material properties, size and boundary conditions of the panel as discussed in section 1.3. But this simplified figure helps to understand the role of the gel surround on the vibrating panel. Therefore dimensions and deflections of the ABS panel ($420 \times 320 \times 2$ mm) and transducer (D44.4 $\times$ 18 mm) in this figure are exaggerated to visualise movements of the panel and transducer.

The reflected transverse waves occurred in the panel, collide with the pistonic waves (the force coming from the transducer) as shown in Figure 4.17 (a). The collision of these two groups of waves results in the mechanical noise, shorter service life, and reduced operating frequency range.

When the gel surround is placed between the transducer and panel, it absorbs the reflected transverse waves, and the collision of the direct and reflected waves are minimised as shown in Figure 4.17 (b).
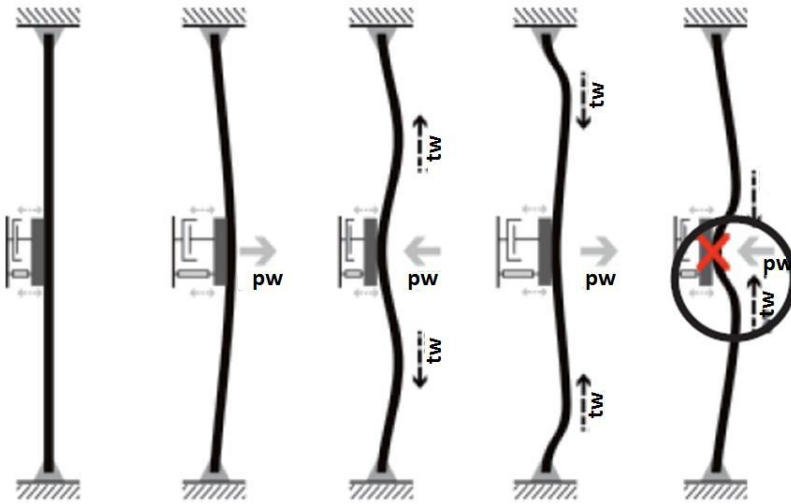
(a) The transducer without the gel surround
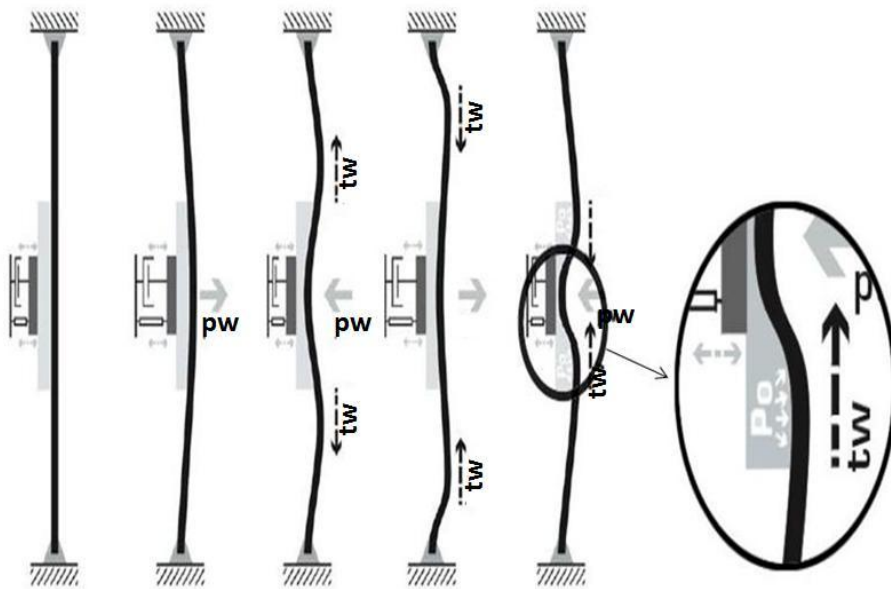
tw: transverse wave, pw: pistonic wave, Po: pressure

(b) The transducer with the gel surround

Fig. 4.17 Absorption of the reflected bending waves on the panel

Therefore the dissipated energy W_d, that is expressed in equation (2.23), of the gel surround needs to be equal or higher than the energy propagated from the bending panel to the transducer. As a result, the gel-type audio transducer can perform even at very low frequency band without creation of a mechanical noise. Commercially available DML (distributed mode loudspeaker) transducers, operating with a solid flat panel bonded, do not incorporate such the "damping mechanism" so they cannot generate a low frequency output signals.

The gel surround also contributes to the impedance matching between the transducer and panel, that maximises the energy transfer and minimise reflection of the force transferred to the panel from the transducer. Equation (4.16) reveals that the mechanical impedance, Z_m is proportional to the stiffness of a system, K_s and the inverse of frequency.

$$|Z_m| \sim \frac{K_s}{2\pi f}$$
(4.16)

The panel and mechanical parts of the gel-type audio transducer have different mechanical impedance due to the difference in the stiffness of the materials used. This causes the mismatch of mechanical impedance between two systems especially at low frequencies. In this case the part of the energy generated by the transducer will be dissipated in the form of heat and mechanical distortion.

However, the presence of the gel surround allows to compensate for the movements of the mechanical parts of the transducer and the panel, so more efficient energy transfer can be achieved. This energy distribution effect leads to the ability of

adopting various types of panels depending on applications for the gel-type audio transducer.

4.3.1.2 Characterisation of vibrations in the panel

The longitudinal and transverse waves occur in the panel, excited by the gel-type audio transducer and form the bending modes. The bending modes vary depending on the driving frequency. At low frequencies, the panel moves as a rigid body. In first vibrating mode, the entire surface of the panel vibrates in phase due to high bending stiffness across the panel and long period of input signal. As frequency increases, the bending mode breaks up over the panel proportionally. Figure 4.18 shows the bending modes. Bending modes can be divided into three groups: in-phase region, anti-phase region, and quadrature region. In the quadrature region, the overall velocity is always zero as in-phase and anti-phase regions occur at the same time.

At high frequencies, the effective moving mass of the panel increases as a frequency of the driving force increases. Also the effective stiffness of the panel increases. So the moving area of the panel is reduced and displacement of the panel is localised around a position of the transducer, whilst the rest of the panel is less affected. This effect allows controlling the displacement on the panel, excited by the gel-type audio transducer.

As the frequency rises higher, these complex series of the vibrations cause a rocking movement of the coil-drive plate assembly which make the panel deforming in a random and unpredictable manner.
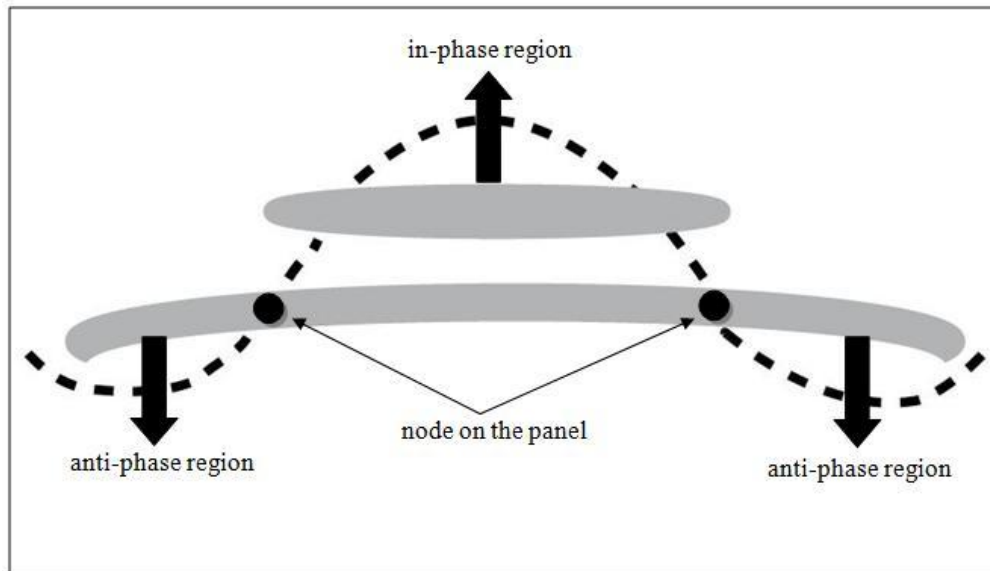
Fig. 4.18 In-phase and anti-phase region on the panel

To observe the role of the gel surround in the energy transfer, the gel-type audio transducer and a DML transducer (a commercially available model) were tested for comparison. The acoustic test was carried out to investigate the mechanical distortion created by both the transducers. Also the FE analysis and laser scanning measurement were used to predict and observe the bending modes of the panel described above.

4.3.2 Simulations and experiments

4.3.2.1 Test procedure

The prototype of the gel-type audio transducer C as described in section 4.2 was used for these experiments. A DML transducer - NXT® transducer with diameter, 28 mm, resistance $R_b = 8\ \Omega$ and nominal power W = 10 W, that is a similar specification to the transducer C was selected for a comparison test as shown in Figure 4.19.
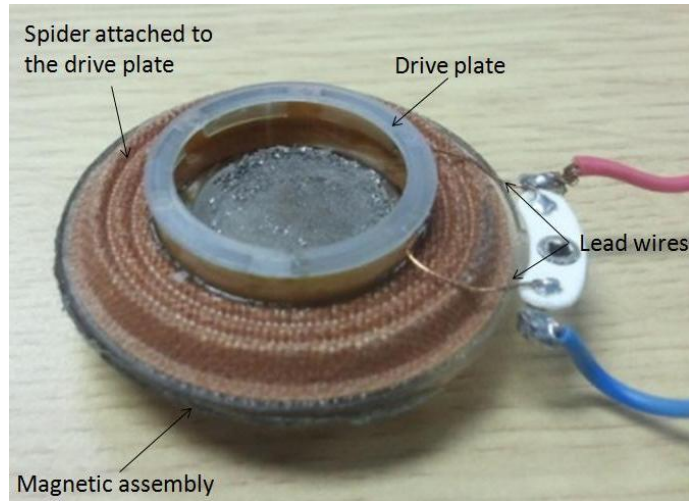
Fig. 4.19 A DML transducer

The transducers were attached to an ABS panel for testing. The DML transducer was attached directly to the surface of the panel with glue, whilst the transducer C was connected to the panel via the gel layer by using the bracket described in section 3.2.5. The main difference between both transducers is illustrated in Figure 4.20.

(a) DML transducer   (b) Transducer A
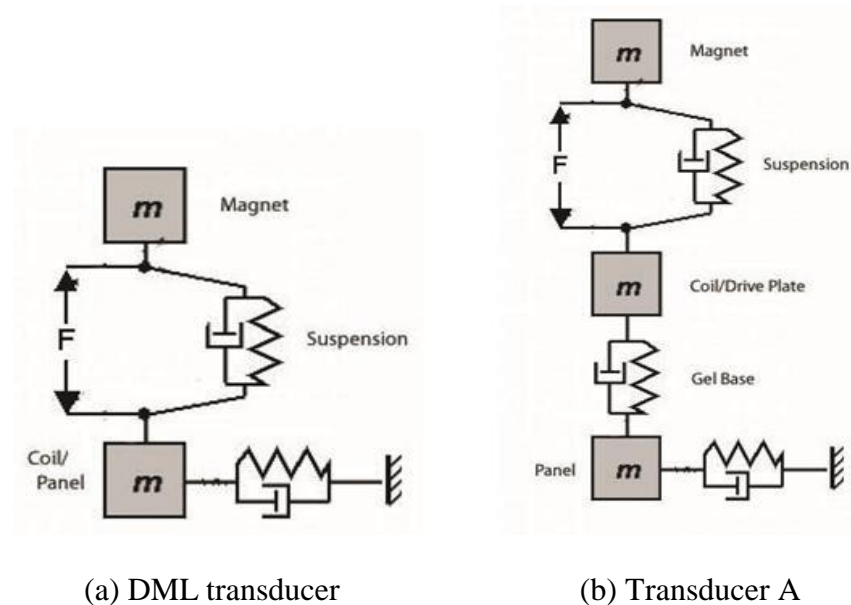
Fig. 4.20 Impedance analogue models of the transducers

The acoustic measurement was carried out to measure the THD % (total harmonic distortion) that represents the level of a mechanical distortion (noise). The COMSOL multiphysics was then used to investigate the behaviour of the bending modes on the panel and they were compared with results of the laser scanning measurement.

4.3.2.2 FE analysis

The stress-structure module was used to predict the bending modes of the panel excited by the transducer. The electrical parameters such as F_e and Z_b, computed for the magnetic simulation in section 4.2, were employed as the input values for the stress-structure simulation. Figure 4.21 shows the geometry of the panel with the transducer attached. Boundary conditions of the all panel edges are "fixed" and the model was the axial-symmetry.
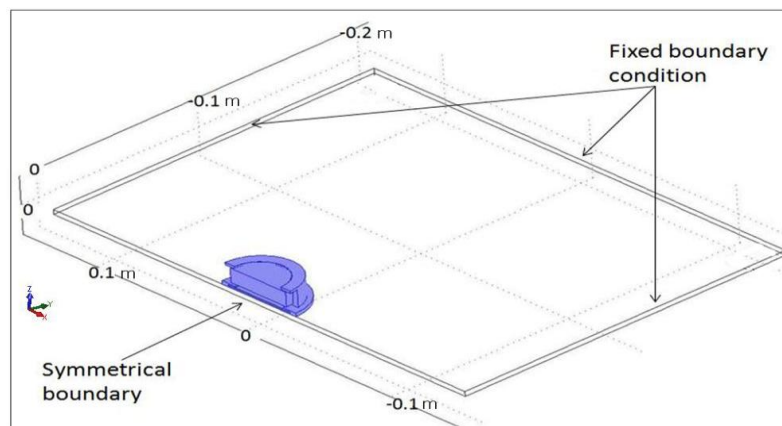
Fig 4.21 The geometry of the model

Figure 4.22 presents the mesh of the domains. Maximum and minimum element sizes of the mesh are 0.0798 m and 0.0168 m respectively. And maximum element growth rate is 1.3. Computed number of mesh elements was 5931.
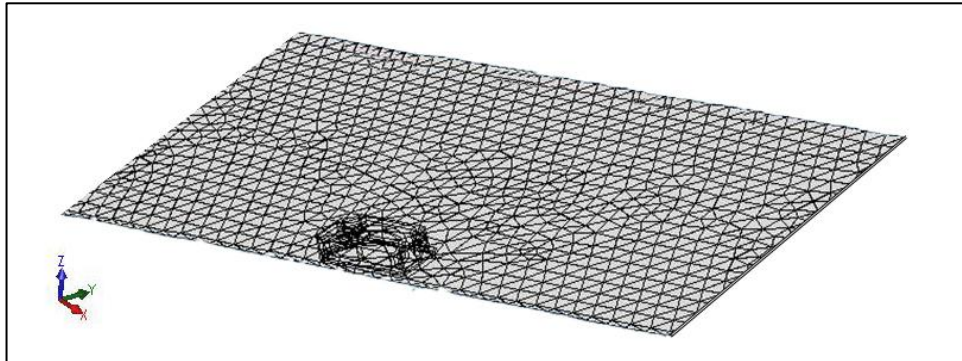
Fig. 4.22 Mesh of the all domains

The F_e computed for the magnetic simulation was applied on both the magnetic and coil-drive plate assembly in opposite direction as shown in Figure 4.23.
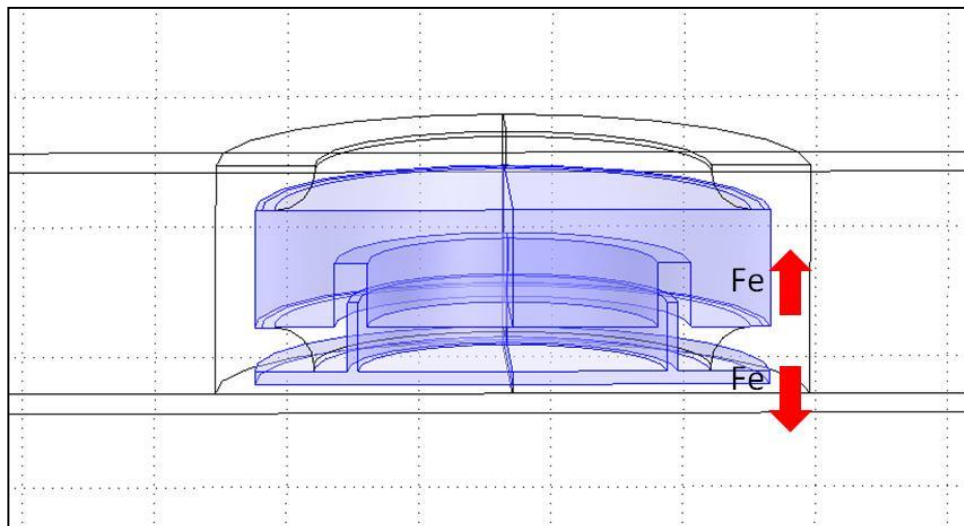
Fig. 4.23 Cross-sectional view of the transducer with the forces applied

Time-harmonic analysis at frequencies in the range 20Hz to 20,000Hz was investigated.

4.3.3 Results and discussions

4.3.3.1. Comparison between the DML and gel-type audio transducer

The gel surround in contact with the panel allows the transducer C to transfer the longitudinal waves to the panel with a minor wave cancellation between the longitudinal waves and bending waves of the panel because the gel surround absorbs such "unwanted" bending waves as described earlier. If those "unwanted" bending waves collide with the longitudinal waves coming through from the transducer, the mechanical distortions (noise) would occur. This is measured by THD % (time-harmonic distortion). The THD(%) is given by[20],

$$THD(\%) = 100 \times (10^{0.1\,THD\,(dB)}/10^{0.1\,SPL(dB)}) \tag{4.17}$$
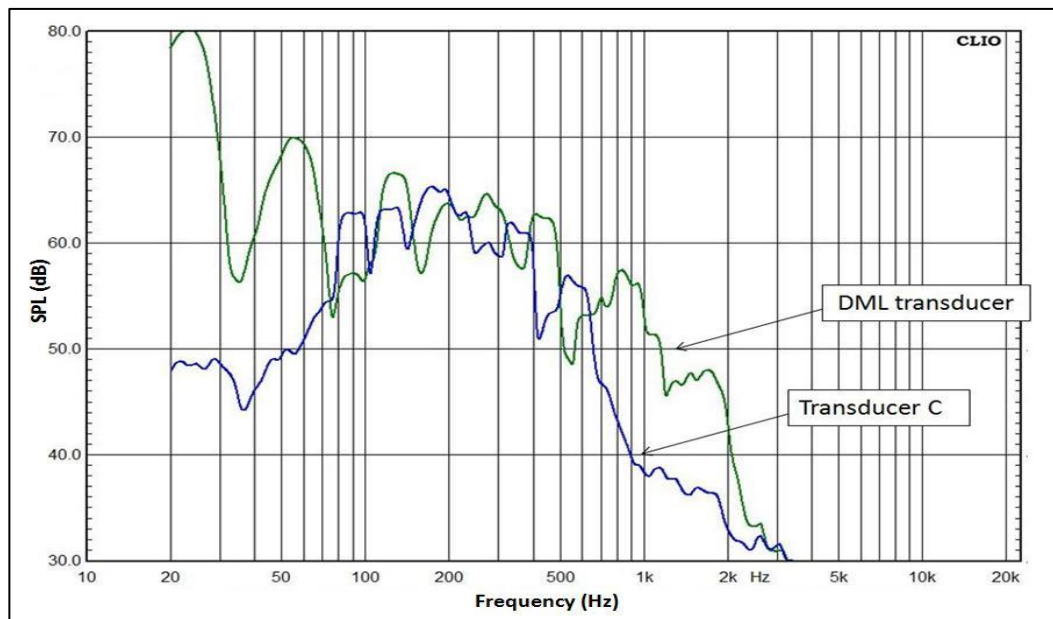
Fig 4.24 The THD% of the transducer C and DML transducer

Figure 4.24 shows the THD% of the transducer C (with the gel surround) and DML transducer (without the gel base between the transducer and the panel). This graph reveals that although the input power of both the transducers was the same at 1 W, the mechanical distortions created by the DML transducer is higher than the transducer C over the full testing frequencies especially below 80 Hz where displacement of the panel becomes the greatest. Figure 4.25 indicates that the panel with the transducer C attached generates 10 dB higher SPL (sound pressure level) than the panel with the DML transducer attached at low and high frequency range. The SPL of the DML measured below 50 Hz resulted from the high mechanical noise. Therefore, since the SPL is directly proportional to displacement of a vibrating panel (this will be discussed more in detail in section 4.4), it has been demonstrated that the role of gel surround is to transfer the mechanical energy more efficiently with a minimal waves cancellations by absorbing bending waves causing mechanical distortions (noise), thereby the transducer can operate down to lower frequencies unlike conventional moving-coil DML transducers.
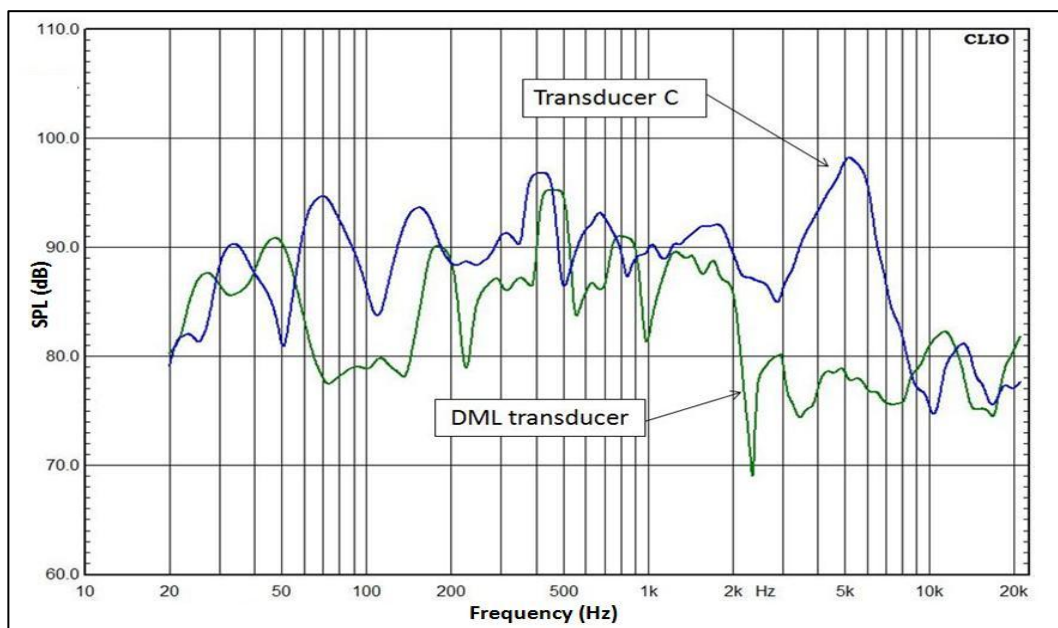
Fig. 4.25 The SPL of the transducer C and DML transducer

4.3.3.2. Bending modes of the panel excited by a single gel-type audio transducer

Figure 4.26 shows the total displacement of the panel computed by the FE analysis at 100 Hz (a), 2,000 Hz (b) and 5,000 Hz (c).
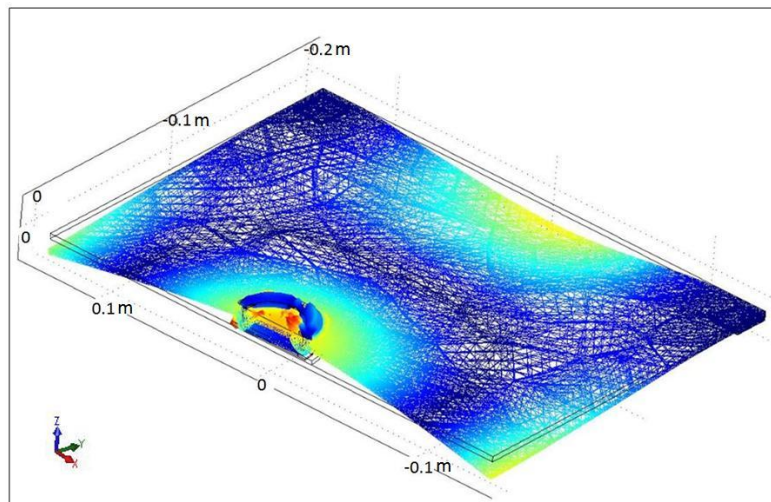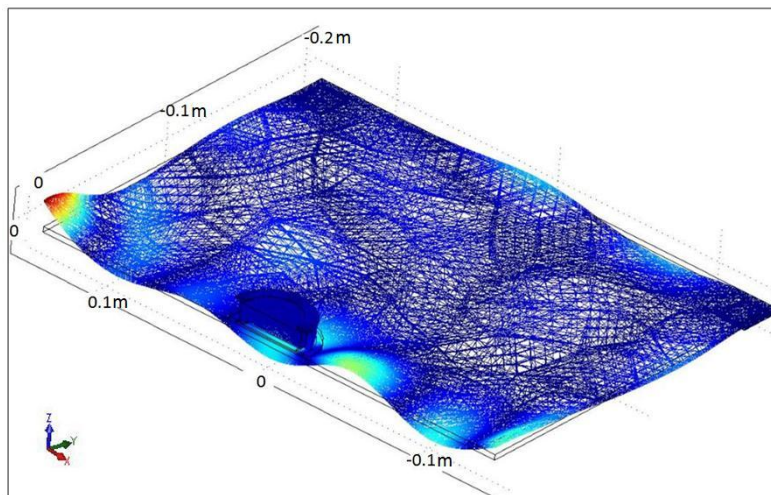
(a) 100 Hz

(b) 2, 000 Hz
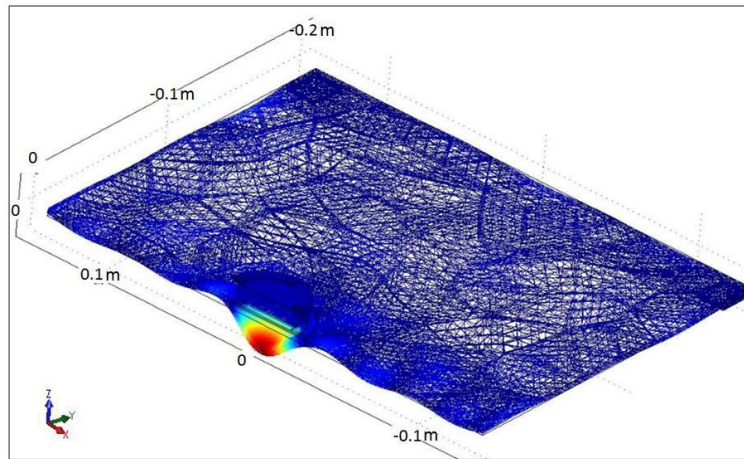
(c) 5,000 Hz

Fig. 4.26 Structural simulation results of the vibrating panel

The vibrating panel at 100 Hz behaves like a rigid piston with only a few bending modes as shown in Figure 4.26 (a). It is because the period of the driving signal at low frequency is long compared to the speed of propagation. So the entire panel moves in essentially the same phase as if it were a rigid piston. As frequency rises, the period of driving signal becomes shorter than the speed of wave propagation. It results in phase shifts so that the panel breaks up into several modes. As frequency increases further, the moving area is limited to the region immediately surrounding the gel-type audio transducer as shown in Figure 4.26 (b). This phenomenon is even more clearly shown at 5,000 Hz as indicated at Figure 4.26 (c).

These simulation results were verified by the laser scanning measurement as shown in Figure 4.27.
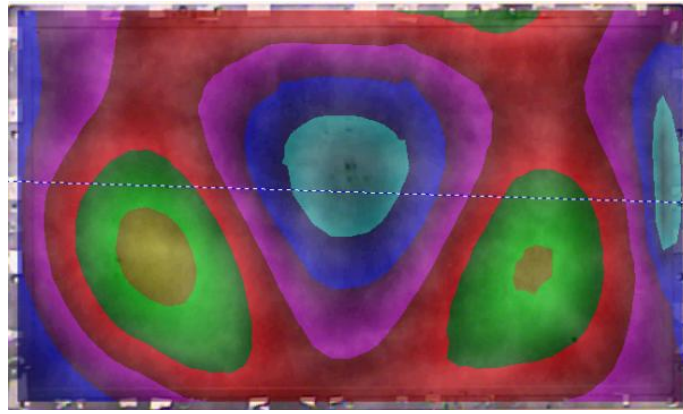
(a) 100 Hz
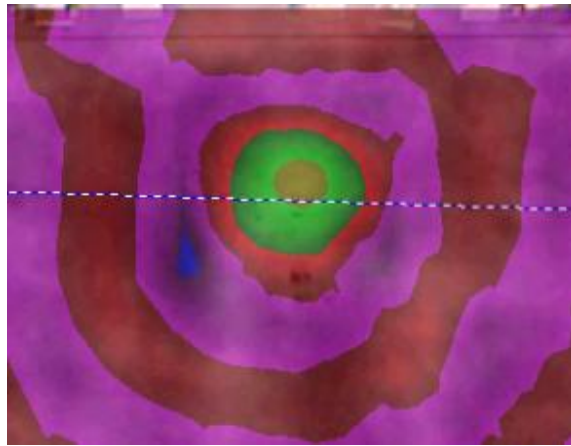
(b) 2,000 Hz
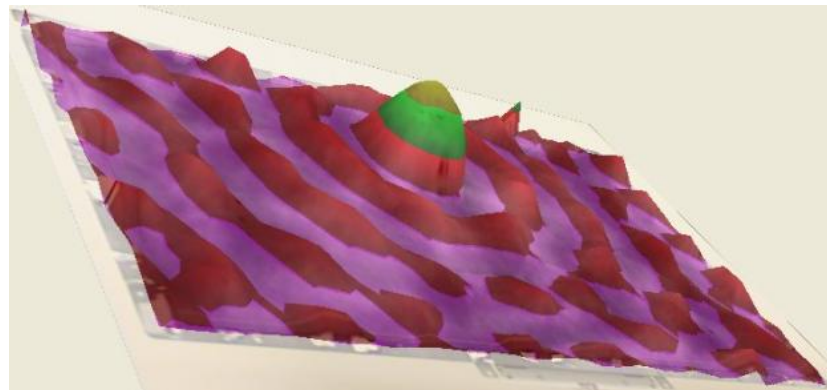
(c) 5,000 Hz

Fig. 4.27 Measured displacement of the profile of the panel excited by the transducer C

Figure 4.27 (a) shows that the panel moves as a rigid body at 100 Hz as predicted and as frequency increases, the moving area of the panel reduces and becomes localised on the position of the gel transducer as shown in Figure 4.27 (b) and (c).

4.3.3.3. Bending modes of the panel excited by two gel-type audio transducer

The bending modes of the panel excited by two transducers C were also measured. Figure 4.28 shows displacement of the profile of the panel excited by two transducers C at different frequencies: 100 Hz (a) and 2,000 Hz (b).
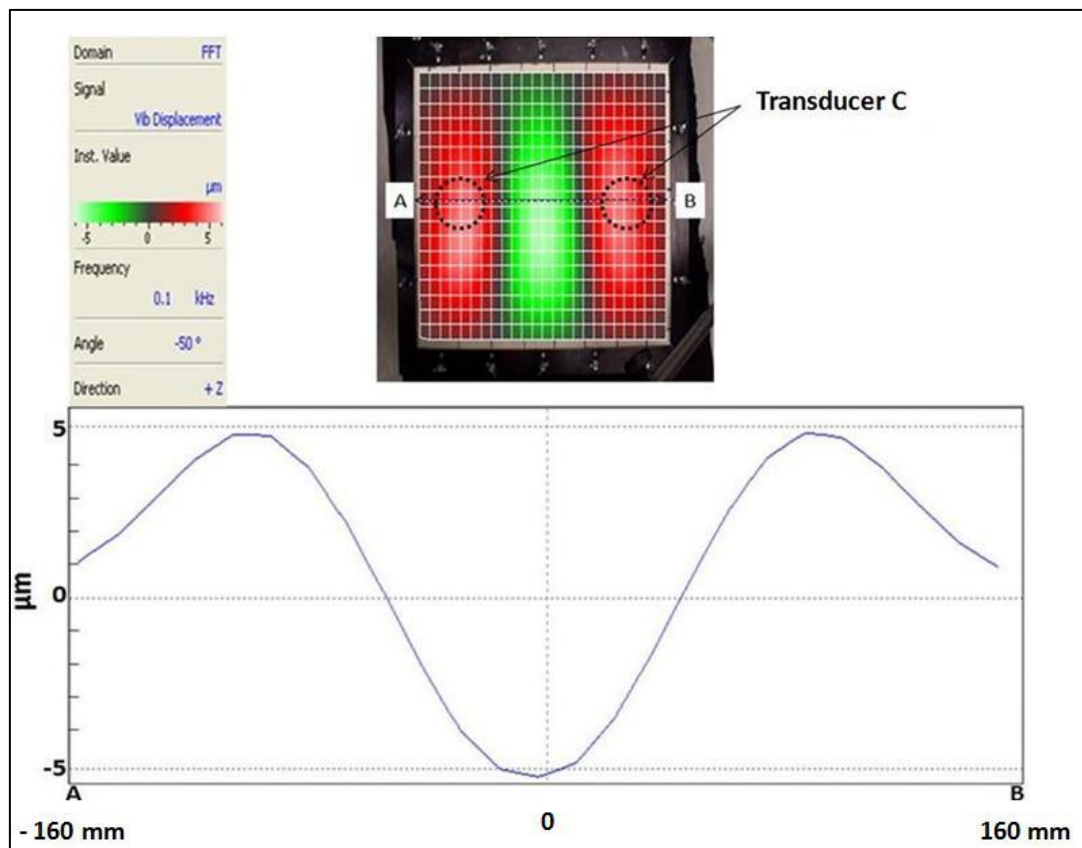
(a) 100 Hz
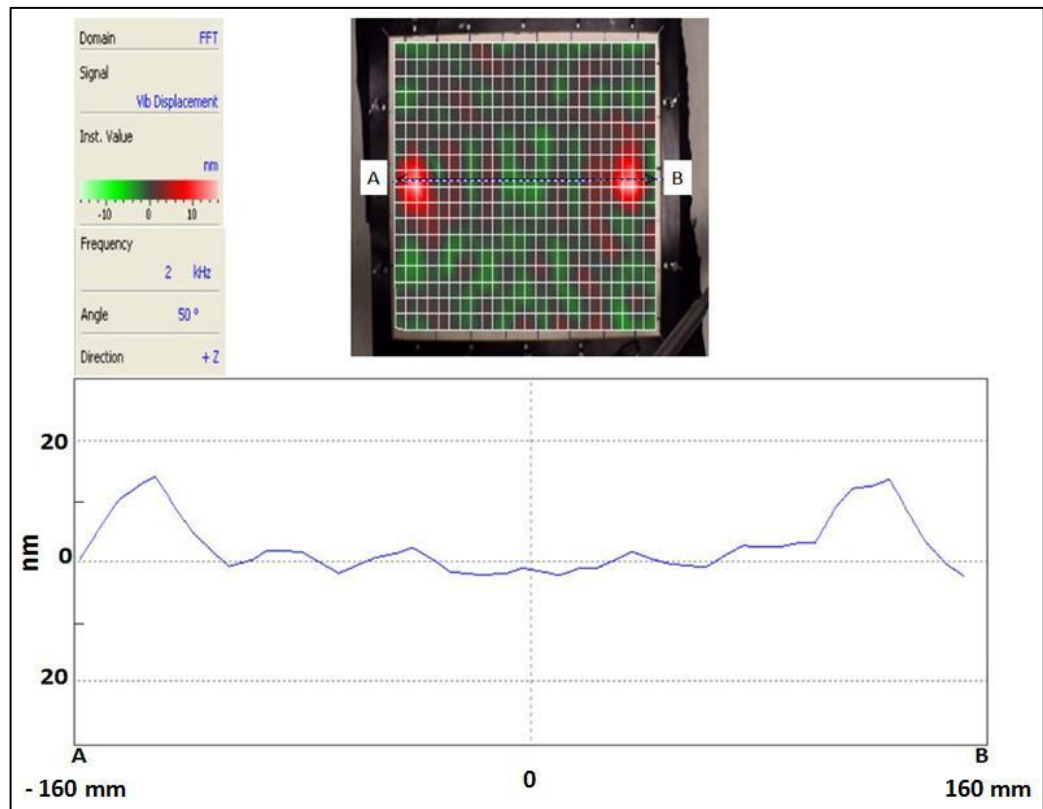
(b) 2,000 Hz

Fig. 4.28 Measured displacement of the profile of the panel excited by the two transducers C

Figure 4.28 (a) and (b) demonstrate that the moving area of the panel reduces and becomes localised on the position of the gel transducer as frequency increases. It was predicted by the FE analysis that the bending modes of the panel, excited by the gel-type audio transducer, change at different frequencies. These simulation results were verified by the laser scanning measurement as shown in Figure 4.27 and 4.28. As a result, this effect allows to give the controlled displacement on a panel excited by the gel-type audio transducer. Additionally, as the driving frequency of the force that is applied to the panel from the transducer, increases, the stiffness of the panel also increases. Therefore the anti-phase region of the panel is consequently minimised so displacement of the panel at high frequencies, comprises mainly of the in-phase regions.

152

This contributes to minimal acoustic cancellations and this will be discussed in the section 4.4.

4.3.4 Summary

It was demonstrated by the comparison test (the gel-type transducer VS the classic DML transducer – a classic moving-coil transducer without a gel layer) that the gel surround of the gel-type audio transducer minimises the mechanical distortions by absorbing bending waves on the panel. Acoustic performance (SPL) of both transducers demonstrated that the gel surround maximises the energy transfer, resulting enhancement of the power output of the gel-type transducer, when compared to the DML. Furthermore this effect enables to extend the operating frequency down to lower frequency band without creating the distortions which causes a system failure. Also the gel surround contributes to the impedance matching between the transducer and panel so it gives the freedom of choosing various types of panels or solid objects in response to the need of applications.
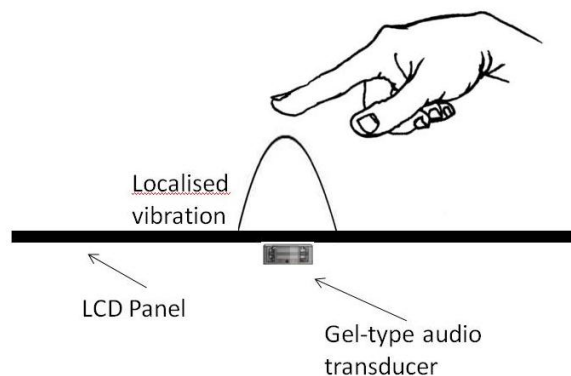
Fig. 4.29 The application of the tactile display

153

Furthermore the behaviour of the vibrating panel in response to that force was identified. The bending modes change at different driving frequencies. In practical terms this implies that as frequency rises, the panel's movement breaks up and the effective moving area becomes localised on the position of the gel-type audio transducer at 2,000 Hz or above. It is therefore possible to generate the controlled displacement on any solid surface with a gel-type audio transducer attached specifically for a tactile display application. This is a physical mechanism or device that provides tactile sense to a user as illustrated in Figure 4.29.

4.4 Effect of soft elastomers on the SPL

It has been investigated in section 4.2 that when the larger M_m or the low-hardness elastomer (greater C) of the gel surround were used, the total output driving force generated by the transducer within low frequency band also increases giving rise to greater panel displacement. The bending modes of the panel excited were experimentally identified at different frequencies. In this section the effect of the compliance C on the SPL will be discussed. Various types of elastomers used to produce gel surrounds were acoustically tested to measure the SPL.

4.4.1 Theoretical problems

Equations (4.18) and (4.19) demonstrate that displacement of a panel $w(j\omega, r_p)$, is proportional to the SPL and equation (4.20) shows that the effective sound radiating area S_P on the panel also decreases by 1/frequency^2 as the bending modes of the panel becomes localised at medium and high frequencies.

$$p(j\omega, r_a) = (\omega^2 \rho_0 / 2\pi) \int_{S_p} [w(j\omega, r_p) / |r_a - r_p|] \, e^{-jk|r_a - r_p|} dS_p \qquad (4.18)$$

$$SPL(\omega, r_a) = 20 \, log[|p(j\omega, r_a)| / P_0] \quad \text{dB} \qquad (4.19)$$

where $p(j\omega, r_a)$ is the sound pressure at the point r_a from the centre point in air, SPL is the sound pressure level at point r_a, P_0 (equals to 2 x 10^{-5} Pa) is the atmospheric pressure, and ρ_0 is density of the air. The integration is taken at each point on the panel r_p, over the sound radiating area S_p.

$$S_p = \pi \left(\sqrt{E / \rho_p} \times 1/\omega \right)^2 = \pi r_{ra}^2 \qquad (4.20)$$

where S_p is the effective sound radiating area on the panel, E and ρ_p are the Young's modulus and the density of the panel respectively, and r_{ra} is the radius of sound radiating area [73].

Figure 4.18 from section 4.3 demonstrates that the bending modes can be divided into three groups: in-phase region, anti-phase region and quadrature region. The in-phase region generates the sound and anti-phase region offsets overall sound pressure by generating out-of-phase sound. In the quadrature region, the total volume velocity is always zero as in-phase and anti-phase regions occur at the same time so no panel's displacement occurs. If the in-phase region is dominant with a minimal anti-phase region, the sound pressure level will be the highest.

At low frequencies, the mechanical impedance of the panel is great due to the high bending stiffness of the panel and the long wavelength of transverse waves on the panel. It causes that the whole panel is engaged in the pistonic movement, that is, the in-phase region dominates the panel. This leads to the low acoustic radiation impedance, R over the panel as described in equation (4.21) so the directivity of the panel radiating the sound is broad. Also since displacement of the panel is directly proportional to the SPL, higher displacement of the panel that is induced by the larger C, results in the greater SPL.

$$R = \rho_0 / \pi r_{ra}^2 \tag{4.21}$$

where R is the real part of the acoustic radiation impedance over the radiating area and ρ_0 is the density of air.

As frequency increases, it was demonstrated in section 4.3 that the moving area of the panel is reduced, resulting in the reduction of the sound radiating area, which leads to the increase of impedance R. Furthermore at higher frequencies, the stiffness of the panel also increases as the driving frequency becomes shorter. So the anti-phase region of the panel is consequently minimised and displacement of the panel comprises mainly of the in-phase regions. This contributes to minimal acoustic cancellations. As a result, the directivity of the sound waves radiated from the panel becomes narrow. This effect allows multiple gel-type audio transducers that are attached to a single panel, to operate at the same time, to radiate independent sound sources without disturbing each other at medium and high frequency band.

In the following sections, gel surrounds made of various types of elastomers with the different hardness were examined to investigate the effect of the *C* on the SPL. Also the FE analysis was used to visualise the directivity of the sound radiated from the vibrating panel. The acoustic testing was carried out to measure the SPL.

4.4.2 Simulations and experiments

4.4.2.1 Test procedure

Gel surrounds made of three different types of elastomers – RTV silicone elastomer, TPE (a styrene block-based copolymer), and silicone foam elastomer – were prepared as shown in Table 4.3. Selection of these materials and manufacturing the gel surround samples using polymer processing techniques were discussed more fully in section 3.2.3.

Then, the acoustic measurement for the gel-type audio transducers assembled with these gel surrounds were carried out. The FE analysis was used to investigate the sound field and directivity radiated by the vibrating panel.

Type of elastomers	Hardness	Density, ρ	Poisson's ratio, v [103]	Young's modulus, E
RTV Silicone	35 Shore 00	1050 kg/m^3	0.49	6.7×10^{-2} MPa
	42 Shore 00	1070 kg/m^3	0.49	9.3×10^{-2} MPa
	48 Shore 00	1080 kg/m^3	0.49	1.3×10^{-1} MPa
	54 Shore 00	1080 kg/m^3	0.49	1.5×10^{-1} MPa
	62 Shore 00	1080 kg/m^3	0.49	3.5×10^{-1} MPa
	70 Shore 00	1090 kg/m^3	0.49	6.2×10^{-1} MPa
TPE	35 Shore 00	1030 kg/m^3	0.49	6.9×10^{-2} MPa
	70 Shore 00	1050 kg/m^3	0.49	5×10^{-1} MPa
Silicone foam	35 Shore 00	300 kg/m^3	0.3	4×10^{-2} MPa
	70 Shore 00	350 kg/m^3	0.3	10×10^{-1} MPa

Table 4.3 Samples of the gel surrounds

4.4.2.2 FE analysis

The acoustic module for the acoustic-structure analysis from COMSOL multiphysics software was used to observe the sound field and directivity radiated from the vibrating panel. The same input parameters described in section 4.3 (the stress-structure simulation) were used for this analysis. The computed F_e was applied to the magnetic and coil-drive plate assembly in opposite direction as shown in Figure 4.23.
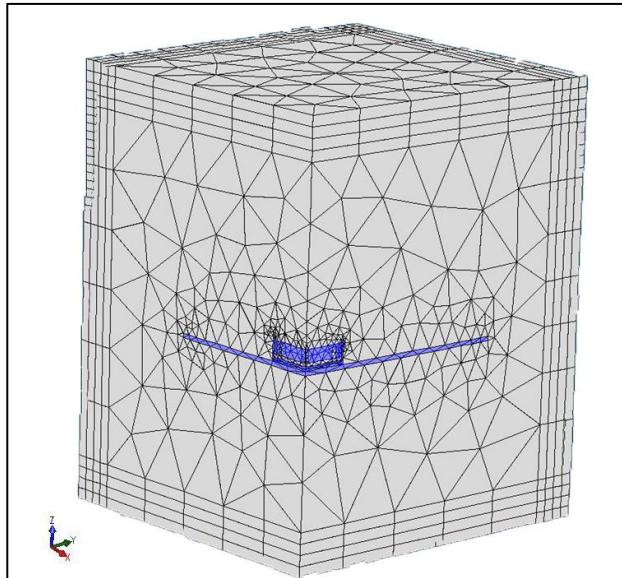
Fig. 4.30 Mesh for the acoustic-structure analysis

Figure 4.30 shows the modelling of the problem as 1/4th of the medium. The mesh of the domains includes the air and PML (perfectly matched layer). Maximum and minimum element size of the mesh are 0.14 m and 0.0196 m respectively, and maximum element growth rate is 1.3. Computed number of mesh elements was 11,116.

4.4.3 Results and discussions

The experimental results presented in Figure 4.31 show that the transducer assembled with the 35 Shore 00 RTV silicone gel surround exhibits higher SPL than 70 Shore 00 transducer over the full frequency range. But the difference in the SPL at low frequency highlighted in a red-dot square is noticeable.

At around first f_0, 80Hz, the SPL of 35 Shore 00 transducer is 10 dB higher than the 70 Shore 00 transducer. This is due to the greater displacement of the panel, excited by the 35 Shore 00 (larger C) transducer at low frequency band when compared to the

70 Shore 00 transducer as discussed in section 4.2. And such displacement of the panel is dominated by the in-phase region as investigated in section 4.3 so the acoustic cancellations are minimised. Thus, as the displacement of the panel is directly proportional to the SPL, the highest SPL is achieved.

Similar effect was also observed for the TPE and silicone foam gel surrounds as presented in Figure 4.32 and 4.33. The SPL of the transducers with the 35 Shore 00 TPE and silicone foam gel surrounds was measured much higher than the 70 Shore 00 transducers especially at low frequency highlighted in a red-dot square.
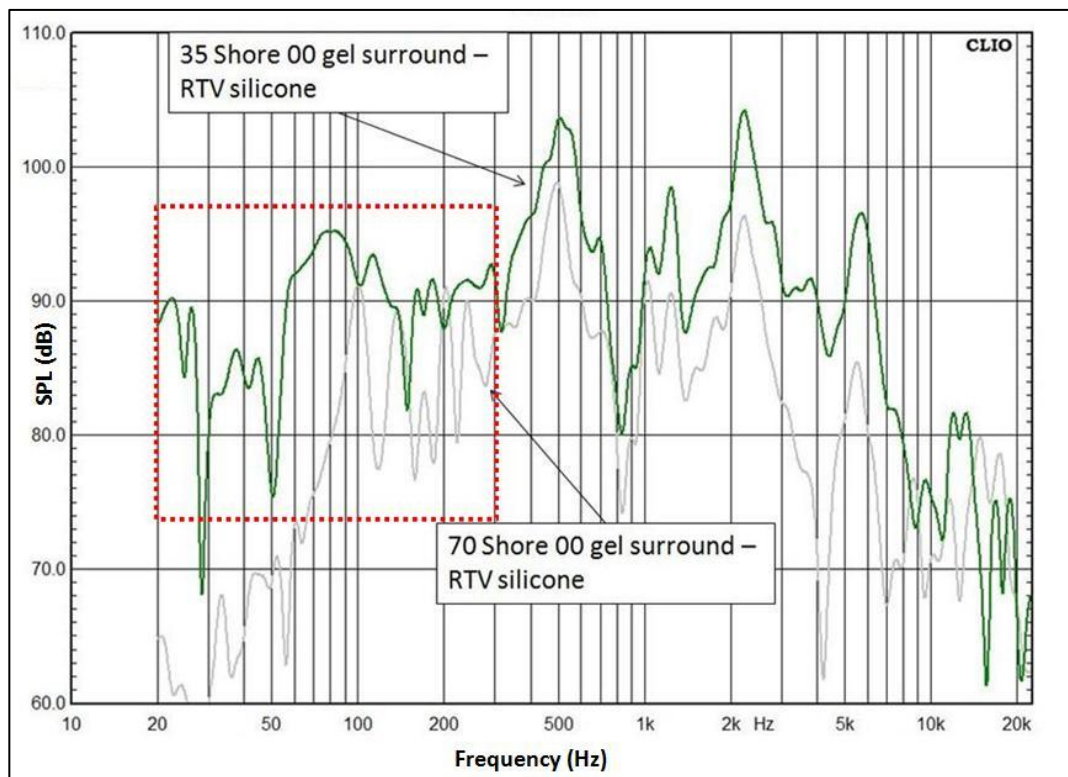
Fig. 4.31 The experimental SPL results for RTV silicone gel surrounds
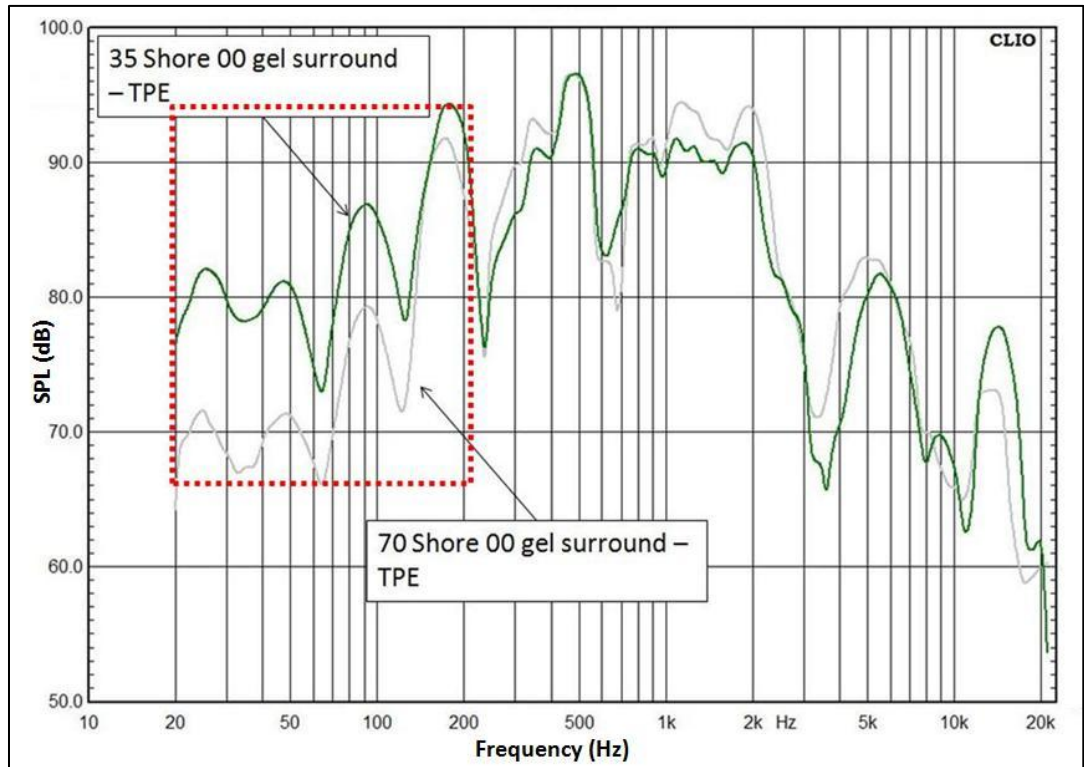
Fig. 4.32 The experimental SPL results for TPE gel surrounds

Therefore the larger C (in this case, the low hardness of the gel surround) that causes larger panel's displacement, contributes to higher SPL. Although there were the differences in the value of the SPL and graph pattern between the testing samples, it was demonstrated that the value of the C of the gel surround has a great impact on the SPL.

$$\text{Acoustic efficiency (average SPL + THD\%)} \tag{4.22}$$

$$= 20 \times log\left[\left(10^{\frac{SPL}{20}}\right) \times ((100 - THD\%)/100)\right]$$

It was also discussed in section 4.3 that the transducer with the gel surround made of larger C produces less total harmonic distortion (THD, measured in %). Thus as equation (4.22) shows, the acoustic efficiency of the transducers increases as the

hardness of the gel surround decreases, that is, the C of the gel surround increases [74]. This result is presented in Figure 4.34.
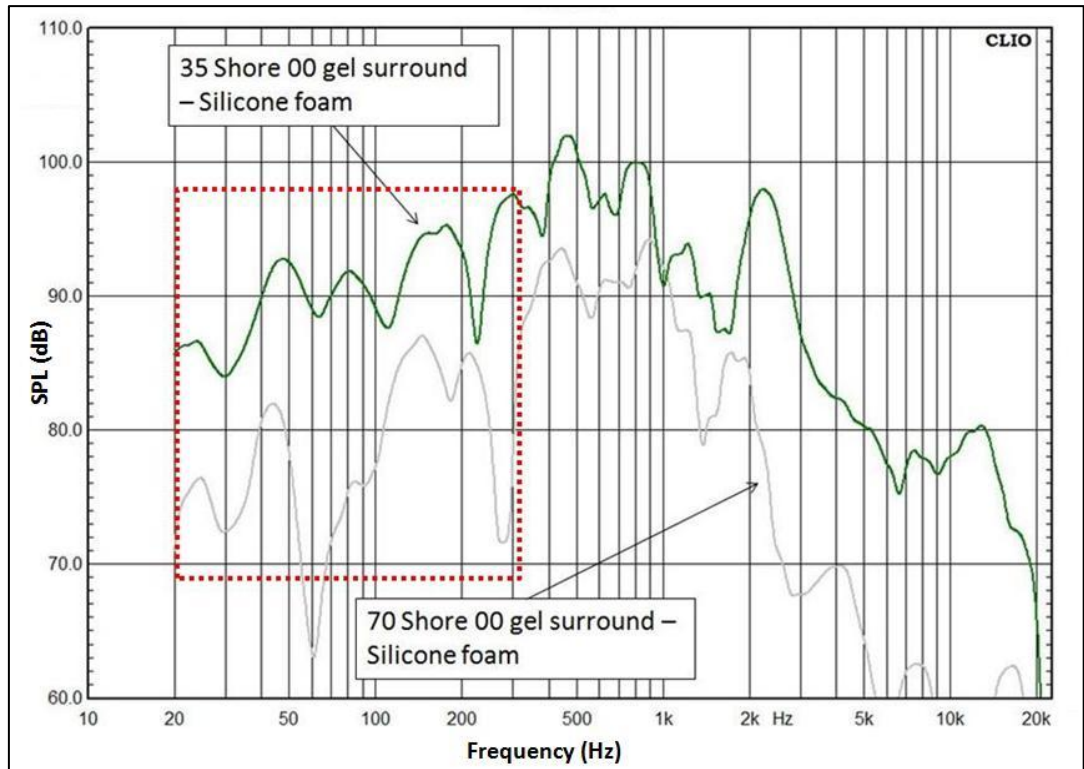
Fig. 4.33 The experimental SPL results for silicone foam gel surrounds
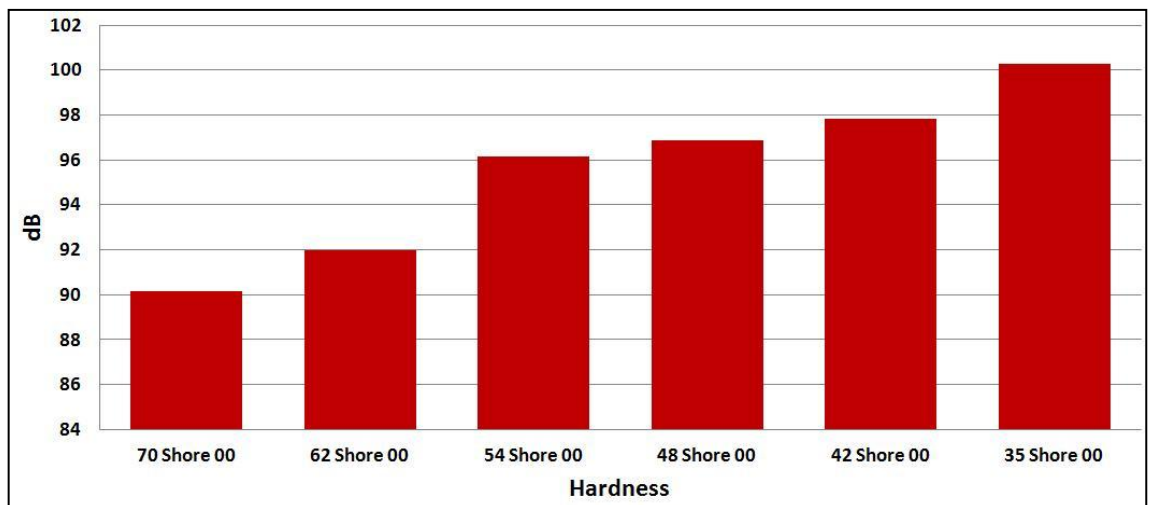
Fig. 4.34 The acoustic efficiency of the different hardness of the gel surrounds made of the RTV silicone elastomer

Figure 4.35 shows the directivity of the sound waves radiated from the vibrating panel at 100 Hz (a), 2,000 Hz (b) and 5,000 Hz (c).
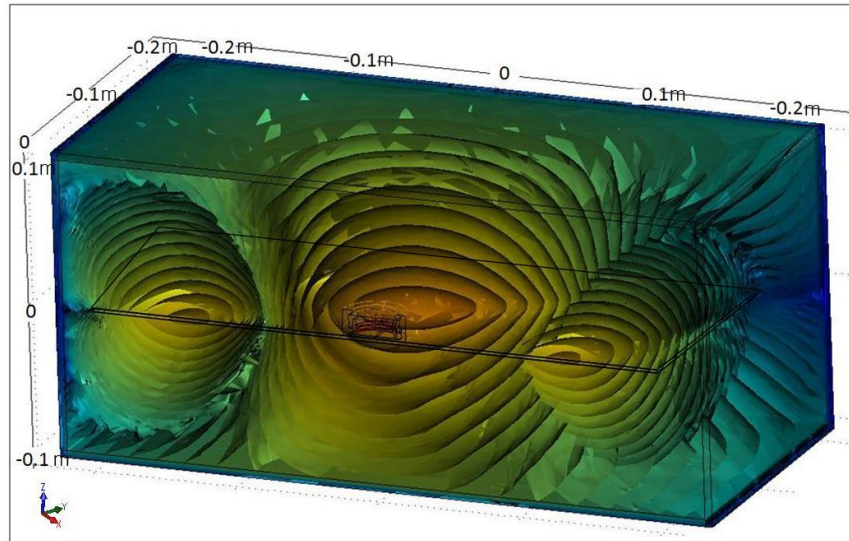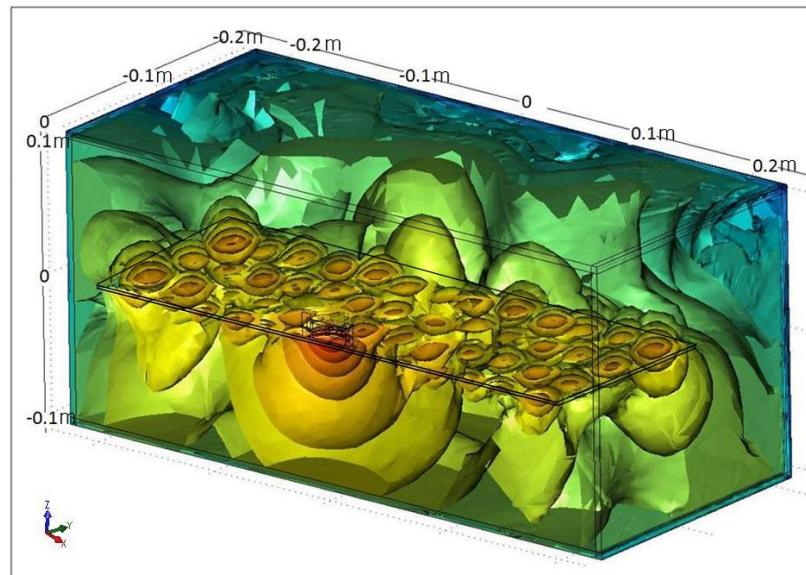
(a) 100 Hz

(b) 2,000 Hz
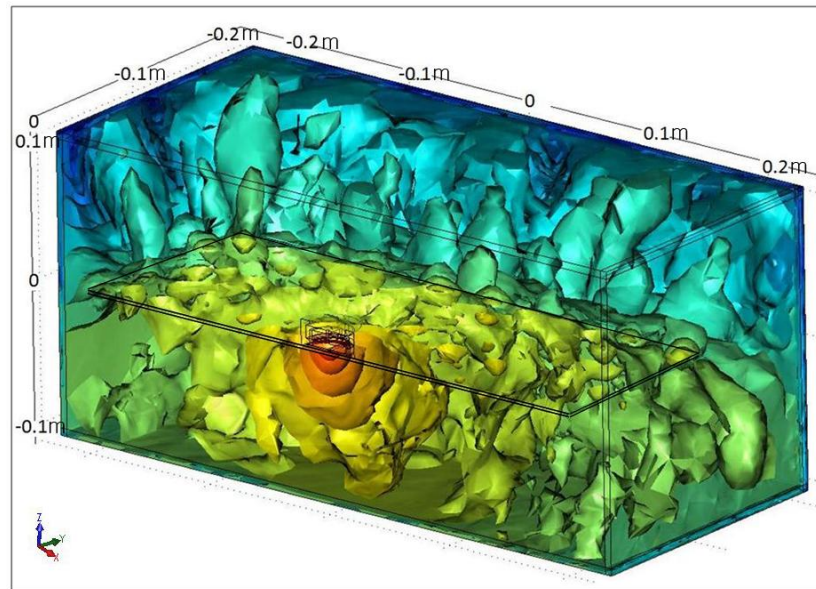
(c) 5,000 Hz

Fig. 4.35 The directivity pattern of the sound projected from the panel

Figure 4.35 (a) indicates that at 100 Hz, the entire panel radiates the sound as the whole panel moves as the experimental result showed in Figure 4.28 (a) [section 4.3.3]. As a result, there would be cancellation of the acoustic waves at low frequencies if two gel-type audio transducers are attached to a single panel and engaged in exciting the panel to radiate the sound. This was illustrated in Figure 4.36 (a). It was also discussed in section 4.3.3 that as frequency increases, the moving area of the panel reduces and becomes localised on the position of the gel-type audio transducer. So when two transducers excite the panel within this frequency range, two independent displacements on the panel can be achieved as presented in Figure 4.28 (b). As a result, the localised moving area causes the narrow directivity of the sound radiation as shown in Figure 4.35 (b) and (c), and thereby it would be possible to utilise two independent sound sources from a single panel as illustrated in Figure 4.36 (b).
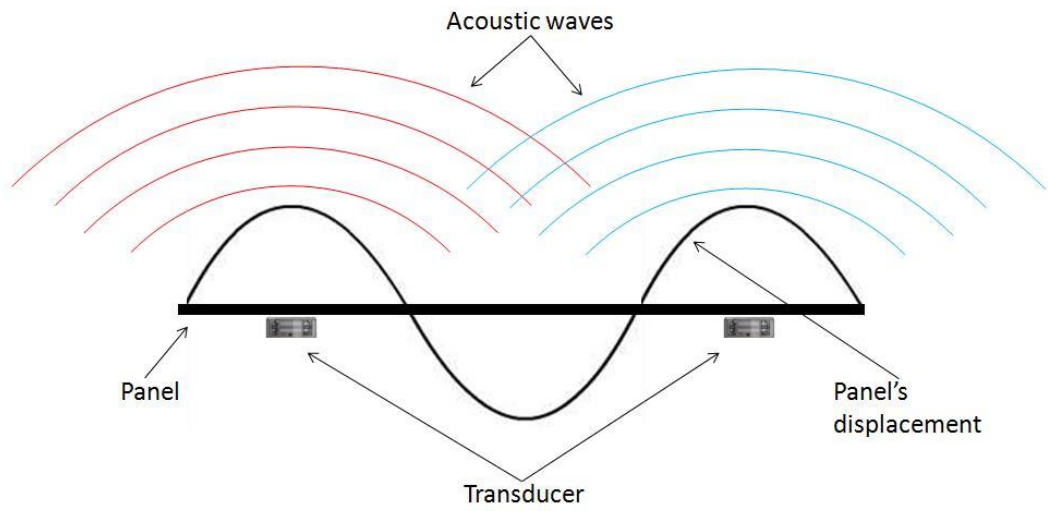
(a) Low frequency

(b) Medium and high frequency

Fig. 4.36 Acoustic and bending waves at different frequency range

This effect was demonstrated in Figure 4.37 which shows the measured SPL of one gel-type audio transducer compared with two gel-type audio transducers. The panel, excited by the two transducers, radiates higher SPL in comparison with the one transducer system at medium and high frequencies in the range 300 Hz to 20,000 Hz. This is due to the localised moving area of the panel generating minimal acoustic interference between the two transducers. At low frequency below 300 Hz where the acoustic and bending waves cancellation occurs, there is no continuous increase of the

SPL radiated by the two transducers against the one transducer. Increase of the SPL at frequencies in the range 20 Hz to 40 Hz can be due to ambient noise.
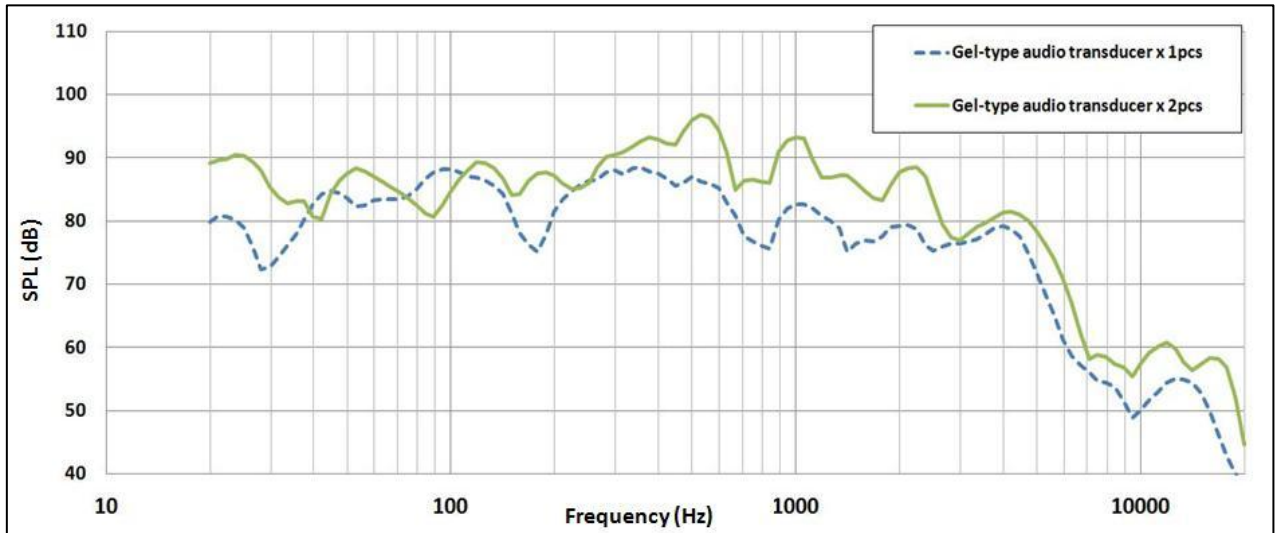
Fig. 4.37 The experimental SPL results for two gel-type audio transducers

4.4.4 Summary

It was demonstrated in section 4.2 that the gel-type audio transducer incorporating the soft gel surround (35 Shore 00) causes greater displacement of the panel when compared to the transducer assembled with the hard gel surround (70 Shore 00). In this section, it was investigated that as displacement of the panel is proportional to the SPL, the transducer with the soft gel surround assembled produces higher SPL than the hard gel surround transducer. The experiments results showed that the transducers, incorporating 35 Shore 00 gel surrounds, exhibit higher SPL than 70 Shore 00 gel surround and especially the difference in the SPL is noticeable at low frequency, where the displacement of the panel is great and in-phase region dominates the panel. This effect was observed for all of three different types of elastomers tested – the RTV silicone elastomer, TPE, and the silicone foam elastomer, although there were the

differences in the value of the SPL and graph pattern between the testing samples. Thus, the C of the gel surround has a great impact on the SPL. Figure 4.34 indicated that the acoustic efficiency increases as the hardness of the gel surround decreases.

It was discussed that the moving area of the panel is reduced as frequency increases. Therefore the effective sound radiating area of the panel also reduces and becomes localised on the position of the gel transducer. Due to this localisation, the volume velocity also decreases. It causes the directivity of the sound field to remain narrow. As a result, it is possible to radiate multiple independent sound sources (i.e. a stereo system) from a single panel excited by the gel-type audio transducers.

4.5 Conclusions

In section 4.2, it was investigated theoretically and experimentally, that the total output driving force of the gel-type audio transducer can be enhanced by increasing values of the M_m or a low-hardness elastomer (great C) of the gel surround (or both) at low frequency band, where the movement of the magnetic and coil-drive plate assembly is great. It is because of a novel mechanism, that takes advantage of the inertial force exerted on the magnetic and coil-drive plate assembly. This was observed by COMSOL multiphysics simulation combined with physical experiments. The results showed that the larger M_m or C of the gel surround (or both) increases the output driving force of the gel-type audio transducer as displacement of the panel excited by the transducer A (80 g of the M_m) and C ($tan\,\delta = 0.95$ at 100 Hz) is higher than the transducer B (40 g of the M_m) and D ($tan\,\delta = 0.65$ at 180 Hz). It was also observed that the larger value of

M_m or C lowers the f_0 of the system, thereby it enables the transducer to operate down to lower frequency range.

In section 4.3, the effect of the gel surround in transferring the force from the transducer to the panel was studied. The gel surround placed between the panel and transducer absorbs the reflected bending waves, so this minimises the collision of the forces between the bending waves on the panel and the pistonic waves coming from the transducer. This was investigated by comparing the transducer C (with a gel base) with the classic DML transducer (a moving-coil transducer without a gel base). As the DML transducer does not have ability to absorb the bending waves on the panel, the THD% of the DML transducer was measured much higher than the transducer C at especially low frequencies in the range 20 Hz to 80 Hz where displacement of the panel becomes the largest. On contrary, the SPL graph shows that the transducer C exhibits higher SPL than the DML transducer. Thus the experimental results demonstrated that the power output of the gel-type transducer is enhanced by incorporating the gel surround, and mechanical distortion is also minimised, when compared to the DML transducer, thereby the transducer can operate at low frequencies unlike conventional DML transducers. Also the gel surround contributes to the impedance matching so this enables various types of panels or solid surfaces to be selected depending on the applications (acoustic results of more panels will be presented in section 5.2, Chapter 5).

The behaviour of the vibrating panel in response to the driving frequency was also investigated in this section. It was observed by the simulation and laser scanning measurement that the whole panel moves like a rigid piston at low frequency range. But as frequency increases, the panel breaks up and the effective moving area becomes localised on the position of the transducer at 2,000 Hz. Therefore as presented in Figure

4.29, the controlled displacement on any solid panel with a gel-type audio transducer bonded can be achieved for the application of the tactile display.

In section 4.4, the effect of the gel surround on the SPL was studied. It was demonstrated that the gel surround with the larger C of the gel surround causes greater displacement of the panel, resulting in the higher SPL radiated. This effect was observed for the three elastomers – RTV silicone, TPE, and silicone foam elastomer. Therefore the C of the gel surround has a great impact on the SPL.

The FE analysis, laser scanning, and acoustic measurement were used to demonstrate the decrease of the effective sound radiating area of the panel as a function of frequency. This also causes the decrease of volume velocity, resulting in the narrowing directivity of the sound field. As a result, multiple independent sound sources radiating from a single panel excited by multiple gel-type audio transducers can be achieved. The experiments showed that overall SPL of the two transducers attached to the single panel was increased at medium and high frequency, where the acoustic cancellation is reduced due to the narrow directivity of the sound field.

In next chapter, some applications incorporating the gel-type audio transducers will be discussed with their commercial values.

Chapter 5 – APPLICATIONS

5.1 Introduction

In this Chapter some applications incorporating the gel-type audio transducer developed throughout this thesis were discussed. The applications include a portable audio speaker designed for all major consumer electronic devices such as a mobile phone and laptop, and loudspeakers for an ultra-slim TV and handheld computer.

Working prototypes were built, and acoustic testing was carried out to demonstrate advantages of incorporating the gel-type audio transducer. The gel-type audio transducer, which was used for a portable audio speaker application, is similar to the one discussed (the transducer C) in previous Chapters. For TV and handheld computer applications, the new gel-type audio transducers were made to fit for the purpose. Commercial benefits of these units addressed.

5.2 Portable audio speaker

A portable gel-audio speaker called "Wowee One" was developed incorporating the gel-type audio transducer. This product could be used for both a fix and portable solution for IPod, mp3, mp4, mobile phone, and computer applications that require an additional woofer device to reinforce their poor acoustic performance at low frequency.

5.2.1 Product specifications

The technical specification of the product is summarised in Table 5.1, and the internal architecture and complete assembly are shown in Figure 5.1(a) and (b) respectively.

Dimensions	$60 \times 120 \times 25.8$ mm
Product weight	200 g
Frequency response	40 Hz ~ 20 KHz
Amplifier	D-class
Output power	2 W RMS
Input power	5 V DC (via mini USB)
Rechargeable battery	Lithium Ion 3.7 V
Playback duration	Up to 20 hours
Audio input	3.5 mm audio jack

Table 5.1 Specification of Wowee One

Wowee One is a compact portable speaker unit which uses a hybrid technology of standard tweeter (8 Ω), delivering the high frequencies, and the gel-type audio transducer delivering the low-med frequencies, when attached to the solid surface. The combination of the two audio transducers and the panel to which the unit is attached, provides the uniform coverage within the full audible range of frequencies from 40 Hz to 20,000 Hz, while standard portable speakers generally lack a low frequency response.

The size of the Wowee One is 120 mm × 60 mm × 25 mm and the bottom surface of the unit is covered with a base gel sheet that gives a firm contact between the unit and panel. An amplifier used for this device is a "D-class" that modulates and amplifies a signal, and then filters the amplified signal back into its original form. This amplifier has been used in portable audio devices, mobile phones and laptops where size, power, and heat dissipation are of great concern. The Wowee One was designed to operate with most types of flat panels, although its acoustical performance is influenced by a panel's properties, size and boundary conditions. The SPL comparison test between the Wowee One and competitor products, employing the ABS panel (420 mm × 320 mm × 2 mm), will be discussed in section 5.2.2.
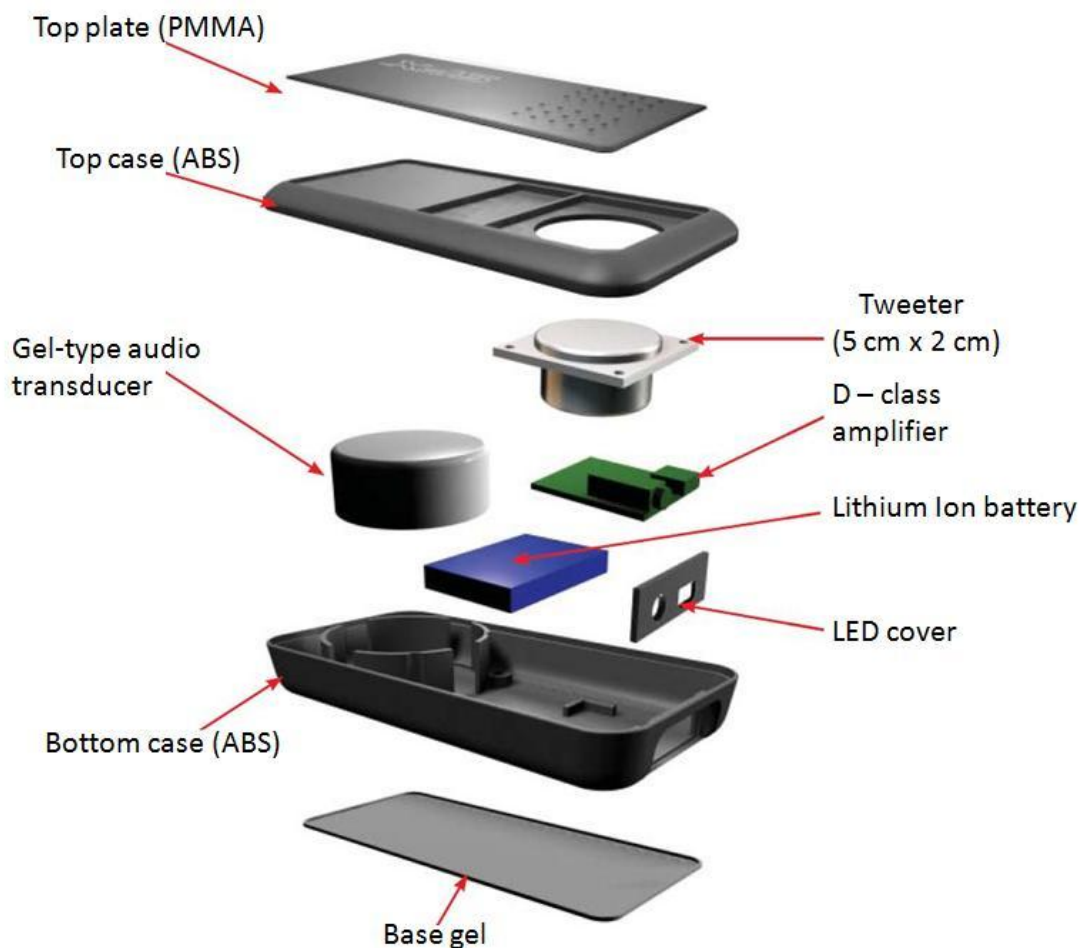
(a) Internal architecture of Wowee One (unit size: 120 mm × 60 mm × 25 mm)

(b) Complete assembly

Fig. 5.1 Wowee One unit

Fig. 5.2 The Sound Station, a portable audio speaker incorporating the gel-type audio transducer developed by SAMSUNG Electronics [75]

A similar concept of the portable audio speaker with enhanced bass sound was also developed by SAMSUNG Electronics, who adopted the gel-type audio transducer to develop the product, called "Sound Station" as shown in Figure 5.2. This device was designed as an audio accessory for a "Galaxy Tab 10.1" tablet. The picture shows the

Galaxy Tab 10,1 being docked on the Sound Station and this product was demonstrated by SAMSUNG Electronics in the International Consumer Electronics Show (CES) 2011 held in Las Vegas, USA.

5.2.2 Comparison with competitor product

The main advantage of the Wowee One speaker in comparison with conventional portable speakers is that the gel-type audio transducer delivers low frequencies by converting the surface to which it is attached into the radiator, whilst the conventional speakers clearly demonstrate lack of low frequency performance.
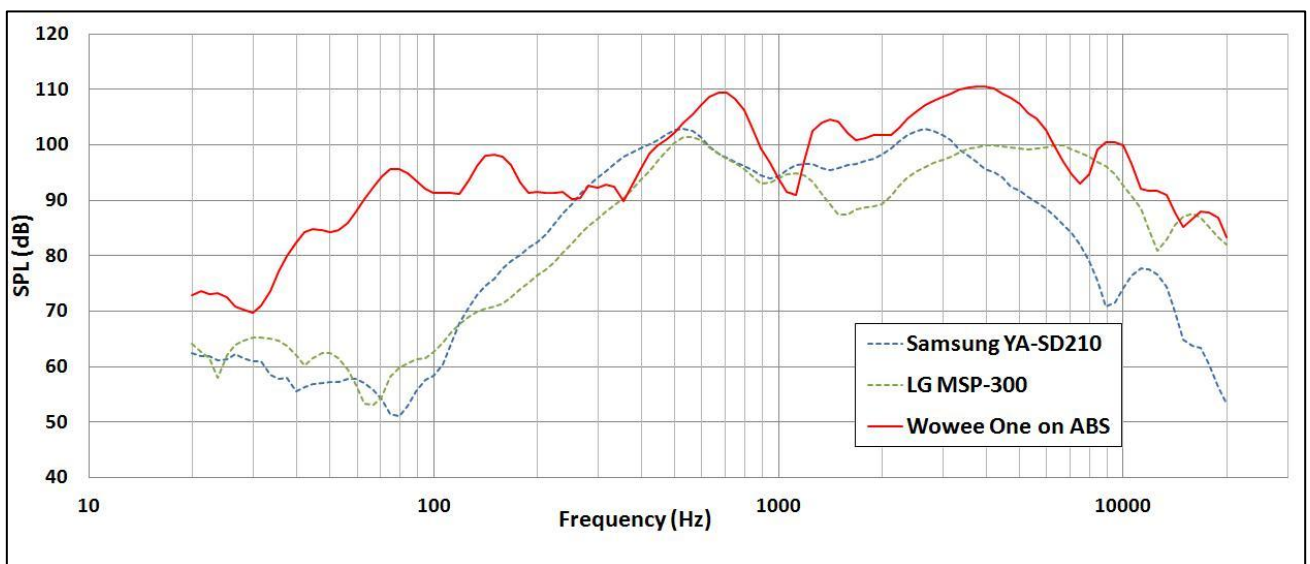
Fig. 5.3 The SPL comparison of Wowee One against standard portable speakers

Figure 5.3 shows the SPL comparison of Wowee One against two standard portable speakers – LG MSP 300 (4 W) and SAMSUNG YA SD 210 (4 W) that have similar characteristics as declared in their specification leaflets. The SPL graph reveals that the Wowee One produces higher SPL over the measured frequencies in the range

20 Hz to 20,000 Hz when compared to LG and SAMSUNG units. The difference in the SPL between the Wowee One and the other units is more significant at low frequencies below 250 Hz, resulting in a flat SPL response of the Wowee One. This made a Wowee One competitive in the market because this unit is considered as only portable speaker that generates the sound with enhanced bass in a small and slim product.

5.2.3 Commercial benefit

Wowee One became a first commercial audio product in SFX Technologies who provided throughout support for this work . The company sold 400,000 units per year since it was released in 2009. This unit was well accepted as a first portable bass speaker in the market. In 2011 Wowee One won Award for Best Mobile Product at the Mobile Excellence Awards.

5.3 Ultra-slim television

TV manufacturers declare year after year that the televisions have to become thinner and thinner to satisfy the aesthetic requirements of the customers. The screen technologies adopted by the manufacturers allow developing very thin TVs, however the sound technology becomes less suitable for usage in these slim products.

Latest OLED TV developed by LG Electronics and presented in the international CES 2011 is shown in Figure 5.4.

Fig. 5.4 OLED LG TV presented in 2011 [76]

5.3.1 Product specifications

Due to a slim trend in the TV market, conventional full range TV speakers cannot be longer employed because they are too big in size. The reduction of the conventional speaker's size results in lack of low frequency sound from the product, which affects the overall customer satisfaction from the product. The gel-type audio transducer was incorporated to one of thinnest LED TVs (SAMSUNG Ultra thin 32" LED TV) to demonstrate that the full range sound solution can be produced with help of innovative gel technology with improved sound at low and medium frequency range.

Figure 5.5 shows a TV prototype built for testing. A speaker originally built-in this TV by the manufacturer was a conventional multi-coil 8 Ω speaker with 10 W output power. A pair of these speakers was used for a stereo sound and a size of each speaker is 225 mm × 23 mm × 20 mm thick. These speakers then were replaced by two gel-type audio transducers specifically designed for this application and the transducers

were attached to the panel as shown in Figure 5.5. A microphone was set up at 1 m from the panel on axis.
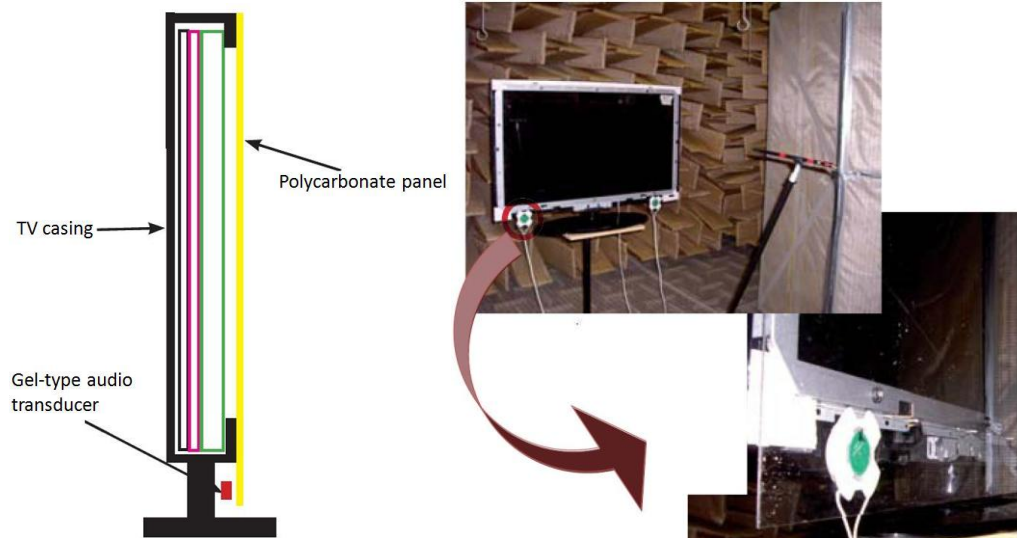
Fig. 5.5 TV prototype

The transducer's specification and assembly drawing are shown in Table 5.2 and Figure 5.6 respectively.

Nominal impedance	6 Ω
Frequency range	60 Hz ~ 10 KHz
Power handling	10 W (RMS)
Dimensions	$42 \times 42 \times 10.5$ mm
Magnet	N48

Table 5.2 Specification of the gel-type audio transducer designed for a TV
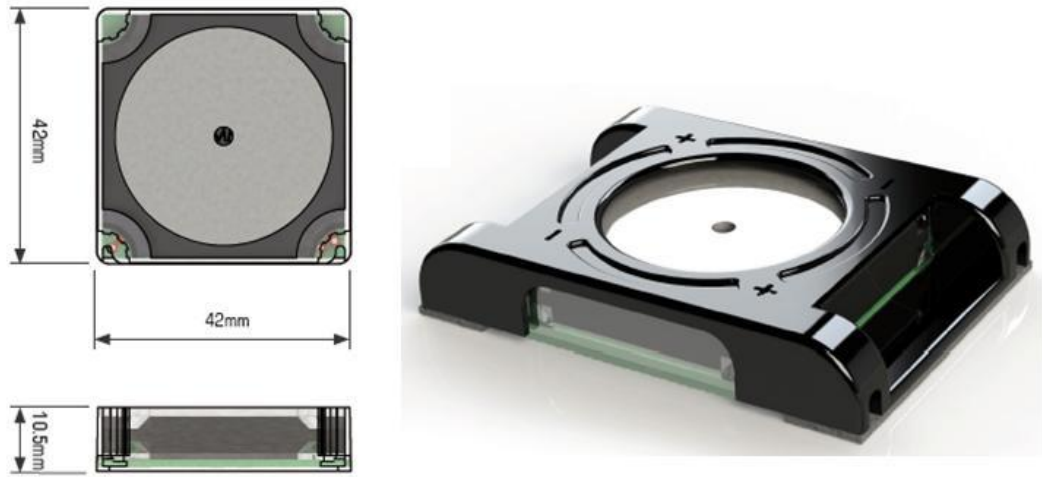
Fig. 5.6 Complete assembly drawing of the gel-type audio transducer designed for TV application

The panel materials used for the comparison tests include polycarbonate [PC], poly(methyl methacrylate) [PMMA] and poly(vinyl chloride) [PVC]. These panels were chosen as they are considered as alternatives to glass display panels. The sizes and the ratios of the length to the width of the panels were shown in Table 1.1. Also the properties of these materials, including the speed of sound in each material, were presented in Table 2.1.

5.3.2 Comparison with competitor product

The SPL graph in Figure 5.7 indicates that the TV speaker could not produce the low range of frequencies between 40 Hz to 300 Hz whereas the gel-type audio transducer generates the high level of sound at these frequencies.

It has been demonstrated that PMMA panel creates the highest level of sound pressure at frequencies in the range 40 Hz to 1000 Hz due to the higher bending

stiffness of the panel compared to the polycarbonate and PVC panels, although there is a slight reduction in the SPL curve at around 150 Hz. The environmental noise affects the SPL at low frequency below 40 Hz. So the unusual increase of the SPL of the PVC panel and TV speaker below 40 Hz is assumed to be caused by the environmental noise. At higher frequencies above 1,000 Hz, the PVC panel shows a higher SPL than the other panels, including the TV speaker at frequencies in the range 3,000 Hz to 18,000 Hz. The PVC panel also creates a high level of SPL at frequencies below 1,000 Hz compared with the PMMA panel. So the panel with the flat response across all measured frequencies – PVC – is recommended for this application. Therefore the TV equipped with the gel-type audio transducers can deliver full frequency sound without a restriction of a TV size and thickness to be able to satisfy the needs of customers for TV industry.
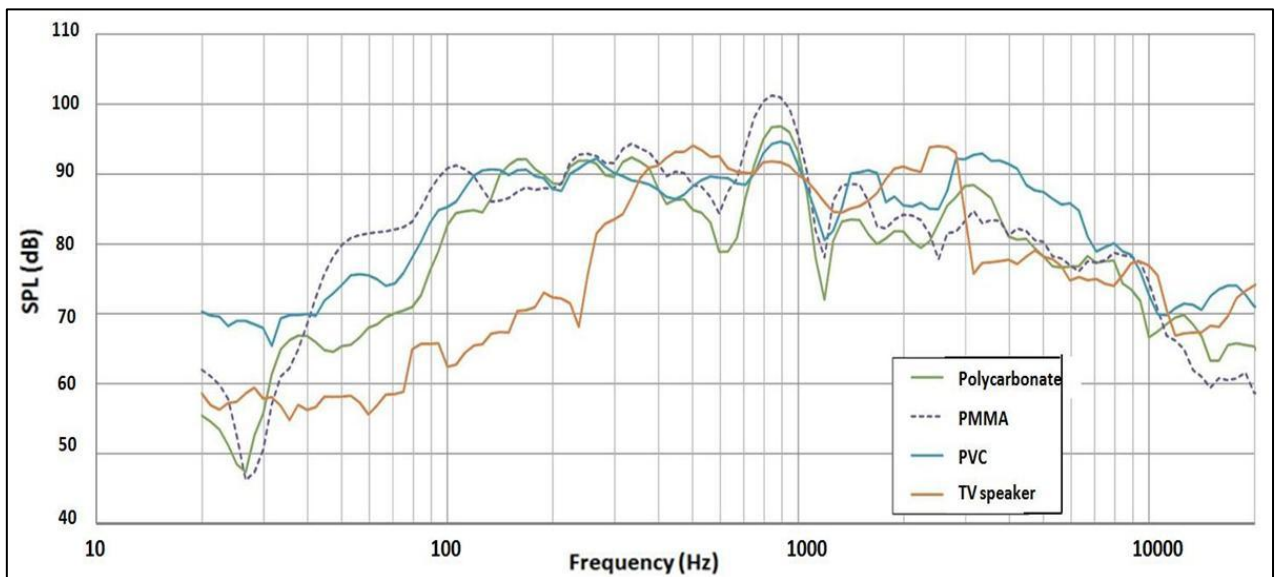
Fig. 5.7 The SPL of the TV prototype

5.3.3 Commercial benefit

Although the TV incorporating the gel-type audio transducer is still under development, this has received great commercial benefits because the TV with the transducer implemented does not require an additional speaker system of which most slim TVs need to reinforce their poor built-in sound system. The gel-type audio transducer is ultra-slim, light weight and there is no need for cut-outs and grills. So this allows TV product designers more freedom and flexibility to deliver high-quality sound. For TV application, there has been a collaboration research project being carried out with SAMSUNG and LG Electronics.

5.4 Handheld computer

Handheld computers are designed specifically for mobile field professionals who need productivity and reliability beyond a smart phone. They are effective for inventory reduction, accurate inventory control and reduction of lead-time from stocking to shipping in the logistics industry. These must combine ruggedness, advanced voice and data communications as well as integrated high-performance scanning capability.

5.4.1 Product specifications

These devices are equipped with two different transducers – a vibrator for the haptic feedback and an audio transducer for generation of multi-tone sound. A gel-type audio transducer can function like both a vibrator and generator of audio signals so a

single gel-type audio transducer can replace both transducers used in handheld computers. The product is shown in Figure 5.8 (a).

A prototype was built by using an Intermec CK3B mobile computer. This device is equipped with a standard ERM (eccentric rotating masses) motor and two conventional tweeters (D20×5.42 mm, 8 Ω) manufactured by Ole Wolff.

A gel-type audio transducer designed for this application, in order to replace two existing tweeters was implemented as shown in Figure 5.8(b). The specification of the transducer is presented in Table 5.3, and the assembly is shown in Figure 5.9.

Nominal impedance	8 Ω
Frequency range	200 Hz ~ 10 KHz
Power handling	4 W (RMS)
Dimensions	$25 \times 25 \times 8.9$ mm
Magnet	N48

Table 5.3 Specification of the gel-type audio transducer designed for a mobile computer

(a) Intermec CK3B mobile computer   (b) Implementation of the transducer

Fig. 5.8 Prototype of the mobile computer
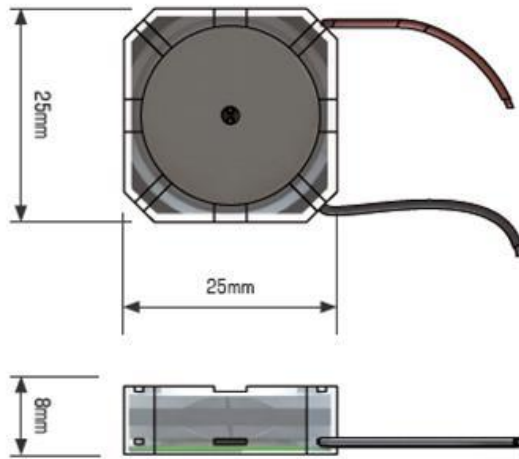
Fig. 5.9 Assembly drawing of the gel-type audio transducer designed for handheld computer application

5.4.2 Comparison with competitor product

The acoustic test was carried out to compare the SPL of the gel-type audio transducer implemented in the computer device against two existing tweeters, and the result was presented in Figure 5.10. Requirement of the frequency response for a tweeter used in these devices is 85 dB at frequencies in the range 500 Hz to 3500 Hz where a beep noise is generated. The SPL graph indicates that the SPL of the gel-type audio transducer measured reaches around 85 dB that is similar to the SPL value of the two tweeters. Also the graph reveals that the transducer generates vibrations at low frequency range so the haptic (vibration) feedback can be achieved. Therefore the gel-type audio transducer can be successfully implemented into handheld computers and serve as both a vibrator and generator of audio signals.
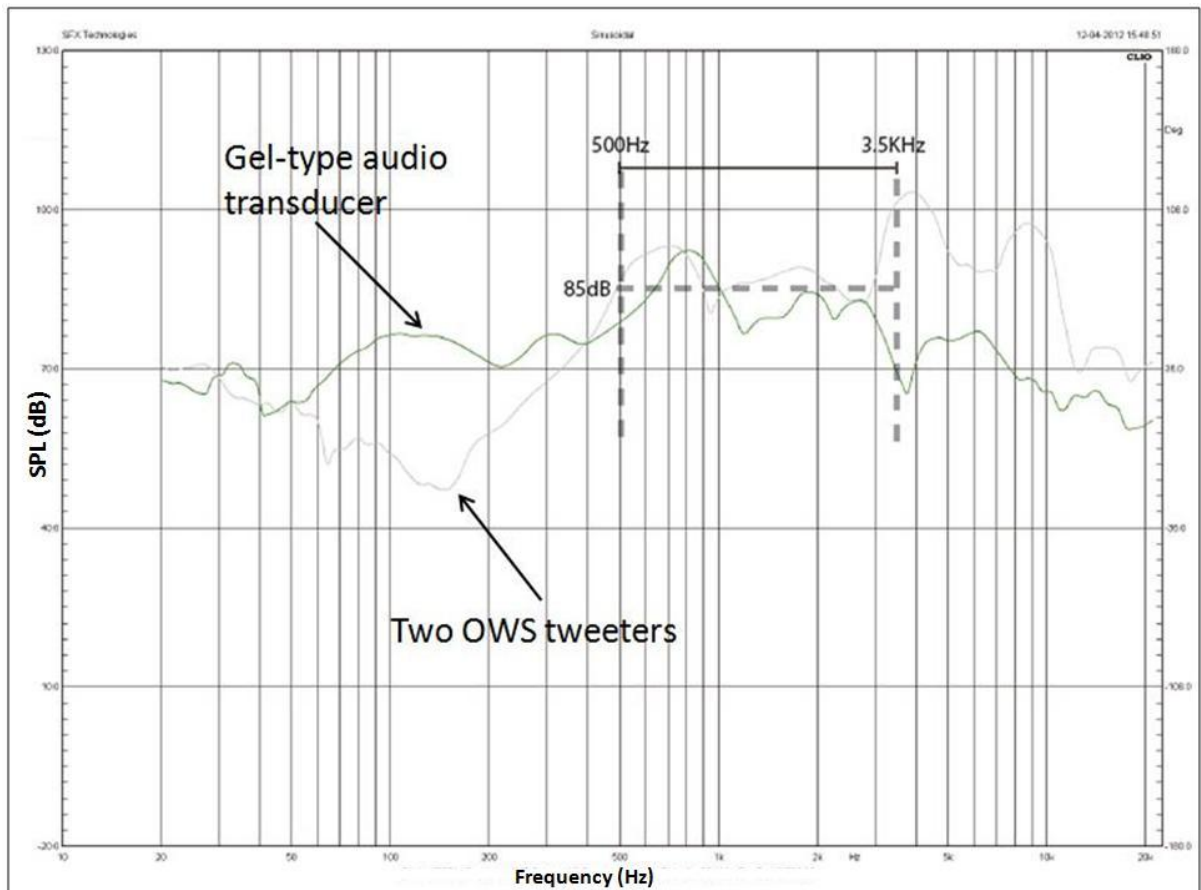
Fig. 5.10. The SPL of the gel-type audio transducer against the two existing tweeters in the mobile computer

5.4.3 Commercial benefit

This application shows great promise that the gel-type audio transducer can deliver not only audio solution but also haptic feedback solution. Furthermore as the transducer does not require cut-outs or grills, this can bring more reliable design for field workers. Currently next generation of a handheld computer incorporating the gel-type audio transducer is underway with Intermec Inc.

5.5 Conclusions

Applications for the gel-type audio transducer developed throughout this research were discussed. Wowee One that is a portable audio speaker incorporating a standard tweeter for high frequency range and the gel-type audio transducer for sound enhancement at low and medium frequency range, was successfully accepted in the market with sales of 400,000 per year since 2009. The SPL graph showed its unique audio performance at low and mid frequency range that makes the unit competitive. This was also observed in the TV application. TV incorporating the gel-type audio transducers radiated flat frequency response over frequencies in the range 40 Hz to 10,000 Hz, while the conventional TV speakers lack the bass sound due to reduction of air cavity in order to fit into a slim TV. A gel-type audio transducer can be also an ideal transducer for handheld computer applications because that works as both an audio transducer and a vibrator for the haptic feedback. Therefore the study on the applications of the gel-type audio transducer showed great promise, and some of the research collaborations with companies such as SAMSUNG, LG electronics, and other manufacturers of consumer electronics are already underway.

CHAPTER 6 – CONCLUSIONS

6.1 Thesis review

The research work presented in this thesis is based on the development of next-generation "gel-type audio transducer" for miniaturisation of a woofer device, in order to overcome the current problems for loudspeaker design.

The gel-type audio transducer, that is driven by the electromagnetic conversion mechanism (a moving-coil transducer), consists of the magnetic assembly and coil drive-plate assembly, and these mechanical parts are coupled by the gel surround made of an elastomer. The gel surround also enables the transducer to be integrated into any solid surface (in this thesis, solid panels were used) to generate controlled vibrations. The gel surround plays an important role in enhancement of the output driving force of the transducer, and the energy transfer from the transducer to a panel that the transducer is attached, resulting in increased acoustic efficiency at low frequencies, especially in the range 20 Hz to 300 Hz. Thus, factors governing the performance of the gel-type audio transducer were identified, and effect of the gel surround on generation of the output driving force and the energy transfer mechanism was investigated. Furthermore, the relationship between the gel surround and sound pressure level (SPL) radiated from the panel excited by the transducer was studied. They were fully investigated in the first instance by utilising simulation software, and subsequently conducting experimental trial, comparison of the results from simulation and experiment enabled verification of the transducer design. For simulations, COMSOL multiphysics was used for various engineering problems. The AC/DC module, stress-structure module, and the acoustic

module were employed to predict the electrical parameters of the transducer, the behaviour of the vibrating panel excited by the transducer, and acoustic performance radiated from the panel respectively. For experiments, various mechanical testing techniques such as the acoustic and laser scanning measurement, and the dynamic mechanical analysis (DMA) were used as discussed in Chapter 3. This Chapter also described the design and fabrication of the gel-type audio transducer used for this research. For evaluation of the gel surround, three different types of elastomers – RTV silicone, thermoplastic elastomer (TPE), and silicone foam elastomer with a range of hardness were selected and investigated.

Successful development of prototypes of next-generation gel-type audio transducer with an enhanced acoustic efficiency at especially low frequency band was achieved throughout the thesis. Furthermore, implementation of the gel-type audio transducers into the consumer applications such as a portable audio speaker, TV, and a handheld computer was carried out, and it was proved that the gel-type audio transducer enhances the acoustic performance of the sound system in those applications as a miniaturised woofer device. The first commercial audio product called "Wowee One", incorporating the gel-type audio transducer developed, was launched and successfully accepted as a first portable bass speaker in the market.

6.2 Main findings of the thesis

a. Output driving force of a classic moving-coil transducer can be greatly enhanced by coupling an elastomer called "the gel surround" to moving parts of the transducer. Larger mass of the magnetic assembly, M_m or compliance, C of the gel surround (or both) increase the output driving force of the transducer.

- This principle takes advantage of the inertial force induced by the movement of the magnetic assembly. This effect is governed by the values of the M_m and C that act as a high-pass filter at low frequency range as described in Figure 4.3, section 4.2.

- Operating frequency range of the gel-type audio transducer is extended to lower values by reduction of the f_0 of the system as a result of larger M_m or C.

- The table 6.1 is the summary of the experimental results, showing that the effect of the M_m and C. That is, the larger values of M_m and C cause the greater displacement of the panel and lower the f_0.

	Testing samples of the gel-type audio transducer	Displacement of the panel excited by the transducer (at the highest peak)	Average displacement of the panel excited by the transducer between 20 Hz and 200 Hz
effect of M_m	Transducer A (80 g of the M_m)	3.5 µm (30 Hz, 1st f_0)	0.5 µm ~ 3.5 µm
	Transducer B (40 g of the M_m)	0.95 µm (60 Hz, 1st f_0)	0.05 µm ~ 1 µm
effect of C	Transducer C ($tan\,\delta$ = 0.9 at 100 Hz)	1.5 µm (120 Hz, 3rd f_0)	0.25 µm ~ 1.5 µm
	Transducer D ($tan\,\delta$ = 0.65 at 180 Hz)	0.55 µm (180 Hz, 3rd f_0)	0.08 µm ~ 0.6 µm

Table 6.1. Experimental results of the panel's displacements

b. The gel surround, coupled with moving parts of the transducer, allows itself to be attached to any solid object and operate with a minimal mechanical interference.

- The panel, excited by the transducer, forms the vibrating modes as a function of a driving frequency, boundary condition, and the panel's shape. The reflected bending waves on the panel collide with the driving force coming from the transducer as depicted in Figure 4.17 (a), section 4.3. This effect results in the mechanical noise, shorter service life, and the reduced operating frequency range. However the gel surround placed between the transducer and panel absorbs the reflected bending waves so the collision of the forces is minimised as shown in Figure 4.17 (b). The ability of the energy absorption of the gel surround is proportional to the loss modulus, E'' and its

strain, ε_0^2. So they must be higher than the energy of the bending waves of the panel expressed as $Z_p v_b \times x_p$ in order to minimize the collision of the forces.

- The gel surround contributes to the impedance matching, as the stiffness of the gel surround reflects the stiffness of both the mechanical parts of the transducer and panel so that efficient energy transfer can be achieved. This enables various types of panels or solid surfaces to be selected depending on the applications. Thus it gives the freedom of choosing various types of panels or solid objects in response to the need of applications.

- The results of the comparison test between the gel-type audio transducer (with the gel surround) and classic DML transducer (without the gel surround) demonstrated that the mechanical distortion created by the DML transducer is higher than the gel-type audio transducer over the full testing frequencies, especially below 80 Hz where displacement of the panel becomes the greatest. On contrary, the panel with the gel-type audio transducer attached projects higher SPL than the panel with the DML transducer attached at low and high frequency band as described in section 4.3.3.

c. The controlled displacement on any solid surface with the gel-type audio transducer attached can be produced.

- The longitudinal and transverse waves occurred in the panel form the bending modes as a function of a driving frequency. At low frequencies, the panel moves as a rigid body so the entire surface of the panel moves in phase. But as frequency increases, the bending mode breaks up over the panel. As the frequency rises higher, the effective moving mass and stiffness of the panel increase. As a result, the moving area of the

panel is reduced and displacement of the panel is localised around a position of the transducer, whilst the rest of the panel is less affected. This phenomenon occurs at 2,000 Hz above. Figures 4.26 and 4.27 in section 4.3 showed the bending modes of the panel that were simulated and also measured experimentally.

d. The SPL of the gel-type audio transducer is greatly enhanced at low frequency band by increasing values of the C of the gel surround.

- The displacement of the panel is directly proportional to the SPL as discussed in section 4.4. Therefore, the greater displacement of the panel, caused by the larger value of the C of the gel surround, results in the highest SPL. Furthermore the in-phase region dominates the panel at low frequencies so the acoustic cancellations are minimized, thereby the enhanced acoustic efficiency is achieved.

- The gel-type audio transducer with the 35 Shore 00 RTV silicone gel surround exhibits higher SPL than 70 Shore 00 transducer over the full frequency range. At around first f_0, 80Hz, the SPL of 35 Shore 00 transducer is 10 dB higher than the 70 Shore 00 transducer.

e. Two independent sound sources radiating from a single panel can be achieved by exciting the panel with the two transducers.

- At frequencies above 2,000 Hz, the moving area on the panel becomes localised so the directivity of the sound radiation becomes narrow over the moving area of the panel. So it would be possible to utilise two independent sound sources from a single panel with the two gel-type audio transducers attached.

6.3 Suggestions for future work

The design process of the gel-type audio transducer can be divided into three stages. The first stage includes the design of electrical parameters (e.g. blocked coil impedance and force factor, BL). According to a target specification, the wire length, thickness, and outer dimension of the coil are determined in this stage. The second stage is to select of the magnet grade (N35~48) and design the external size of the magnetic assembly based on the coil design (a target frequency range is determined). Designing the gel surround, to maximize the movement of the magnetic assembly and the energy transfer to a panel, is the last stage of the driver development process. The overall size of the transducer is decided in the first stage of design process and this size limits the mass of the magnetic assembly, M_m and the C of the gel surround that determine the operating frequency range and acoustic performance of the transducer.

Furthermore the driving mechanism of the gel-type audio transducer is based on the interaction between an electrical force (created from a coil intersecting the flowing magnetic flux) and a mechanical force (created by the movement of the magnetic assembly – an inertial force, and damping force of the gel surround). Those forces are closely related and interacted in a non-linear manner and the gel surround exhibits non-linear viscoelastic characteristics as a function of frequency so it is very challenging to make the gel-type audio transducer scalable and customizable. Thus for each application, the completely new design (configuration) of the gel-type audio transducer is required. This process slows down development of the gel audio driver so it is difficult to produce a wide range of the gel-type audio transducer for different types of applications. Further

research on overcoming these issues will encourage manufacturers of consumer applications to adopt the gel-type audio transducer for applications.

The gel-type transducer developed throughout this thesis was investigated for an audio application. However a range of applications can be extended to an active vibration cancellation and energy harvesting system. It would be worth considering implementation of the gel-type audio transducer for those applications.

References

[1] J. Eargle., 2003. Loudspeaker handbook, 2nd ed. Springer (2003)

[2] W. Carroll & Jr. Pursell., 1990. Technology in America: a history of individuals and ideas, 2nd ed. MIT Press (1990)

[3] G. M. Ballou., 2005. Handbook for sound engineers, 3rd ed. Elsevier (2005)

[4] V. Dickason., 1991. The loudspeaker design Cookbook, 4th ed. Audio Amateur Press (1991)

[5] J. Wang., 2007. Polymer Deformable Mirror for Optical Auto Focusing. ETRI J., December, 2007, **29**, no. 6, pp. 817-819

[6] D. Kim, J. Yeo, J. Choi., 2008, Compact Spatial Triple-Band-Stop Filter for Cellular /PCS/IMT-2000 Systems. ETRI Journal, October 2008, **30**, no. 5, pp. 735-737

[7] G. Bank. N. Harries, 1998. The distributed mode loudspeaker – Theory and Practice. AES 13th Conference, 3-5 March 1998

[8] C.S. Lee., 2003. An Approach to Durable Poly (vinylidene fluoride) Thin Film Loudspeaker. J. Mater. Research, December 2003, **18**, pp. 2904-2911

[9] T. Horikawa & K. Kobayashi., 2008. Application of Ceramic Piezoelectric Device to Audio Speaker. Proc. SICE Annual Conference, April 2008

[10] C. Shearwood., 1996. Application of Polyimide Membranes to MEMS Technology. Microelectron. Eng., 1996, **30**, pp. 547-550

[11] H. Kim., 2005. Bi-directional Electrostatic Microspeaker with Two Large-Deflection Flexible Membranes Actuated by Sing/Dual Electrodes. Proc. IEEE Sensors, 2005, pp. 89-92.

[12] J.J. Neumann, Jr. K.J. Gabriel., 2002. CMOS-MEMS Membrane for Audio-Frequency Acoustic Actuation. Sensors and Actuators A: Physical, January 2002, **95**, no. 2, pp. 175-182.

[13] N. Harris., 1997. The distributed-mode loudspeaker (DML) as a broad-band acoustic radiator. AES convention, September 1997

[14] G. Bank & G.T. Hathaway., 1982. Three-dimensional energy plots in the frequency domain. Audio Engineering Society Conference, January 1982

[15] NXT Ltd, October 2012. Sound wave fields of DML transducers. Accessed from www.vxm.com/nxt

[16] H. Azima & N. Harris., 1997. Boundary interaction of diffuse field distributed-mode radiators. AES 103rd Convention, September 1997

[17] Mitch Tashiro. G. Bank & M. Robers, 1997. A new flat panel loudspeaker for portable multimedia. AES 103rd Convention, New York, September 1997

[18] N.J. Harris, M.O.J. Hawksford., 2000. Introduction to distributed mode loudspeaker (DML) with first-order behavioural modeling. IEE Proc.- Circuits devices syst., June 2000, **147**, No. 3, pp.153-157

[19] Martin Logan, September 2012. Accessed from www.martinlogan.com

[20] John Borwick., 2001. Loudspeaker and headphone handbook, 3rd ed. Wiley (2001)

[21] Lindenberg, Theodore., 1953. Design of an electrostatic loudspeaker. J. Audio. Eng. Soc. October 1953, **1**, issue 4, pp. 273-275

[22] Glen M. Ballou., 2005. Handbook for sound engineers, 3rd ed. Elsevier (2005)

[23] M.I. Haller. Khuri-Yakub, B.T., 1996. A surface micromachined electrostatic ultrasonic air transducer. IEEE transactions on ultrasonics, ferroelectrics and frequency control, January 1996, **43**, Issue 1, pp. 1-6

[24] H.J. Kim. S.Q. Lee. S.K. Lee. K.H. Park., 2009. A Piezoelectric microspeaker with a high quality PMN-PT single-crystal membrane. J. Kor. Phys. Soc., February 2009, **54**, pp. 930-033

[25] S.H. Yi, E.S. Kim., 2005. Micromachined Piezoelectric microspeaker. Jpn. J. Appl. Phys., March 2005, **44**, no. 6A, pp. 3836-3841

[26] C.H. Han, E.S. Kim., 2000. Parylene-Diaphragm piezoelectric acoustic transducers. Proc. IEEE Micro Electro Mechanical Systems, IEEE MEMS, June 2000, pp. 148-152

[27] Murata Ltd, September 2012. Murata is a developer of a piezo-type audio transducer. Accessed from www.murata.com

[28] Asia Electronics Industry (AEI) magazine, 2007. Dempa publications, November (2007)

[29] SFX Technologies White paper, August 2009

[30] Norman H. & Ian H., 2001. Loudspeaker driver assemblies, U.S. Patent 7,889,876 B2. Filed 17th Jun 2003. Assigned 17th June 2004

[31] A. W. Leissa., 1969. Vibration of plates. Aeronautics and space administration (1969)

[32] Kuonan Li., 2010. A critical review of bending wave loudspeaker technology and implementation. Chalmers University of Technology (2010)

[33] Davidson, September 2012. The education website showing bending modes of the panel. Accessed from www.phy.davidson.edu/stuhome/derekk/chladni/pages/menu.htm

[34] J.E. Mark., 2003. Some Recent Theory, experiments, and simulations on rubberlike elasticity. J. Phys. Chem. B., 2003, **107**, no.4, pp. 903-913

[35] E.T. Bishop. S. Davison., 1969. Network characteristics of the thermoplastic elastomers. J. Polymer. Science. Part C: polymer symposia, 1969, **26**, issue 1, pp. 59-79

[36] J. C. Gerdeen., 2006. Engineering design with polymers and composites. Taylor & Francis Group (2006)

[37] D.W. Herrin. T.W. Wu. A.F. Seybert., 2000. Case study evaluation of the Rayleigh integral method. J. Acoust. Soc. Am. December 2000, **108**, issue 5, pp. 2451

[38] J.Heijboer., 19690. Modulus and damping of polymers in relation to their structure. British polymer Journal, January 1969, **1**, issue 1, pp. 3-14

[39] Morton, M., 1987. Rubber technology. Van Nostrand Reinhold, New York (1987)

[40] Donnet, J.& A. Voet., 1976. Carbon black − Physics, Chemistry and Elastomer reinforcement. Marcel Dekker, New York (1976)

[41] Andrew Ciesielski., 2000. An introduction to rubber technology. Rapra technology Ltd (2000)

[42] R.C. Edwards., 1983. Automotive elastomers and design. March (1983)

[43] Y.C. Fung., 1997. Biomechanics circulation, 2nd ed. Springer-Verlag Berlin (1997)

[44] K. Xiang. Xiaoan Wang. Guangsu Huang., 2012. Thermal ageing behaviour of styrene-butadiene random copolymer: A study on the ageing mechanism and relaxation properties. Polymer degradation and stability, September 2012, **97**, issue 9, pp. 1704-1715

[45] K. G. Budinski., 2010. Engineering materials: properties & selection, 9th ed. Pearson (2010)

[46] T.C.T. Ting., 1965. The contact stresses between a rigid indentor and a viscoelastic half-space. Brown University, December (1965)

[47] C. A. Tweedie. Krystyn J. Van Vliet., 2006. Contact creep compliance of viscoelastic materials via nanoindentation. J. Materials Research, 2006, **l21**, Issue 06, pp. 1576-1589

[48] T. M. Nair. M.G. Kumaran. G. Unnikrishnan. V.B. Pillai., 2008. Dynamic mechanical analysis of ethylene-propylene-diene monomer rubber and styrene-butadiene rubber blends. J. Polymer Science, December 2008, **112**, issue 1, pp. 214-215

[49] R.J. Schaefer., 1995. Dynamic Properties of Rubber. Rubber world, January (1995)

[50] N.G. McCrum., 1991. Anelastic and dielectric effects in polymer solids. Dover publication Inc (1991)

[51] R. F. Barron., 2001. Industrial noise control and acoustics. Marcel Dekker Inc (2001)

[52] J.D. Ferry., 1980. Viscoelastic properties of polymers, 3rd. ed. Wiley, New York (1980)

[53] L. E. Kinsler., 2000, Fundamentals of acoustics, 4th ed. John Wiley & Sons Inc (2000)

[54] W. T. Tomson., 1998. Theory of vibrations with applications, 5th ed. Pearson (1998)

[55] E. E. Ungar. Edward M. Kerwin Jr., 1962. Loss factors of viscoelastic system in terms of energy concept. J. Acoust. Soc. Amer., 1962, **34**, no.7, pp. 954-957

[56] Hajime Kishi. Manabu Kuwata. Satoshi Matsuda. Toshihiko Asami. Atsushi Murakami., 2004. Damping properties of thermoplastic − elastomer interleaved carbon fibre − reinforced epoxy composites. Composites Science and Technology, December 2004, **64**, issue 16, pp. 2517-2523

[57] R. Lakes., 2009. Viscoelastic materials. Cambridge University Press (2009)

[58] R. Solecki., 2003. Advanced mechanics of materials. Oxford University Press (2003)

[59] C.R. Calladine., 1969. Engineering Plasticity, 1st ed. Pergamon Press (1969)

[60] I.G. Bubnov., 1914. Theory of ship structures. St. Petersburg (1914)

[61] B.G. Galerkin., 1915. Series solution of some problems in elastic equilibrium of rods and plates. Vestn. Inzh, Tech (1915)

[62] A.E.H. Love., 1927. A teatise on the mathematical theory of elasticity, 4th ed. Cambridge University Press (1927)

[63] S.P. Timoshenko & S. Woinowski-Krieger., 1959. Theory of Plates and Shells, 2nd ed. McGraw-Hill, New York (1959)

[64] Sasadhar De., 1971. Problem on the vibrations of plates. Pure and applied geophysics, 1971, **92**, no. 1, pp. 45-51

[65] J.W.S. Rayleigh., 1945. The theory of sound, Dover publications, New York (1945)

[66] L. Cremer, M. Heckl, & E. E. Ungar., 1988. Structure-Borne sound, 2nd ed. Springer-verlag, Berlin (1988)

[67] F. Fahy., 1987. Sound and structural vibration. Academic Press, London (1987)

[68] L. Beranek., 1996. Acoustics. Acoustic society of America, New York (1996)

[69] P. M. Morse & K. U. Ingard., 1968. Theoretical acoustics, Section 7.4. Mcgraw Hill, New York (1968)

[70] J. Panzer., 1998. Distributed-mode loudspeaker radiation simulation, AES 105th convention, September 1998

[71] J. Krautkramer., 1990. Ultrasonic testing of materials, 4th ed. Springer-Verlag, Berlin (1990)

[72] B. B. Bauer. Shure Brothers., 1976. Equivalent circuit analysis of mechano-acoustic structures. J. Audio Eng. Soc, October 1976, **24**, issue 8, pp. 643-655

[73] W. Klippel. Schiechter Joachim, 2006. Measurement and visualization of loudspeaker cone vibration. J. Audio Eng. Soc. October 2006, **54**, pp. 1251-1252

[74] J. Eargle., 2003. Loudspeaker handbook, 2nd ed. Kluwer academic publisher (2003)

[75] SAMSUNG Electronics, September 2012. Sound station presented by SAMSUNG at 2010 MWC . Accessed from www.samsung.com

[76] LG Electronics, September 2012. 2011 LG TV application presented at 2011 CES. Accessed from www.cesweb.org

List of publications

a. M. Cho, M. Barker and E. Prokofieva, "Effect of elastic gel layer on energy transfer from the source to moving part of loudspeaker", the AES 134th Convention in Rome Italy, May 2013

b. M. Cho, M. Barker and E. Prokofieva, "Enhancing the power output of moving coil actuators by incorporating soft polymers", J. Sensors and Actuators: A Physical, Apr 2013, vol 193, pp. 161-169

c. E. Prokofieva, M. Cho, and M. Barker, "Methods of effecting the directivity and the magnitude of vibrations transferred over multilateral surfaces", IX All-Russian Conference on Non-linear vibrations of mechanical systems, Nizhny Novgorod, Russia, Sept 2012

d. M. Cho, E. Prokofieva and M. Barker, "A novel design for a gel-type DML transducer incorporating a solid panel projecting multiple independent sound sources", 40th AES International Conference, Tokyo, Japan, Oct 2010

e. M. Cho, E. Prokofieva and M. Barker, "Improvement of sound quality by means of ultra-soft elastomer for the gel-type inertia driven DML transducer", 128th AES International Convention, London, UK, May 2010